Microstructural, Mechanical and Tribological Investigation of Copper-Based Coatings for Extreme Environments

Martin Asuquo

A Thesis

In the Department of

Chemical and Materials Engineering

Presented in Partial Fulfillment of the

Requirements for the Degree of

Master of Applied Science (Chemical Engineering)

at

Concordia University

Montréal, Québec; Canada

August 2024

CONCORDIA UNIVERSITY

School of Graduate Studies

This is to certify that the thesis prepared

By: **Martin Asuquo**

Entitled: **Microstructural, Mechanical and Tribological Investigation of Copper-Based Coatings for Extreme Environments**

and submitted in partial fulfillment of the requirements for the degree of

Master of Applied Science (Chemical Engineering)

complies with the regulations of the University and meets the accepted standards with respect to originality and quality

Signed by the final examining committee:

_____ Chair
Dr. Sixu Deng

_____ Examiner
Dr. Moussa Tembely

_____ Examiner
Dr. Sixu Deng

_____ Supervisor
Dr. Pantcho Stoyanov

_____ Supervisor
Dr. Christian Moreau

Approved by _____
Dr. Zhibin Ye, Graduate Program Director
Department of Chemical and Materials Engineering

August, 2024 _____
Mourad Debbabi, Dean
Gina Cody School of Engineering and Computer Science

ABSTRACT

Microstructural, Mechanical and Tribological Investigation of Copper-based Coatings for Extreme Environments

Martin Asuquo

Thermal spray coating methods such as Atmospheric Plasma Spray (APS), High-Velocity Oxygen Fuel (HVOF), and newly developed High-Velocity Air Fuel (HVAF) offer one of the best technique to effectively protect new parts from high temperature, wear, corrosion, and residual stresses as well as produce hard and dense coatings which in turn helps in the improvement of the lifespan of the material. These techniques provide coatings that enable the enhancement and prolongment of component life and the reduction of component cost due to the improvement in the functionality of a low-cost material. There is also an opportunity to revamp worn parts to their original dimensions, without the need to replace the entire component. However, traditional thermal spray techniques tend to produce coatings with high oxide content and porosity resulting in undesirable coating properties. On the other hand, Cold Spray (CS), a more recent coating technique, can produce highly dense coatings with strong bonding through the plastic deformation of powder feedstock, thus avoiding most of the aforementioned issues.

The main purpose of this research is to study the tribological properties of copper-based coatings deposited by APS, HVAF and Cold spray (i.e. from high temperature to low temperature deposition methods) to determine their suitability for extreme environments. This thesis is comprised of two research studies, The first study emphasizes on development of APS-CuNi coatings on different substrate materials to investigate the influence of the substrate materials as well as the tribological performance of the coatings at various temperatures (room and elevated temperature). The second study focuses on the evaluation of copper coatings by low temperature deposition systems (HVAF and CS) to understand their microstructural, mechanical and tribological behavior (room and elevated temperature).

The microstructural evaluation of coatings produced by both studies was analysed using the scanning electron microscope (SEM). Also, the Vickers microhardness tester was used to measure the coatings hardness in both studies. Furthermore, the tribological performance of

coatings developed in both studies was conducted with a reciprocating tribometer using a ball-on-flat configuration and wear profiles were measured using confocal laser microscopy. Ex-situ characterization of the worn coatings was performed using a scanning electron microscope (SEM), energy-dispersive X-ray spectroscopy (EDS), and Raman spectroscopy. In the first study, APS coatings showed lower wear rates at room temperature in comparison to high temperature sliding. With regards to the second study, cold sprayed copper coatings showed a better wear resistance compared to the HVAF copper coatings.

Keywords: APS. HVAF. Cold spray. Cu-Ni coating. Cu coating. Friction. Wear. RT. Elevated temperature

Acknowledgement

My sincere and profound gratitude goes to my supervisors, Dr. Pantcho Stoyanov, and Dr. Christian Moreau for their guidance, encouragement, and motivation through this project work. I'm extremely grateful for the opportunity they provided me to carry out this exciting project. I would also like to appreciate the contributions of Rakesh B Nair, Yinyin Zhang, Mostafa Fotoohinezhadkhales, Ali Akbarnozari, and Golnoush Asadiankouhidehkordi for their valuable collaboration and reviews on this research work.

A special thanks to all members of the Thermal Spray Laboratory and tribology group for their support, suggestions and productive discussions during the research work. I would also like to thank Dr. Fadhel Ben Ettouil and Dr. Dmytro Kevorkov for their assistance in the experimental aspect of this project.

Thanks to Concordia University for providing a conducive environment and resources to carry out this research in a seamless manner

Finally, I would like to express my gratitude to Parents and siblings for their support throughout this project. To my amazing wife, thank you for your support, prayers, love, and care throughout this journey.

Dedication

To my lovely, supportive, caring and amazing wife, Damilola

Contribution of Authors

This thesis consists of peer-reviewed and under-review research articles. All the manuscripts were written by me as the first author and my supervisors, Dr. Pantcho Stoyanov and Dr. Christian Moreau in collaboration with others as co-authors. The major aspects of the experimental work were performed by me as the principal author and the supervisors provided technical guidance over the project. I acknowledge the contribution of each co-authors towards the successful production of the articles.

- Chapter 3: Asuquo, M.; Nair, R.; Fotoohinezhadkhales, M.; Akbarnozari, A.; Stoyanov, P.; Moreau, C. Tribological behavior of atmospheric plasma sprayed Cu-Ni coatings. Submitted to Journal of Thermal Spray Technology.
  - Asuquo M was responsible for conceptualization, experimentations, analysis of the results, and writing of the original manuscript draft. Nair R was responsible for the critical review of the manuscript. Fotoohinezhadkhales M was responsible for data analysis. Akbarnozari A was responsible for data analysis and critical review of the manuscript. Stoyanov P and Moreau C were responsible for the conceptualization, supervision, data analysis, and critical review of the manuscript.
- Chapter 4: Asuquo, M.; Zhang, Y; Asadiankouhidehkordi, G.; Fotoohinezhadkhales, M.; Moreau, C.; Stoyanov, P. Influence of solid-state deposition processes on the tribological behavior of copper coatings. To be submitted.
  - Asuquo M was responsible for conceptualization, experimentations, analysis of the results, and writing of the original manuscript draft. Zhang Y was responsible for the critical review of the manuscript. Asadiankouhidehkordi G was responsible for providing coated samples for experimental work. Fotoohinezhadkhales M was responsible for data analysis. Moreau C and Stoyanov P were responsible for the conceptualization, supervision, data analysis, and critical review of the manuscript.

Table of Contents

List of Figures

List of Tables

Abbreviations

COF – Coefficient of friction

SEM – Scanning electron microscope

EDS – Electron dispersive spectroscopy

XRD – X-ray diffraction

APS – Atmospheric Plasma Spraying

HVAF – High velocity air fuel

CS – Cold spraying

RT – Room temperature

CuNi – Copper nickel

Cu – Copper

Organization of thesis

i. Chapter 1 presents the introduction as well as the motivation, and scope of the thesis.

ii. Chapter 2 provides background information on thermal spraying and different deposition methods. Also, characteristics of thermal spray coatings along with copper-based tribological coatings are presented.

iii. Chapter 3 presents the tribological behavior of atmospheric plasma sprayed Cu-Ni coatings.

iv. Chapter 4 presents the Influence of solid-state deposition processes on the tribological behavior of copper coatings.

v. Chapter 5 outlines the main conclusions and potential future works of this thesis

Chapter
1. INTRODUCTION AND SCOPE

In this chapter…

the introduction, motivation, and scope of the thesis are presented.

1.1 Introduction

Surface modification of materials is crucial to the durability and efficiency of components for different applications such as aerospace engineering, automotive, chemical, biomedical, nuclear industries, electronics cooling, household appliances, boiling heat transfer, etc. [1]. Various surface modification techniques are usually applied to improve the functionality of materials for different applications. These techniques include electrochemical deposition, reactive sputtering, thermal evaporation, electron beam evaporation, thermal spraying, etc. [1]. However, thermal spraying is essentially a more effective and feasible process in comparison to the other surface modification processes, due to its low cost, high scalability, and involvement of a single step [1]. Indeed, an estimate of 2 billion euros at the beginning of the XXI century was made for the entire thermal spraying market. This grew to 7.4 billion US$ (which is equivalent to 6.6 billion euros) in 2018 and a further projection of about 13,5 billion US$ (12 billion euros) has been made for 2026 [2]. Thermal spraying methods are used to produce functional coatings with improved tribological performance as well as higher corrosion and oxidation resistance. They are environmentally friendly protective coatings with improved fuel efficiency, when used for gas turbine applications, as they also have less impact on the environment than other surface modification techniques [3].

Aerospace components are faced with harsh conditions during operation. Thus, high-performance alloys such as Ti-6Al-4V, are conventionally used for structural sections of aircraft. This is due to their high specific strength, low density, corrosion, and oxidation resistance [4]. However, these alloys face limitations regarding their usage, such as poor thermal conductivity, high coefficient of friction, and low hardness and they are easily affected by fretting fatigue failure [4]. Fretting wear is the most predominant failure in aerospace parts, resulting in fatigue crack initiation and subsequently reduction in the lifetime of components. Typically, fretting failure occurs between the compressor blade dovetail and the fan. The existence of normal pressure between contacting surfaces results in relative slip, which creates a fretting wear condition [5]. Thermal spray techniques such as APS are applied to alleviate the problem of fretting failure in titanium alloys by improving their fretting wear resistance and reducing the coefficient of friction of the titanium alloy parts.

Copper is known to have good ductility as well as remarkable thermal, electrical, and formability properties, to be applied as coatings on different substrate materials for various applications such as aerospace, power, automotive, nano-devices, and metallurgical industries [6]. Also, Cu-based coatings can be used in other industries for medical applications to serve

as antimicrobial materials, thermal conductors, corrosion, antifriction, wear-resistant materials, and cost-effective electrical contact materials [7]. Copper-based coating such as copper-nickel coating is a good candidate for protecting wear between two component interfaces such as titanium alloy parts in gas turbine engines, thereby reducing material removal by fretting, adhesion, galling, and cavitation. This coating combination can also reduce the coefficient of friction of titanium alloy parts. Cu-based coatings can be used as an anti-fretting coating that protects the contact area of the dovetail part of the compressor blade root from fretting fatigue failure. This is because copper-based coatings like CuNiIn have good plastic deformation ability and toughness [5,8,9]. In addition, these materials exhibit good corrosion resistance, lubricity, non-magnetic, and are excellent for machining [10].

Cu-based coatings utilized in tribological interfaces of gas turbine engines are fabricated by conventional thermal spray methods such as atmospheric plasma spray (APS) and high-velocity oxygen fuel (HVOF). However, these high-temperature deposition techniques produce coatings with high oxidation levels and enhanced porosity, resulting in poor wear performance of coatings. While a significant amount of work has previously been performed on copper-based coatings, there are a limited number of studies addressing the influence of substrate materials as well as assessing low-temperature deposition processes for copper-based coatings in tribological systems.

1.2 Thesis Objectives

The main goal of this thesis is to develop and critically evaluate next-generation copper-based tribological coatings for extreme environments. The sub-objectives of this thesis are stated below:

1. Development of APS-CuNi coatings on different substrate materials to investigate the influence of the substrate materials as well as the tribological performance of the coatings at various temperatures (room and elevated temperature).

2. The evaluation of copper coatings by low temperature deposition processes (HVAF and Cold spray) to understand their microstructural, mechanical and tribological behavior (room and elevated temperature).

References

1. Atul Ranjan, Aminul Islam, Manabendra Pathak, Mohd Kaleem Khan, and Anup Kumar Keshri. Plasma sprayed copper coatings for improved surface and mechanical properties. Vacuum 168 (2019) 108834. https://doi.org/10.1016/j.vacuum.2019.108834

2. Leszek Latka, Lech Pawlowski, Marcin Winnicki, Pawel Sokolowski, Aleksandra Malachowska, and Stefan Kozerski. Review of Functionally Graded Thermal Sprayed Coatings. Applied Sciences (2020) 10, 5153. https://doi.org/10.3390/app1015513

3. V. Viswanathan, Nirmal Kumar Katiyar, Gaurav Goal, Allan Matthews and Saurav Goal. Role of thermal spray in combating climate change. Emergent materials (2021) 4:1515-1529. https://doi.org/10.1007/s42247-021-00307-1

4. Amin Ma, Daoxin Liu, Xiaohua Zhang, Guangyu He, Dan Liu, Chengsong Liu, and Xingchen Xu. The fretting fatigue performance of Ti-6Al-4V alloy influenced by microstructure of CuNiLn coating prepared via thermal spraying. Tribology International 145 (2020) 106156. https://doi.org/10.1016/j.triboint.2019.106156

5. Yong-Sheng Xhu, Xiao-Tao Luo, Yin-Qiu Sun, Yuan Ren, and Chang-Jiu Li. Atmospheric plasma-spayed CuNiInB coatings of high fretting wear performance enabled by oxide-free metallic droplet deposition. Surface and Coatings Technology 464 (2023) 129537. https://doi.org/10.1016/j.surfcoat.2023.129537.

6. Vineeth Menon, Clodualdo Aranas Jr., and Gobinda Saha. Cold Spray Additive Manufacturing of Copper-Based Materials: Review and Future Directions. Materials Science in Additive Manufacturing (2022), 1(2): 1-20. https://doi.org/10.18063/msam.v1i2.12

7. Mohamed Ibrahim, Mohammed Abdul Samad, Khaled Al-Athel, Abul Fazal Arif, and Nasirudeen Olalekan. Evaluation of Tribological Properties of Thermally Sprayed Copper and Copper Alloy Coatings. Arabian Journal for Science and Engineering (2018) 43:4899-4910. https://doi.org/10.1007/s13369-018-3222-2.

8. Shujuan Dong, Yihui Wang, Jinyan Zeng, Xiong Yang, Panpan Liang, Dezheng Wang, Huiqi Liao, and Hanlin Liao. Performance of plasma sprayed CuNiIn coatings and Mo Coatings subjected to fretting fatigue. Nano Materials Science 2 (2020) 140 -150. https://doi.org/10.1016/j.nanoms.2019.07.003.

9. Righton Blackburns (Aerospace and Defence). www.rightonblackburns.co.uk.

10. J.K. Xiao, W. Zhang, L.M. Liu, X.P. Gan, K.C. Zhou, and C. Zhang. Microstructure and tribological properties of plasma sprayed Cu-15Ni-8Sn coatings, surface coating technology. 337 (2018) 159 -167. https://doi.org/10.1016/j.surfcoat.2018.01.016.

Chapter
2. BACKGROUND INFORMATION AND LITERATURE REVIEW

In this chapter…

A brief introduction to thermal spray technology and different deposition techniques is presented. Also, the characteristics of thermal spray coatings and the tribology of copper-based coatings are discussed.

2.0 Thermal Spray Technology

The first thermal spray device for flame generation was developed by Schoop, which was based on melting wire to produce coatings. After this stage, the metalizing process was improved, which led to the introduction of another technique called electric arc for high-melting material application [1]. Based on the historical and technological developments of thermal spray coating methods and their prospects, there is a clear indication of advancements and progressive trajectory paths it offers due to its expanded potential application range. Max Ulrich Schoop (Zurich, Switzerland) during 1882-1889 [1], developed the earliest patent on thermal spray. The feeding of lead and tin wires into a modified oxyacetylene welding torch was well explained by this patent. Later on, advancements in the torches were made to accept feedstock in the form of powder, before extending to spraying powders in a hot expanding jet flow [2].

A group of processes used to deposit layers of metallic or non-metallic materials on a prepared substrate surface is referred to as thermal spraying. In this technique, feedstock material such as powder, ceramic rod, wire, etc., is heated or melted full or partially by a concentrated heat source such as gases, an electric arc, or plasma, etc., and with the help of a process jet, the molten particles (fully or partially) is transported towards a prepared substrate material. When the feedstock material hits the surface of the substrate, it solidifies rapidly into splats build-up, consequently forming a coating [3]. Figure 2.1 displays the generic schematic illustration of the thermal spray coating process development. With thermal spray technology, it is possible to spray feedstock materials such as metals and their alloys, ceramics (oxides and carbides), polymers, composites of metal, and alloys etc. Also, the substrate material can be made of metals and alloys, ceramics, polymers, etc. [4]. Figure 2.2 shows the coating formation through the successive build-up of individual splats formed via the impact of the particles/molten droplets on the substrate surface. The properties of the individual splats depend on several factors such velocity and temperature of the particles/droplets before impact on the substrate. The angle of projection of the particles/droplets on the substrate, the chemistry of the coating environment, the substrate temperature and its preparation. Defects in coating formation can arise due to non-melted or partially melted particles, oxidized particles, and the formation of voids/pores due to improper spreading of the splats, which can affect the properties and performance of the coating [5]. Proper substrate preparation is essential to have quality coatings, as the adhesion of the coating to the substrate is related to its roughness, cleanliness, and good machining of the substrate. Depending on the level of accuracy and repeatability of

the final product that is required, thermal spray coatings can be done manually, in semi-automatic and robotic mode. Also, coating thickness ranging from 25μm to 2.5mm can be obtained, depending on the component or system [6].

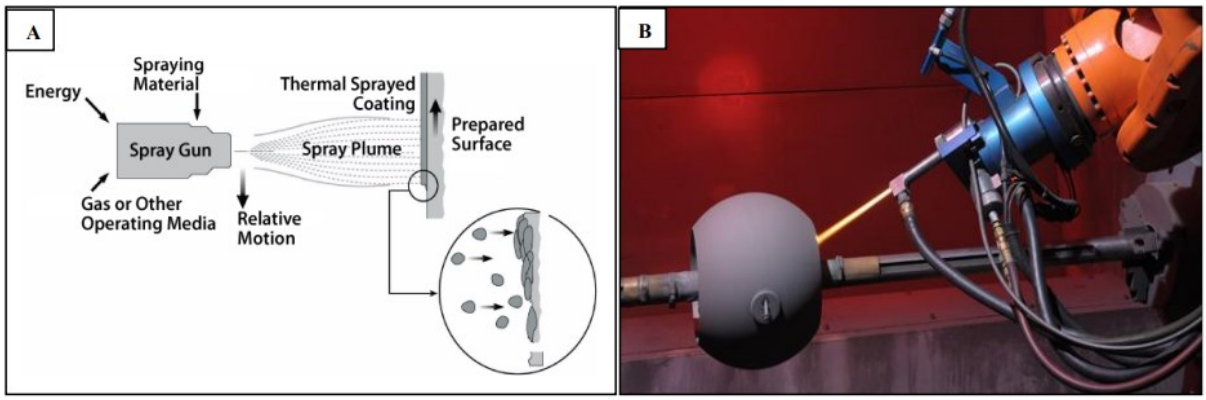

Figure 2.1 (A) General schematic diagram of thermal spray coating processes and (B) The set-up of thermal spray [7].

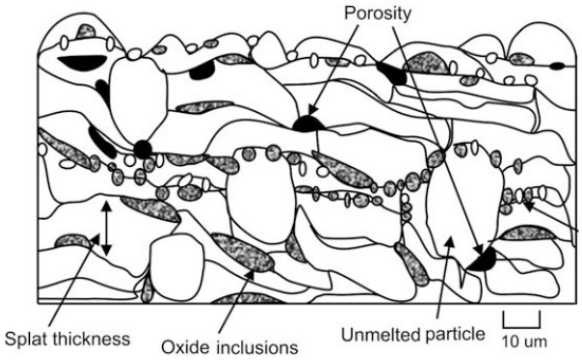

Figure 1.2 Schematic illustration of the coating build-up mechanism through the compilation of successive splat formation [5].

Thermal spray processes offer advantages such as the possibility to use a wide range of materials for developing coatings, as long as the material can melt without decomposing. Also, a coating can be done on a substrate without heating it significantly, providing the likelihood of coating high melting points materials on a substrate without thermal distorting and changing the properties of the substrate. However, the gun or torch of these processes is limited to depositing only what it can see (line-of-sight nature). In addition, there are size limitations that prohibit the deposition of small and deep cavities [7].

2.1 Thermal Spray Methods

The thermal spray coating process is divided into three broad categories 1) The application of chemical energy and combustion heat sources: consisting of the flame spray, detonation gun, High-velocity oxygen fuel spray (HVOF), High-velocity air fuel (HVAF) 2) The application of electrical energy for melting of consumable feedstock materials: namely Plasma and wire arc process. 3) The latest addition to the thermal spray family is the cold spray also known as the kinetic spray, utilizing the energy from the expansion of gas. Figure 2.3 describes an overview of different thermal spray processes.

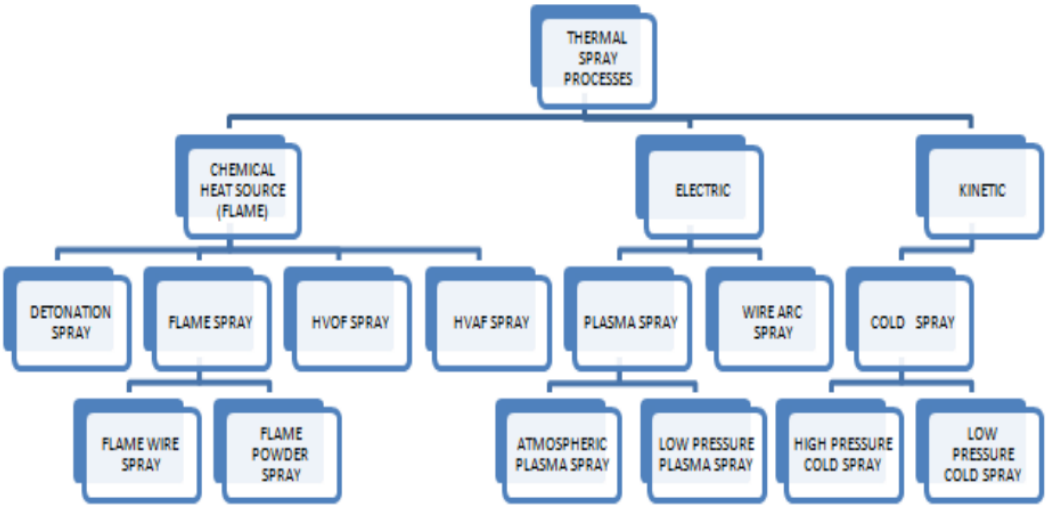

Figure 2.3 Classification of various thermal spray coating processes [8]

The copper-based coatings developed in this thesis were via atmospheric plasma spray (APS), High-Velocity Air Fuel (HVAF) and Cold spray (CS). Hence, these deposition techniques are discussed in the following sub-sections.

2.1.1 Atmospheric Plasma Spraying (APS)

Atmospheric plasma spray is a common thermal spray coating technique. The first patents attributed to the design of this method were made at the beginning of the 1960s [4]. In this technique, an electric arc is ignited between the copper anode and the thoriated tungsten cathode, resulting in ionization, heating, and expansion of plasma gases to form a plasma jet. Then, with the help of carrier gas, feedstock particles are transported to the hot stream of the plasma jet, to be subjected to heating and acceleration by drag force. With this acceleration, the molten particles hit the substrate with relatively high kinetic energy to form splats, which

solidify to form a coating build-up [4]. The working gas composition of this process consists of 1) Primary gas such as Argon (Ar) and sometimes Nitrogen (N_2), whose function is to stabilize the arc inside the torch nozzle. 2) secondary gases such as Hydrogen and helium, which function to increase the heat conductivity of the plasma [2,9]. Other essential spray parameters for this process include electric power, plasma gas flow rates, feed rate of the powder as well as its size distribution (20 – 90 microns), and the relative speed of the plasma torch with regards to the substrates [4]. The typical commercial plasma torches available include low-power one-cathode torches which can operate up to 80 kW such as SG100 (Praxair, Indianapolis, IN, USA) or F4 (Oerlikon Metco, Pfaffikon, Switzerland), etc., The high-power torches which operate with an electric power input up to 200 kW such as Plazjet (Praxair, Indianapolis, IN, USA), Axial-III (Northwest Mettech, Surrey, BC, Canada), etc. [4]. Typical powders sprayed by the APS technique include the oxide ceramics, metals and their alloys, carbides, nitrides, cermet, and borides, etc. The schematic diagram of a plasma spray method is depicted in Figure 2.4. The open discharge mode of this process can result in partial oxidation of metallic particles and oxidation-sensitive ceramics. This is due to the modification of the jet structure and temperature level to which the coating materials are exposed, arising from the incorporation, and mixing of ambient air with the plasma jet [5]. However, APS offers an economic advantage as well as freedom of shape and dimensions of parts to be sprayed in an open discharge mode. This coating technique can be used to prepare dense and uniform coating for various applications. Also, there is flexibility in choosing the substrate and coating materials, as they can both be of the same materials such as copper on copper or of different materials. With this, the properties of surfaces produced can be tailored for different applications such as wear-resistant, antifriction materials, thermal barrier coating, etc. [3].

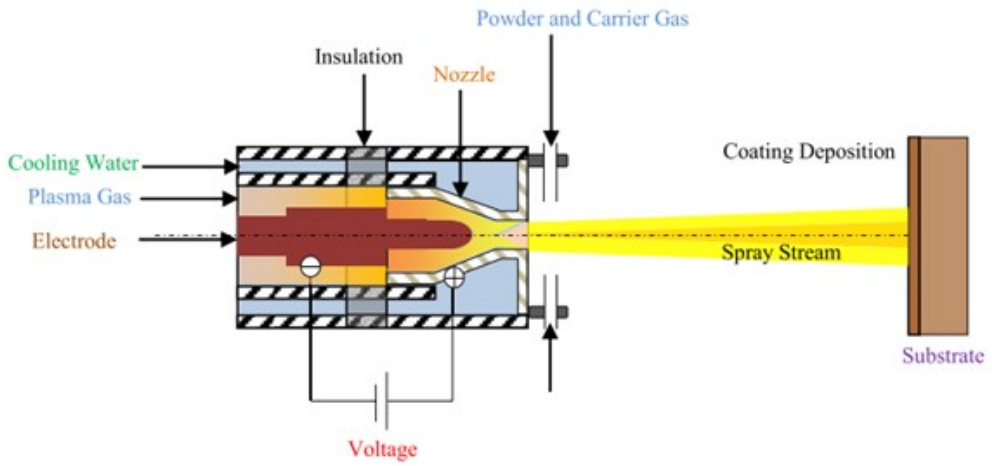

Figure 2.4 Schematic of plasma gun [3].

2.1.2 High-Velocity Air Fuel (HVAF)

This is a relatively new thermal spray technique in comparison to the conventional and established high-velocity oxygen fuel (HVOF). Coatings obtained from this technique are suitable for wear-resistant alloys and cermet-based applications. For instance, nickel-based coatings deposited steel material for hydro turbines and boiler applications [10]. In this process, gaseous fuel such as propylene, propane, or natural gas is mixed with compressed air in a premixing chamber, after which the mixture is ignited in front of a ceramic plate. This reaction creates a high-temperature and high-pressure gas in the combustion chamber, which heats and accelerates the powder injected in the system by nitrogen gas, resulting in the acceleration of the gas flow at supersonic speeds via a divergent nozzle. After which the molten and semi-molten powder particles are deposited on the substrate material, to produce a protective coating [10]. The use of compressed air instead of oxygen (as in the case of HVOF), helps to reduce flame and particle temperatures, which in turn reduces fine particle oxidation during spraying. This technique also produces coatings with high deposition efficiency, highly dense, low porosity, higher particle velocities, and superior wear performance [10]. Figure 2.5 shows the schematic of a high-velocity air fuel (HVAF) system.

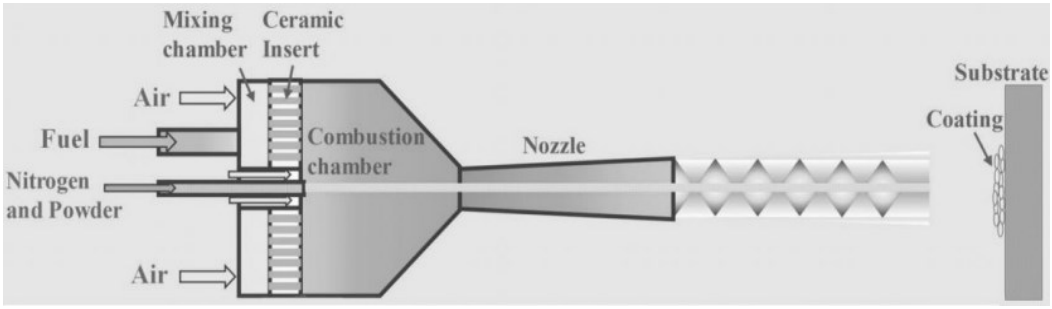

Figure 2.5 shows the schematic of a high-velocity air fuel (HVAF) system [10]

2.1.3 Cold spray

The cold spray process was first demonstrated in the mid-1980s by Dr. Antolli Papyrin and colleagues at the Russian academy of science [11]. The cold spraying method is a low-temperature process with high particle velocities. It is a solid-state process that utilizes a supersonic particulate jet rather than a molten droplet jet of conventional thermal spray coatings. In this coating method, the process gas is preheated (for compensation of adiabatic

cooling due to expansion) at a temperature (300 - 800°C) lower than the melting temperature of the feedstock and fed into a converging-diverging de Laval nozzle to form a supersonic gas jet, while also reducing process gas consumption. Spray powder is introduced into the gas jet by a carrier gas such as compressed air, helium, or nitrogen, resulting in a supersonic particle jet. The gas and feedstock material is accelerated and cooled down at the divergent section of the nozzle, exiting the spray gun nozzle at a lower temperature, even less than room temperature. Plastic deformation of feedstock particles which occurs due to the high kinetic energy of the particles upon impact on the substrate materials enables the formation of interlinking splats, resulting in a coating, as the coating depends on the velocity of spray particles upon impact [6,12]. A high velocity of about 300 – 1,200 m/s is developed with the converging/diverging nozzle to transport feedstock particles on the substrate [11]. Adhesion of particles on the substrate only occurs if the impact velocity is above a critical value, within a range of 500 to 900 m/s [5]. Fine feedstock powders with a size range of 1 to 50 μm are more effective for the cold-spray system in comparison to other types. Feedstock particles arrive on the substrate in a solid state, below their melting point, as the particles are exposed to the hot process gas for a short period of time inside the spray gun after injection and before the expansion of the gas jet at the diverging portion of the nozzle [13]. Deposition efficiencies as high as 70% can be achieved with cold spray with a spray rate of 3-5 kg/h. Ductile metals are most suitable for spraying with this system. Examples include Ag, Zn, Ti, Al, Cu, Nb, Mo etc. Alloys such as Ni-Cr and Cu-Al can also be sprayed [5]. The initial pressure of the working gas enables the division cold spray technique into (1) high-pressure cold spray HPCS (gas pressure > 1 MPa) and (11) low-pressure cold spray LPCS (gas pressure < 1 MPa) [4]. The parameters influencing the quality of coatings produced by cold spray include density, size, temperature, and velocity [11]. The advantages of the cold spraying coating technique over coatings obtained from conventional thermal spray include reduced residual stress in the coating, development of high density and low porosity, reduction of oxidation, no powder melting, no grain growth, no phase changes, minimum thermal input to the substrate, high bond strength, etc. [14]. Figure 2.6 shows a diagrammatic illustration of the cold spray process.

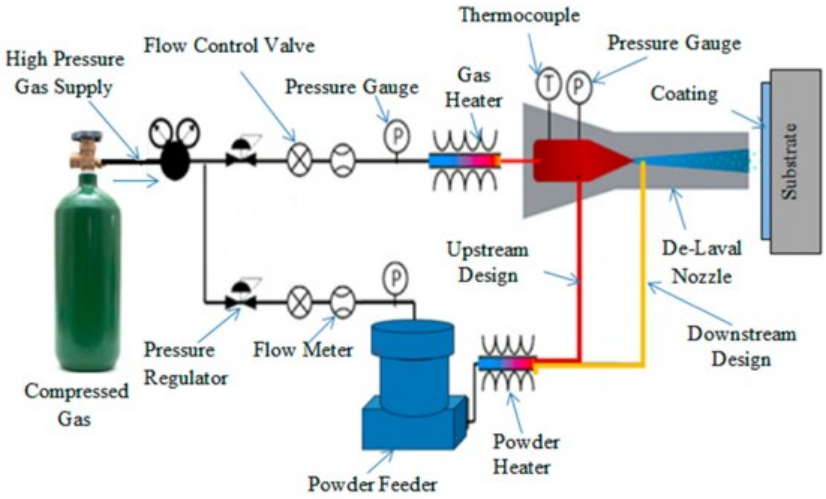

Figure 2.6 Schematic illustration of the cold spray process [1].

2.2 Characteristics of Thermal Spray Coatings

The different industrial applications of thermal spray coatings require certain functional requirements to be met for specific usage of these coatings. This chapter discusses key characteristics of thermal spray coatings in three groups, namely mechanical properties, microstructural characteristics and tribological behavior.

2.2.1 Mechanical Properties

The most important mechanical properties obtained from thermal spray coatings include microhardness, bond strength, elastic modulus, fracture toughness, etc. However, only microhardness is discussed as related to this thesis.

2.2.1.1 Microhardness

Hardness is not considered an intrinsic property of a material or a coating, rather it value is dependent on the method used for measurement and in terms of coatings, the direction where the test was performed, such as coating surface, cross-section parallel to splats or orthogonal to splats [5]. Therefore, it is referred to as the coating resistance to permanent deformation by penetration of an indentation [4,15]. Depending on the nature of the coating, the substrate may or not influence the hardness properties. For instance, the substrate may be influential for thin coatings, while coatings with a thickness of 250 µm or more render the influence of the substrate to be inconsequential [5]. Microhardness properties of coatings correlate well with abrasive and wear resistance. Common indenters used for measurements of hardness of thermal-sprayed coatings include Vickers, Knoop, Berkovitch, and conical (Rockwell test) indenters [4]. Atul et al. [3] reported an improvement in the hardness of copper coatings when the plasma power was increased from 20kW to 25kW. They reported an increase in plasma power helps to produce a completely melted feedstock particle, which easily spreads out to

form a better lamellar structure upon impact on the substrate with less porosity. The increase in plasma power also improves the oxidation of the coatings, which in turn increases the hardness. The increase in the percentage of Al_2O_3 added to cold-sprayed copper coatings, has been reported to slightly improve the microhardness of the coatings in comparison to pure copper cold-sprayed coating [12].

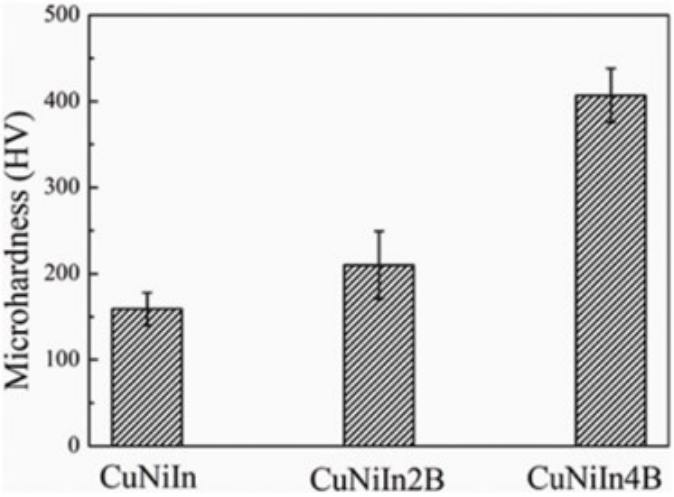

Figure 2.7 shows the improvement in the microhardness of CuNiIn coatings with the addition of boron (B), which acts as a deoxidizer to produce oxide-free CuNiIn [16]

2.2.2 Microstructure of coatings

Some important characteristics of coatings include thickness, porosity, and oxide content of the coatings, etc. In thermal spray, thickness ranging from a few micrometers up to a few millimeters can be obtained for coatings produced, depending on the spray coating method. The introduction of certain thermal energy to the structure of the coatings brought up by subsequent spray passes, is in alignment with thickness, residual stresses, and bond strength [4]. Also, these characteristics are determined by splat morphology, interfacial strength of splat-splat interface, and splat-substrate interface [17]. For instance, PS-CuNiIn coating was reported to have a well-flattened laminar feature in comparison to HVOF-CuNiIn coating [18]. This is because the flight speed for the plasma process was lower, creating a longer residence time for the heat transfer between the CuNiIn feedstock and the high-temperature plasma. This results in a fully melted powder particle and upon impact on the substrate, a flattened laminar structure is formed. In terms of oxide inclusions, thermal spraying of metallic coatings exposes feedstock material to oxidation due to particle and atmospheric interaction as well as heating

of the process gas with spray particles, such as the APS process. Longer exposure times of particles and higher particle temperatures improve the thickness of the oxide on the particles which results in to increase in the concentration of oxide stringers within the coating, with a characteristic dark phase in the coating cross-section [11]. However, several studies have reported the improvement of the hardness of coatings as the dispersion of oxide inclusion increases [3,11,19,20,21], as oxides have a hardness that exceeds 1,000 DPH [11], higher than the metallic particles. As a result of this, metal and metal oxides produce a higher microhardness in comparison to just the metal coating itself. However, in some cases, the increase in the content of oxides can result in brittle coatings, affect the splat-to-splat cohesion, and lower the strength, toughness, machinability, and corrosion resistance properties of coating [11]. The presence of pores in coatings affects the thermal and mechanical properties of the produced coatings as well as the creation of poor coating cohesion. As an important microstructural feature of thermal spray coating, porosity is referred to as turbulent processes of flattening and solidification of impacting molten droplets [15]. The various causes of porosities include (1) entrapment of a large number of unmelted, partially melted, or resolidified particles in a coating, resulting in the formation of voids (2) Porosities arising from the inherent feedstock powder manufacturing process (3) inter-splat or intra-splat cracking (4) Shrinkage of material on cooling from the liquid state (5) Poor wettability between adjacent surfaces or flattening droplets to the splats solidified underneath [11]. The most common measuring technique used to quantify porosity is the image analysis (IA) method. Other methods include electrochemical tests, ultrasound, gas pycnometry (Helium pycnometry), mercury intrusion porosimetry (MIP), water absorption/immersion (Archimedes method), etc. [15].

2.2.3 Tribology Behavior

Tribology is the science and engineering of interacting surfaces in relative motion. It deals with the study and application of principles of friction, lubrication, and wear. The term tribology became mainstream after the Jost report was published in 1966, where it highlighted the impact of the cost of friction, wear, and corrosion on the United Kingdom economy. Effects of wear, friction, and heat cannot be completely eradicated, though they can be minimized [22,23]. With the knowledge of the tribological behavior of materials, the amount of energy that is required to overcome the friction between two moving parts can be reduced, as friction requires 20% of all energy used globally [24]. In addition, a good understanding of interacting surfaces is essential for the long-term reliability of components, economic viability, and optimal

functioning of machine component systems as well as reduction in additional operational expenditures [24, 25]. The resistance force that occurs between two surfaces in contact during sliding is referred to as friction. In tribological characterization, the coefficient of friction (COF) is a quantitative parameter that defines the frictional behavior of the investigated material. The coefficient of friction for all coatings characterized is normally obtained at the steady state region without considering the run-in stage of the material. This is because the run-in phase does not give a true representation of friction, as the contact is not stable at this point. On the other hand, the progressive loss of material from mating surfaces in relative motion during the sliding process due to mechanical and/or chemical action is referred to as wear. Wear initiates dimensional alteration of components, affecting the operating efficiency and resulting in misalignments and vibration [26]. Friction and wear behavior tends to dissipate energy and deteriorate materials during relative motion. Wear resistance as well as the thickness of the material is crucial to the determination of the lifespan of coatings, this can get to 10 mm with PTA coatings [gt5]. The tribology behavior of coating material is not an intrinsic property, rather they depend on processing conditions, operating parameters (applied load, sliding velocity, and sliding distance), characteristics of the coating material, contact condition, etc. [27]. The most common wear mechanisms include adhesive, abrasive, and erosive wear. Others include cavitation erosion, corrosion, fatigue, fretting, and impact wear [4]. Abrasive wear occurs when a hard particle slides against a softer coating surface resulting in material loss due to cutting or deformation. This is represented by grooves, pits, and scores [5,17]. Erosive wear occurs due to solid particles moving at a high speed carried by a fluid, striking the surface of the coating, resulting in the degradation of material/surface damage [5,17]. The degradation of coating materials due to the interaction of two surfaces in relation to motion, resulting in the transfer of particles from one surface to the other is referred to as adhesive wear. The transfer is normally from the weaker to the harder material [5,17]. The tribological performance of thermal spray coatings is normally investigated by a tribometer made with different configurations, such as pin on disc, pin on plate, and block on ring. As depicted in Figure 13a, the addition of tungsten of different wt.% to copper has been reported to improve the specific wear rate resistance of cold-sprayed copper-tungsten coatings [28]. Cu+Al2O3 cold sprayed coatings with different wt.% of Al2O3, have also been reported to have a superior wear resistance in comparison to pure copper coating [12]. Cu 4%Sn twin arc-sprayed coating was said to have a lower C.O.F in comparison to pure copper coating. The uniform and dense microstructure with splats that were well adhered to each other was reported to be the reason for the lower coefficient of friction behavior of the Cu4%Sn coating [29].

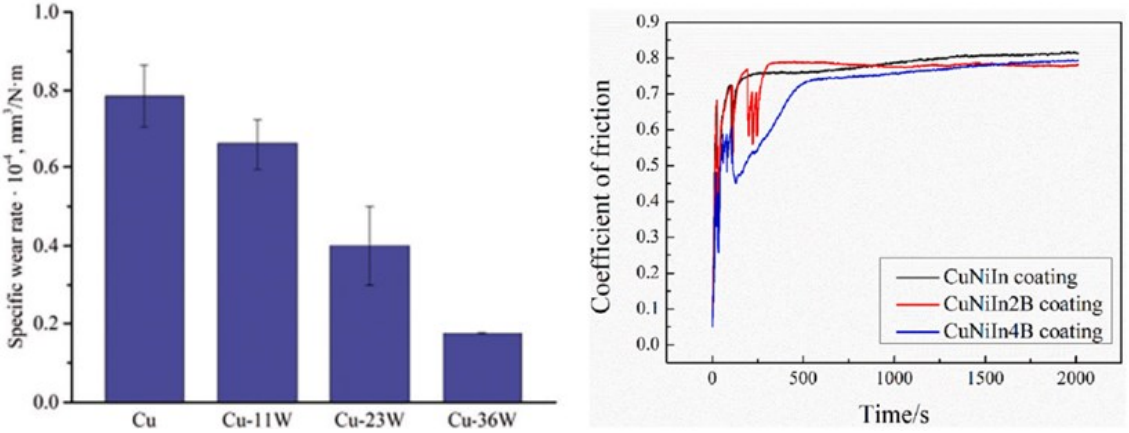

Figure 2.8a Specific wear rate of CuW coatings. **(b)** shows a lower coefficient of friction of CuNiInB compared to CuNiIn [28,16].

It is important to note that tribology investigation of materials under laboratory test configurations does not represent a perfect real condition for final decisions on materials. They are regarded as a helpful screening tool, as field tests and product validation are considered the final choice for the right material combination and essential step before introducing novel components into service [30, 31].

2.3 Copper-based tribological coatings

Thermally sprayed copper and copper alloy coatings are used as coating materials for a variety of applications. These include medical applications, thermal conductors, antimicrobial materials, corrosion, antifriction and wear-resistant materials [29]. The tribological performance of these coatings is connected with their composition, microstructure, and surface characteristics [32]. These coating materials are endowed with superior properties making them suitable for extreme environment applications such as gas turbine engines. Also, the tribological performance of copper-based materials can be enhanced to broaden their applications making them suitable for heavy loads or high sliding speeds functions by the incorporation of reinforcements and hard particles such MoS_2, SiC, Al_2O_3, graphene, Tio_2 etc [12,33]. For instance, the superior wear resistance of cold sprayed Cu + Al_2O_3 coating and plasma sprayed Cu + Al_2O_3 compared to copper coating has been reported [12,34]. Also, the reduction in friction and enhancement in wear resistance of cold sprayed copper-graphene compared to pure copper coatings has been previously reported [35]. Therefore, the mixture of copper-based powder with a proper content of reinforcements can further improve the plastic deformation of copper-based coatings and also enhance the tribological performance of the coatings. Concerning other copper-based materials, aluminum-bronze (CuAI) alloys are known

to have good friction reduction and corrosion resistance, making them suitable candidates for lead-free self-lubricating materials in marine applications [36]. Superior tribological performance of plasma-sprayed CuAl coatings under seawater conditions in comparison to pure water and dry sliding was reported by Jie et al. [37]. Also, CuNiIn coatings are commonly used to inhibit the fretting damage to titanium alloy engineering components of aircraft engines. Yang et al. [38] stated that CuNiIn coatings showed a high accommodation and cooperation capacity for plastic deformation when subjected to fretting conditions, indicating the ability to mitigate the stress concentration of the contact area and reduce the nucleation risk of the fretting fatigue cracks.

References

1. Santosh Kumar and Rakesh Kumar. Influence of Processing Conditions on the Properties of Thermal Sprayed Coating: A review. Surface Engineering, 2021, 37(11). https://doi.org/10.1080/02670844.2021.1967024

2. 4. David JR, Davis, Associates. Handbook of Thermal Spray Technology. Materials Park, OH: ASM International, 2004.

3. Atul Ranjan, Aminul Islam, Manabendra Pathak, Mohd Kaleem Khan, and Anup Kumar Keshri. Plasma sprayed copper coatings for improved surface and mechanical properties. Vacuum, 2019, 168 (108834). https://doi.org/10.1016/j.vacuum.2019.108834

4. Leszek Latka, Lech Pawlowski, Marcin Winnicki, Pawel Sokolowski, Aleksandra Malachowska, and Stefan Kozerski. Review of Functionally Graded Thermal Sprayed Coatings. Applied Sciences, 2020, 10 (5153). https://doi.org/10.3390/app1015513

5. Maher I. Boulos., Pierre L. Fauchais., and Joachim V.R. Herberlein. Thermal Spray Fundamentals. From powder to part, second edition, 2021. https://doi.org/10.1007/978-3-030-70672-2

6. R.J. Talib, S. Saad, M.R.M. Toff, and H. Hashim. Thermal spray coating technology – A review. Solid state science and technology, 2003, 11(1), p109-117.

7. Sagar Amin and Hemant Panchal. A Review on Thermal Spray Coating Processes. International Journal of Current Trends in Engineering and Research (IJCTER), 2016, 2(4), p 556 – 563.

8. Rakesh Kumar and Santosh Kumar. Thermal spray coating: A study. International Journal of Engineering Sciences and Research Technology, 2018, 7(3). https://doi.10.5281/zenodo.1207005

9. Pawlowski, L. The Science and Engineering of Thermal Spray Coatings, 2nd ed.; Wiley and Sons: Chichester, UK, 2008.

10. Yasemin Yildiran Avcu, Mert Guney, and Egemen Avcu. High-Velocity Air Fuel Coatings for Steel for Erosion-Resistant Applications. J.Electrochem. Sci. Eng, 2023, 13(2), p 407-420. https://dx.doi.org/10.5599/jese.1369

11. Jyotsna Dutta Majumdar. Thermal and Cold Spraying Technology in Manufacturing. Handbook of Manufacturing Engineering and Technology, 2013. https://doi.org/10.1007/978-1-4471-4976-7_31-2

12. Kostoula I. Triantou, Dimistris I. Pantelis, Vincent Guipont, and Michel Jeandin. Microstructure and tribological behavior of copper and composite copper + alumina cold sprayed coatings for various alumina contents. Wear, 2015, 336-337, p 96-107. https://dx.doi.org/10.1016/j.wear.2015.05.003.

13. M.F. Smith. Comparing Cold Spray with Thermal Spray Coating Technologies. Sandia National Laboratories, USA.

14. Julio Villafuerte. Morden Cold Spray, Materials, Process, and Applications. 2015. https://doi.org/10.1007/978-3-319-16772-5.

15. Andrew Siao Ming Ang and Christopher C. Berndt. A review of Testing Methods for Thermal Spray Coatings. International Materials Reviews, 2014, 59 (4). https://doi.org/10.1179/1743280414Y.0000000029

16. Yong-Sheng Zhu, Xiao-Tao Luo, Yin-Qiu Sun, Yuan Ren and Chang-Jiu Li. Atmospheric plasma-sprayed CuNiInB coatings of high fretting wear performance enabled by oxide-free metallic droplet deposition. Surface and Coatings Technology, 2023, 464(129537). https://doi.org/10.1016/j.surfcoat.2023.129537

17. Manish Roy. Surface Engineering for Enhanced Performance against Wear. 2012. https://doi.org/10.1007/978-3-7091-0101-8.

18. Righton Blackburns (Aerospace and Defence). www.rightonblackburns.co.uk.

19. Shujuan Dong, Yihui Wang, Jinyan Zeng, Xiong Yang, Panpan Liang, Dezheng Wang, Huiqi Liao, and Hanlin Liao. Performance of plasma sprayed CuNiIn coatings and Mo Coatings subjected to fretting fatigue. Nano Materials Science, 2020, 2, p140 -150. https://doi.org/10.1016/j.nanoms.2019.07.003.

20. Goudarzi Masoumeh, Saviz Shahrooz, Ghoranneviss Mahmood, and Salar Elahi Ahmad. Investigation of stand-off distance effect on structure, adhesion, and hardness of copper coatings obtained by the APS technique. Journal of Theoretical and Applied Physics, 2018, 12, p 85-91. https://doi.org/10.1007/s40094-018-0277-0.

21. Jin-Kun Xiao, Wei Zhang, Li-Ming Liu, Xue-Ping Gan, Ke-Chao Zhou, and Chao Zhang. Microstructure and tribological properties of plasma sprayed Cu-15Ni-8Sn coatings. Surface

and coatings technology, 2018, 337, p159 – 167. https://doi.org/10.1016/j.surfcoat.2018.01.016.

22. U.S Bongarde and V.D Shinde. Review on natural fiber reinforcement polymer composites. International journal of engineering science and innovative technology, 2014.

23. H.P Jost, Lubrication (Tribology) – a report on the present position and industry's needs, Department of Education and Science, H.M. stationary office, London, UK, 1966.

24. Maitham Mohammed Al-Asadi, Hamza A. Al-Tameemi. A review of tribological properties and deposition methods for selected hard protective coatings. Tribology International, 2022, 176(107919). https://doi.org/10.1016/j.triboint.2022.107919.

25. Temesgen Berhanu Yallew, Pradeep Kumar and Inderdeep Singh. Sliding wear properties of jute fabric reinforced polypropylene composites. Procedia Engineering, 2014, 97, p 402-411.

26. Rajdeep Paul, Krushna Gouda, and Sumit Bhowmik. Effect of different constraint on tribological behavior of natural fiber/filler reinforced polymeric composites: A review. Silicon, 2021, 13 p 2785-2807.

27. A. Shalwan and B.F Yousif. In state of art: Mechanical and tribological behavior of polymeric composites based on natural fibers. Materials and Design, 2013. p 14-24.

28. Vlasdislav S. Shikalov, Tomila M. Vidyuk, Artem A. Filippov, and Ivanna D. Kuchumova. Microstructure, mechanical and tribological properties of cold sprayed Cu-W coatings. International Journal of Refractory Metals and Hard Materials, 2022, 106 (105866). https://doi.org/10.1016/j.ijrmhm.2022.105866.

29. Mohamed Ibrahim, Mohammed Abdul Samad, Khaled Al-Athel, Abul Fazal Arif, and Nasirudeen Olalekan. Evaluation of Tribological Properties of Thermally Sprayed Copper and Copper Alloy Coatings. Arabian Journal for Science and Engineering, 2018, 43, p 4899-4910. https://doi.org/10.1007/s13369-018-3222-2.

30. Klaus Friedrich, Zhong Zhang and Alois K. Schlarb. Effects of various fillers on the sliding wear of polymer composites. Composites Science and Technology, 2005, 65, p 2329- 2343. https://doi.org/10.1016/j.compscitech.2005.05.028.

31. Mitchell R. Dorfman. Thermal Spray Coatings. Handbook of Environmental Degradation of Materials, 2018. https://doi.org/10.1016/B978-0-323-52472-8.00023-x.

32. Jin X, Gao L, Lui E, Yu F, Shu X and Wang H. Microstructure, corrosion and tribological and antibacterial properties of Ti-Cu coated stainless steel. J. Mech. Behav. Biomed. Mater., 2015, 5, p 23-32.

33. Beibei Chen, Jin Yang, Qing Zhang, Hong Huang, Hongping Li, Hua Tang and Changsheng Li. Tribological properties of copper-based composites with copper coated $NbSe_2$ and CNT. Materials and Design, 2015, 75, p 24-31. https://dx.doi.org/10.1016/j.matdes.2015.03.012

34. Kangwei Xu, Jiajia Tian, Shufeng Xie and Pin Wu. Facile Fabrication of Micron-Laminated Cu-Al_2O_3 Coating with Long-Lasting Antifouling Performance and Excellent Wear Resistance. Journal of Thermal Spray Technology,2023,32, p 2170-2186. https://doi.org/10.1007/s11666-023-01624-z

35. Jongbeom Choi, Nana Okimura, Takatoshi Yamada, Yuki Hirata, Naoto Ohtake and Hiroki Akasaka. Deposition of graphene-copper composite film by cold spray from particles with graphene grown on copper particles. Diamond and Related Materials, 2021, 116(108384). https://doi.org/10.1016/j.diamond.2021.108384

36. Rui Gao, Yanfei Huang, Xinuuan Zhou, Guozheng Ma, Guo Jin, Tianhao Li, Haidou Wang and Ming Liu. Material system and tribological mechanism of plasma sprayed wear resistant coatings: Overview. Surface and Coatings Technology, 2024, 483(130758). https://doi.org/10.1016/j.surfcoat.2024.130758

37. Jie Yang, Zhipeng Li, Guoliang Hou, Yulong An, Huidi Zhou and Jianmin Chen. Sliding friction and wear behaviors of plasma sprayed aluminum-bronze coating in artificial seawater. Surface and Interface Analysis, 2015, 47, p 390-397. https://doi.org/10.1002/sia.5724

38. Qi Yang, Welong Zhou, Xiabing Zheng, Zhqiang Niu, Zhiqiang Li, Bowel Zhou and Fu Xuesong. Investigation of shot peening combined with plasma-sprayed CuNiIn coating on the fretting fatigue behavior of Ti-6AI-4V dovetail joint specimens. Surface Coatings and Technology, 2019, 358, p 833-842.

Chapter 3. Tribological Behavior of Atmospheric Plasma Sprayed Cu-Ni Coatings

In this chapter…

The tribological studies of copper-nickel powder deposited on three different substrates by atmospheric plasma spray technique are provided. The tribological testing at varying temperatures and various characterization techniques were performed to understand the friction and wear behavior of the coatings.

3.1 Abstract

Atmospheric plasma-sprayed (APS) copper-nickel-based coatings are commonly used for the prevention of fretting wear of components in aerospace engines. In this study, Cu-Ni alloy was deposited using plasma spraying on different substrate materials such as stainless steel, carbon steel, and aluminum alloy to investigate the influence of the substrate materials as well as the performance (mechanical and tribological behavior) of the coatings. Microstructural studies revealed a homogeneous microstructure with the presence of splats for coatings deposited on each substrate. The porosity and microhardness of coatings deposited on each substrate were found to be within the range of (1.22±0.27-1.65±0.33%) and (117±10 –136±23 $HV_{0.05}$) respectively. The tribology results also showed an increase in the frictional coefficient for each substrate from 0.41 at 25° to 0.73 at 300°C, However, a steady state was not obtained at 450°C. Similarly, the wear rates of coatings for each substrate increased from 300°C to 450°C test conditions, with no significant wear obtained at 25°C. The results showed that the substrate materials had no significant effect on the performance of the coatings, as the thickness, porosity, surface roughness, and microhardness of coatings for each substrate material were comparable with no remarkable difference.

Keywords: APS. Cu-Ni coating. Friction. Wear. Transfer film. RT. Elevated temperature

3.2 Introduction

Copper-nickel alloys (Cu-Ni) have garnered significant attention across various industrial sectors, including electronic, marine, and aerospace [1-3]. Copper-nickel alloy exists as a binary system with a remarkable single solid solution phase because of the total solubility of copper and nickel in each other [4-6]. These alloys exhibit impressive attributes such as high strength and toughness, exceptional corrosion resistance, superior fretting wear resistance, and excellent thermal conductivity [1,3,4,7,8]. With a single-phase solid solution structure and outstanding solubility between constituents, Cu-Ni alloys excel in frontline applications, particularly in combating wear and corrosion [8-10].

While the exceptional properties of Cu-Ni alloys are highly regarded, their fabrication plays a crucial role in ensuring optimal performance against fretting wear [11-14]. Fretting wear is a form of wear that occurs at the contact interface between two surfaces undergoing slight relative motion or vibration under load, resulting in a reduction in the lifespan of components [15-17]. One such example of the fretting wear damage observed between the compressor blade dovetail and the fan, which undermines the safety and longevity of aero-engines [9,18,19]. A feasible approach to address fretting wear involves enhancing the surface properties of components by means of thermal spraying. Thermal spraying emerges as a viable surface modification technique to enhance the surface properties of Cu-Ni alloys [1,9,20]. Thermal spraying, acknowledged for its versatility, cost-effectiveness, and widespread industrial adoption, is extensively utilized in various sectors such as aerospace, turbines, and oil and gas due to its wide range of applications [21]. This process involves feeding feedstock material such as powder, wire, rod, or suspension into a spray torch, heating it to a molten or near-molten state, and then propelling it towards a base substrate material to create thick coatings [20-21]. Among thermal spray techniques, atmospheric plasma spraying (APS) CuNi coatings are commonly preferred due to their affordability and higher deposition efficiency [9,22].

Numerous studies have been conducted to explore the application of Cu-Ni alloys with various additional elements (such as Sn, In, etc.) using thermal spraying methods such as detonation gun spraying, high velocity oxy fuel (HVOF), cold spraying (CS), and atmospheric plasma spraying (APS) [1,9,10,13,22,23,24]. Cu-Ni alloy coatings produced through cold spraying have been utilized for corrosion resistance applications [25-26]. However, only a limited number of studies have focused on addressing fretting wear using Cu-Ni alloy coatings via APS. For instance, Xiao et al. [1] investigated the tribological characteristics of Cu-Ni alloy coatings with the addition of Sn (Cu-15Ni-8Sn) using APS on stainless steel substrates. The

authors observed delamination and spalling as the dominant wear mechanisms of the APS coating. In another study, Ma et al. [10] reported on the fretting wear behavior of Cu-Ni-In alloy coatings on Ti-6Al-4V substrates produced through APS and HVOF techniques. Their findings revealed that the CuNiIn coatings manufactured by means of APS exhibited a more pronounced lamellar microstructure and demonstrated superior fretting fatigue resistance. This outcome was attributed to the combined impact of the coatings high toughness and low microhardness, effectively impeding fatigue-crack initiation. Another study investigated by Shujuan et al. [22] reported the fretting wear mechanisms of CuNiIn coatings on Ti6Al4V and AI1050 substrates. Their study identified galling, third-body abrasive wear, and material transfer as the predominant fretting wear mechanisms in their investigation. Nevertheless, despite demonstrating the potential of APS Cu-Ni alloy coatings for tribological interfaces, evaluating their performance under extreme environmental conditions remains unexplored. Specifically, there is a significant gap in understanding Cu-Ni alloy coatings produced through APS without the addition of elements such as In and Sn. Additionally, the impact of producing APS-based Cu-Ni alloy coatings on different substrate materials and their influence on bonding and tribological performance at various temperatures (room temperature and elevated temperature) is also lacking.

In light of this, the present study aims to fabricate Cu-Ni alloy coatings through APS on different substrate materials, including carbon steel, stainless steel, and aluminum alloy. This investigation seeks to elucidate how different substrate materials affect the sliding wear performance of APS-based Cu-Ni alloy coatings at different temperatures (25°C, 300°C and 450°C). Cu-Ni feedstock was chosen to develop next-generation copper-based coatings suitable for tribological interfaces i.e. coatings with reduced coefficient of friction and enhanced wear resistance.

3.3 Experimental Details

3.3.1 Materials and Methodology

Commercially available Cu38Ni (Metco 57NS, Oerlikon Metco, USA) with a particle size distribution of -75 + 45 µm (as received from the manufacturer) was utilized as the feedstock for the deposition process. The substrates used in this study were medium carbon steel 1''× 1''× 0.19" (25.4mm × 25.4mm × 4.7mm), 304L stainless steel 1" × 1" × 0.19"(25.4mm × 25.4mm × 4.7mm), and Aluminium 6061-T6 alloy 1" × 1" × 0.26"(25.4mm × 25.4mm × 6.5mm). Prior to the spraying process, the substrates were grit blasted using #20 mesh alumina grit abrasive particles to improve the surface roughness as well as the adhesion of the coatings onto the substrates. The substrates were subsequently cleaned with compressed air to remove any sand residue from the sample surface. Prior to deposition, preheating was performed to reduce any residual stresses and improve bonding between the coating and the substrate. Preheating was conducted for five passes using the plasma gun without feedstock feeding. The substrate temperatures after preheating were measured to be 220°C for medium carbon steel, 245°C for stainless steel, and 265°C for aluminum alloy using the IR camera. Subsequently, the Cu-Ni alloy powder was introduced immediately after the preheating. The Cu-Ni feedstock powders are deposited to these substrates by employing 3-MB plasma spray gun (Oerlikon Metco, USA). Table 3.1 lists the spraying parameters used for the spray process. The powders from the Thermach Inc. AT-1200 powder feeder were injected into the plasma by radial injection. The torch velocity and stand-off distance were kept constant with the help of a fixed robot assembly (HP-20, Motoman Yaskawa Electric Corp, Waukegan, IL, USA) to avoid any inconsistency in the deposition process. Ten passes were used for the coating deposition and two coatings for each substrate were produced for each test. Argon and hydrogen were used as the primary and secondary gases respectively. The schematic of the spraying process is shown in Fig. 3.1.

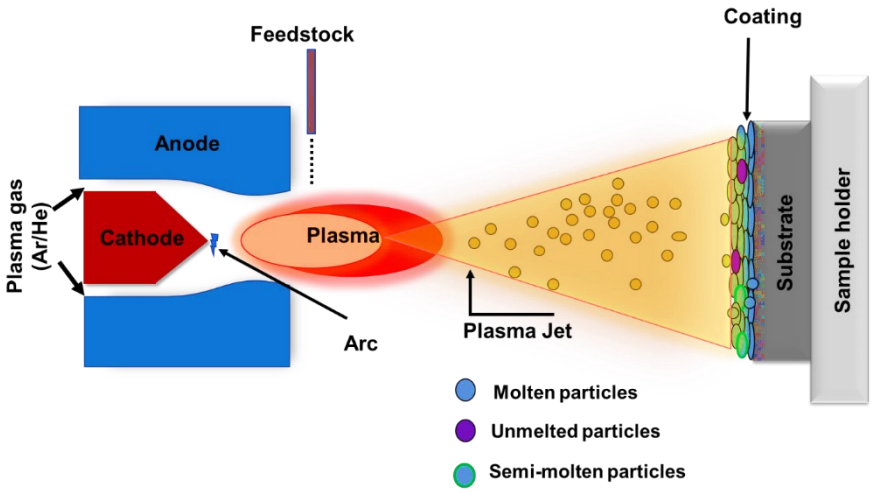

Figure 3.1 Schematic diagram of the atmospheric spray (APS) spraying process

Table 3.1 Atmospheric plasma spray parameters used for depositing Cu-Ni coatings

Parameters	Values
Primary gas flow Ar (nlpm)	36.6
Secondary gas flow H_2 (nlpm)	6.6
Current (A)	500
Voltage (V)	60
Power (kW)	30
Carrier gas flow (nlpm)	5.9
Feed rate (g/min)	35
Spray distance (mm)	64
Preheat passes	5
Number of spray passes	10
Gun linear speed (m/s)	1

3.3.2 Characterization

The feedstock powder was characterized by using scanning electron microscopy (SEM) (SU8230, Hitachi, Japan) to evaluate the morphology. The particle percentiles (d_{10}, d_{50}, and d_{90}) were analysed by using Spraytec (Malvern Instruments, UK) made with a wet dispersion (water) accessory to measure the particle size distribution of the Cu-Ni powder. The cross-section and top surface of the as-sprayed Cu-Ni coatings were analysed using the scanning electron microscope (SU8230, Hitachi, Japan). The cross-sectional surfaces were cold mounted using epoxy resin and dried for 24 hours. The samples were then ground down to 1200 grit emery sheets followed by diamond polishing as per the ASTM Standard E1920-03 [27]. Also, the chemical composition of the coatings was obtained using energy-dispersive X-ray spectroscopy (EDS). The coating thickness on each substrate was measured from the cross-sectional SEM images. Ten measurements were taken, and the average was reported as the coating thickness. To investigate the phase patterns of the spray powder and CuNi coatings, X-ray diffraction (XRD) analysis was performed using (X'pert, Malvern α , UK) with Cu-kα radiation (step size = 0.02°, λ = 1.54 Å, 2θ = 20°-90°). This was operated using a voltage of 45 kV and a current of 35 mA. The surface roughness of the as-sprayed coatings was measured

using a confocal laser microscope (Olympus LEXT 4000, Houston, USA). At least 10, measurements were taken for each coating and the average value as well as the standard mean error was reported. Image J analysis software was used to measure the porosity of the coatings. To ensure statistical repetition of results, fifteen high-magnified SEM images at 2.00K magnification of 20 µm scale bar on different locations of the as-sprayed coatings were taken according to ASTM E2109-01 standard [28]. The high magnification was chosen, to allow resolution of the voids and best fills the screen with the entire coating thickness. With this, inherent porosity (voids) can be clearly seen and are only measured. Defects such as oxides, artifacts (pullouts, smearing), embedded grit, and other unwanted features are not taken into consideration. The average value as well as the standard mean error was reported. Microhardness measurements were carried out on the polished cross-sectional coatings using a Vicker's microhardness tester (Anton Paar Micro combi tester-MCT^3, Switzerland). A Vickers diamond indenter was used for the testing with an applied load of 500g ($HV_{0.05}$) and a dwell time of 10 seconds. 10-point measurements were carried out to report an average microhardness value for each coating.

3.3.3 Wear Tests

Wear tests under dry sliding conditions were conducted with a reciprocating tribometer (Anton Paar, TriTec SA, Corcelles, NE, Switzerland) using a ball-on-flat configuration. Table 3.2 lists the parameters used for the wear test derived from previous studies in the same research group [29,30], which are based on the capability of the tribometer. The counterface material consisted of a 6.3 mm diameter Al_2O_3 ball, employed against the Cu-Ni coatings deposited on each substrate. The choice of alumina as the counter body for the sliding test is due to its high hardness of 1500 HV (verified by McMaster-Carr, USA) and superior wear resistance [31-33]. The relative humidity was maintained below 20% with the help of a desiccator. The wear testing was performed at a constant load of 5 N by varying the temperature conditions. i.e., (room temperature (RT), 300°C, and 450°C) to determine the influence of heating on the friction and wear performances. For the high-temperature test condition, the coatings were heated with the help of a furnace connected to the tribometer. After which the surface of the sample was measured with a pyrometer. It should be noted that the highest temperature used in this study is above the typical operating temperature for the aluminum-based substrate. However, it has been included in this study as a reference to the other substrates and to validate the testing procedure. The maximum linear speed of the sample during the reciprocating test

was 3.14 cm/s. All sliding wear tests performed for this study were conducted on unpolished coating samples. The rationale behind testing the as-sprayed coatings is to replicate real-world conditions without additional surface finishing processes. The methodology not only ensures the applicability of the results to practical conditions but also helps reduce the lead time and overall component costs. Three repetitions were performed on each coating, and the average value was reported as the average C.O.F. The depth of the wear tracks was measured using confocal laser microscopy (Olympus LEXT 4000, Houston, USA) to calculate the wear rates. About 30 profiles were analysed across the wear track and data obtained from this measurement was used to plot the wear depth profile as well as to obtain the wear area (mm^2) using the OriginLab software. Material pile-up from the wear profile was discarded during the calculation. The wear area (mm^2) was multiplied by the track length (mm) to obtain the wear volume (mm^3). The specific wear rate (k) (mm^3/N.m.) is calculated according to the wear equation below [34], by dividing the wear volume with applied load (N) and the total sliding distance (m).

$$K = \frac{V}{S.W} \tag{1}$$

where V is the total volume loss (mm^3), S is the Sliding distance (m), and W is the applied load (N). The wear tracks and counter balls were subsequently analysed using the field emission scanning electron microscope coupled with energy dispersive spectroscopy to investigate the wear mechanism of the coatings.

Table 3.2 Ball-on-flat reciprocating sliding test parameters

Parameters	Values
Frequency (Hz)	1
Applied load (N)	5
Stroke length (mm)	10
Velocity (cm/s)	3.14
Number of cycles	5000
Total sliding distance (m)	100
Temperature	RT, 300°C, 450°C
Counter ball	Al_2O_3 (Ø 6.35)

3.4 Results and Discussion

3.4.1 Feedstock material

Figure 3.2 shows the SEM morphology of the powder used for spraying. As seen in Fig. 3.2a, the FE-SEM micrograph of the copper-nickel feedstock obtained at 200 µm magnification, displays a spherical morphology with the presence of satellite. Gas-atomized powders are known to have this morphology [22]. Figure 3.2b shows the morphology of a single copper-nickel dense particle showing a dendritic nature. The particle size distribution of copper-nickel powder is shown in Fig. 3.2c. The d_{10}, d_{50} and d_{90} values obtained from this measurement are 52.1µm, 68.8µm, and 90.9µm respectively. EDS analysis was done on the powder to understand the elemental spread of the feedstock. As seen from Table 3.3, the presence of a small amount of oxide was obtained on the different points considered for the analysis which might be due to oxidation during the gas atomization of the powder. This further explains the inevitable oxidation of CuNi droplets in the plasma jet [9]. Figure 3.3 reveals a uniform distribution of elements of the powder feedstock when analysed with the EDS color mapping.

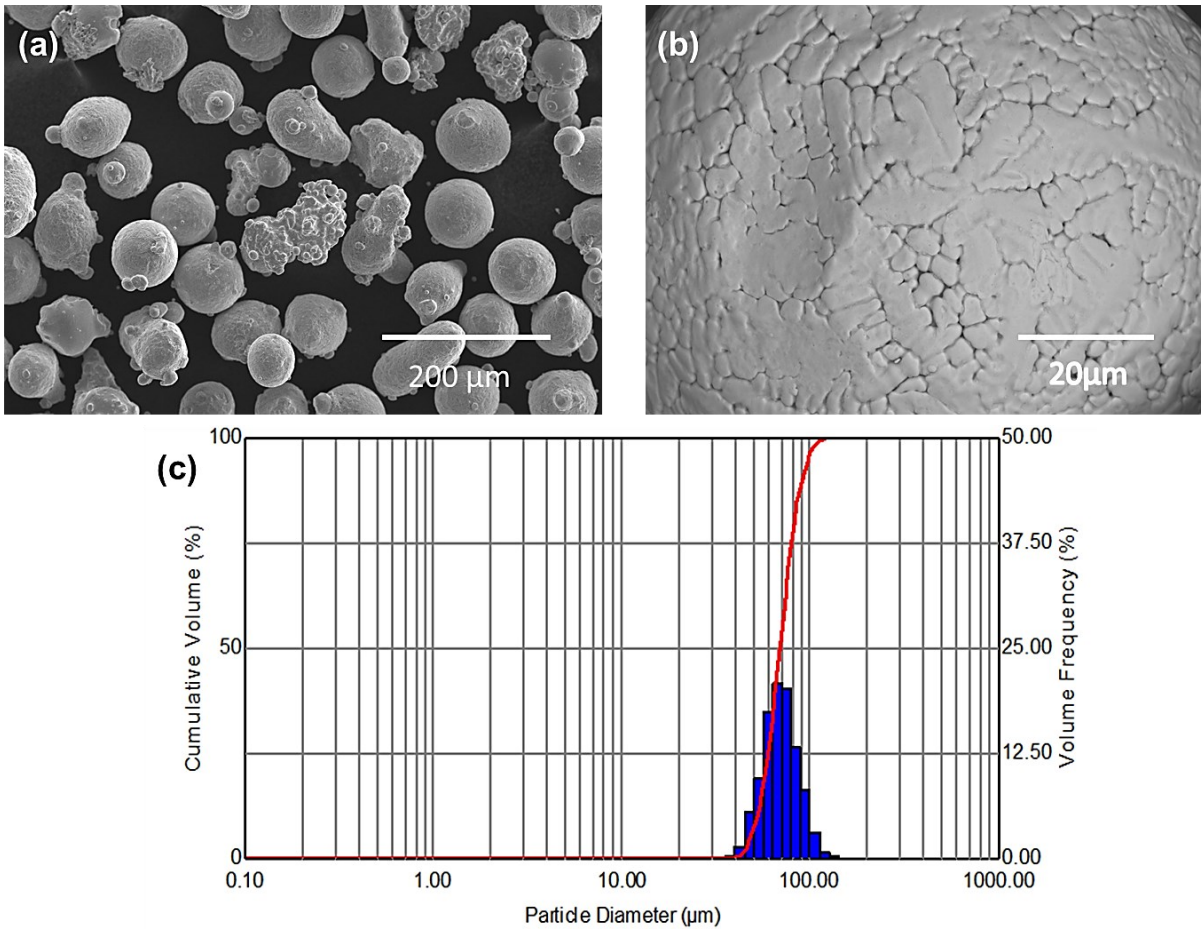

Figure 3.2 Scanning electron micrographs showing (a) low-magnified images of powder Cu-Ni powder particles, (b) high-magnification images showing dendritic nature and (c) particle size distribution of Cu-Ni feedstock.

Table 3.3 Chemical composition of the spraying powder in weight percentage.

Spectrum Label	Spectrum 1	Spectrum 2	Spectrum 3	Spectrum 4	Spectrum 5	Spectrum 6	Spectrum 7
O	0.85	1.81	0.94	0.25	0.33	1.68	1.48
Ni	30.34	42.21	35.00	85.92	70.49	45.24	36.18
Cu	68.81	55.98	64.06	13.84	29.17	53.08	62.34
Total	100.00	100.00	100.00	100.00	100.00	100.00	100.00

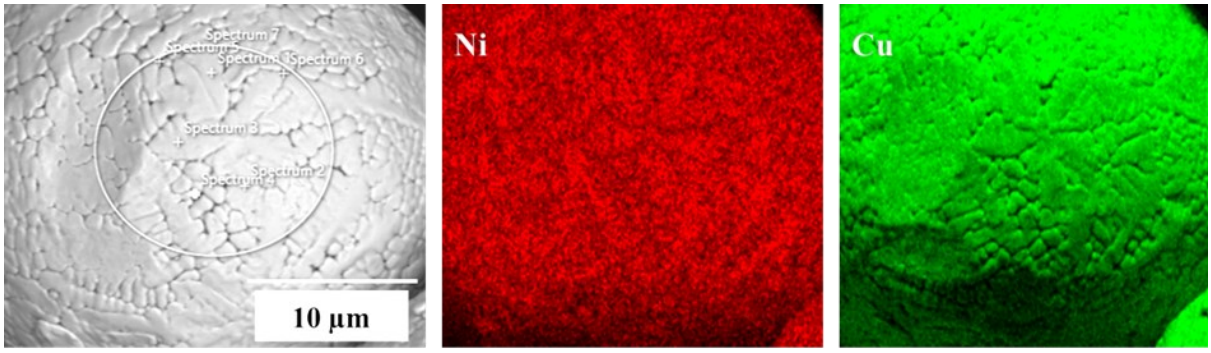

Figure 3.3 Energy dispersive spectroscopy mapping analysis of copper-nickel powder.

3.4.2 Microstructure of coatings

Figure 3.4 shows the coating morphology on the top surfaces. The top morphology of Cu-Ni coating showed the presence of pores, built-up splash particles and splat formations. It should be noted that there is no significant difference in the coating morphology for all the coatings, as shown in Fig. 3.4(a, b, and c). During the plasma spray process, the flight speed of feedstock particles is typically low, resulting in particles staying in the high-temperature zone of the plasma for a longer time, leading to sufficient heat transfer between the powder particles and high-temperature plasma. As a result of this, particles remain molten upon impact on the substrate, leading to the formation of flattened splats [10]. Furthermore, the surface roughness of the coating was within a similar range and is listed in Table 5 to be 23±1 µm, 22±1 µm and 23±0.5 µm on carbon steel, stainless steel, and aluminum alloy substrates respectively.

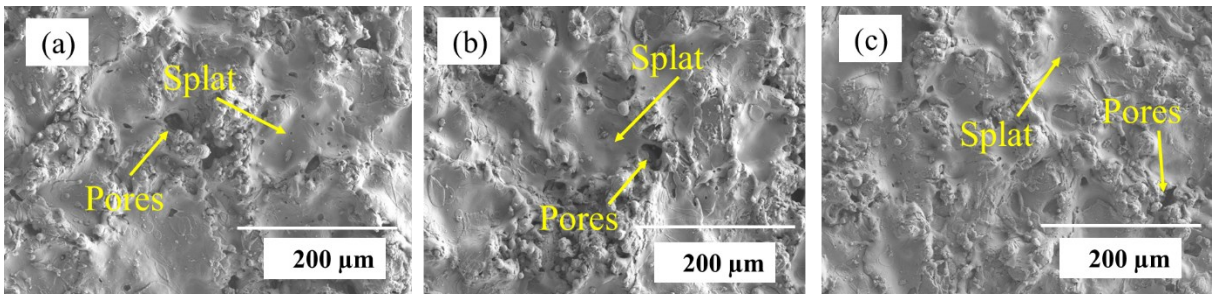

Figure 3.4 Scanning electron micrographs of top surface of copper-nickel coatings deposited on (a) carbon steel (b) stainless steel (c) aluminum alloy substrates.

The cross-sectional SEM images of plasma sprayed Cu-Ni coatings deposited on different substrates are shown in Fig. 3.5. It is noteworthy that the Cu-Ni coating deposited on each substrate demonstrated a homogeneous microstructure as there were no visible distinct regions on the coatings. Nevertheless, the occurrence of intersplats pores can be seen in the coatings deposited on the carbon steel and stainless steel substrates, respectively. This is mainly attributed to the splats overlapping, splashing, incomplete splat stacking, creating pores, and stress releasing mechanisms [35,36]. The dark gray region in the cross-section SEM images represents the formation of oxides for all the coatings. The weight percentage of oxide contaminations is tabulated in Table 3.4. The occurrence of oxide contaminations is mainly due to in-flight oxidation during spraying. It is noteworthy that oxides were mostly found at the boundaries of the inter-splat in the coating. Furthermore, the presence of pores was also evidently found in each coating, indicated by a black region. The air or plasma gas that is dissolved in the feedstock particles is trapped upon impact on the substrate resulting in the accumulation of splats which in turn leads to the formation of voids [37]. The average apparent porosity measured for all the coatings was less than 2% (see Table 5). A study conducted by study conducted by Yong-sheng Zhu et al. [9] also reported an average porosity of APS CuNiIn coatings to be 1.5%, within the range of this study. Porosities developed by plasma-sprayed coatings help to reduce the stress created by coating, however, excess pores can affect the service life as well as the properties of coatings [35]. Copper-nickel coating deposited on aluminum alloy substrates produced a wavy interface, indicating a better adhesion between substrate and coating in comparison to coatings deposited on other substrates. Nevertheless, the black zones in the interface region between the coating and stainless steel substrates are alumina grit that arises from the grit blasting of the substrate.

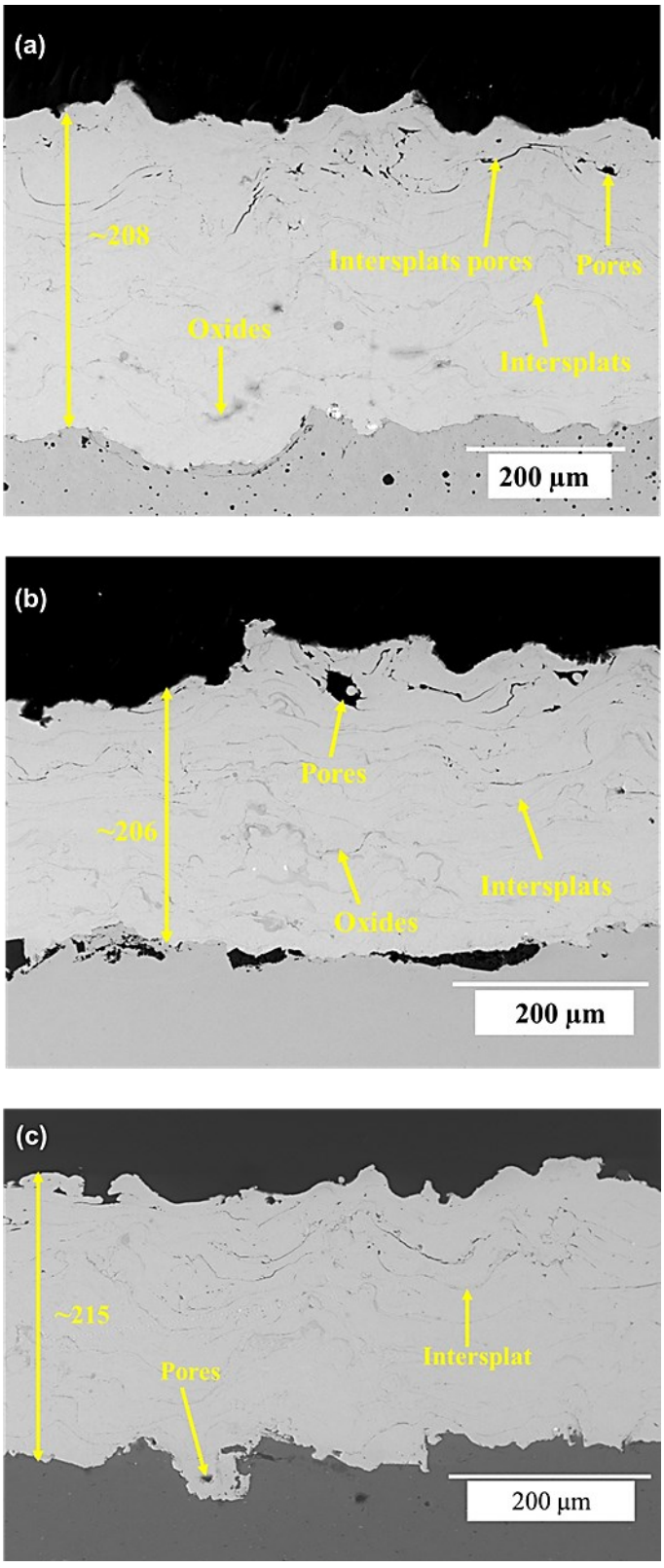

Figure 3.5 Scanning electron micrographs showing coating deposited on a) carbon steel (b) stainless steel (c) aluminum alloy substrates

Table 3.4 Chemical composition of CuNi coatings on carbon steel, stainless steel, and aluminum alloy substrates (wt.%)

Type of Substrate	Cu	Ni	O
Carbon steel	50±13	42±16	8±3
Stainless steel	56±15	38±17	6±3
Aluminum alloy	55±12	39±13	6±3

Table 3.5 Properties of copper-nickel coating

Type of Substrate	Thickness (µm)	Porosity (%)	Roughness Sa (µm)	Microhardness ($HV_{0.05}$)
Carbon steel	208±4	1.65 ±0.33	23±1	128± 33
Stainless steel	205±3	1.43 ±0.27	22±1	117± 10
Aluminium alloy	215±8	1.32 ±0.27	23.5±0.5	136± 23

Figure 3.6 shows XRD spectra of Cu-Ni feedstock and coating. As shown in Figure 6, no phase transformation was observed from the feedstock before and after the spray, as shown by the sharp peaks. This indicates similar characteristics peaks in the XRD pattern of the Cu-Ni powder and coatings. The three sharp peaks for both the powder particles and coatings at 43.77°, 51.11°, and 75.11° correspond to Cu-Ni, which perfectly matches the standard data (PCD 1907590). while the two additional small peaks for the coating at 37.13° and 62.83° correspond to NiO, which resembles the standard data (PCD 1817392). The analysis depicts that a significant amount of Cu-Ni was retained, while a little amount of NiO was formed in the coating. A small amount of NiO was formed due to the oxidation process that took place during the high temperature heating process of the air plasma spray. In the APS process, the powder particles are exposed to a high temperature, alongside the oxygen present in the plasma jet due to air entrainment. This increases the likelihood of oxide formation of the molten particles in flight [22]. The XRD analysis validates the formation of oxides on the microstructure of coatings produced. In analysing the diffractograms produced with the standard database of the XRD device, it was found that copper and nickel have the same crystal structure. As a result of this, the three sharp peaks for both the Cu-Ni feedstock and coatings contain copper and nickel peaks in between each other, (i.e., a single peak consisting of copper and nickel mixture). This indicates a solid solution in which the atoms of copper and nickel are mixed. This was affirmed by the phase diagram of the Cu-Ni binary system, where Cu-Ni is found to be in a complete solid solution [38].

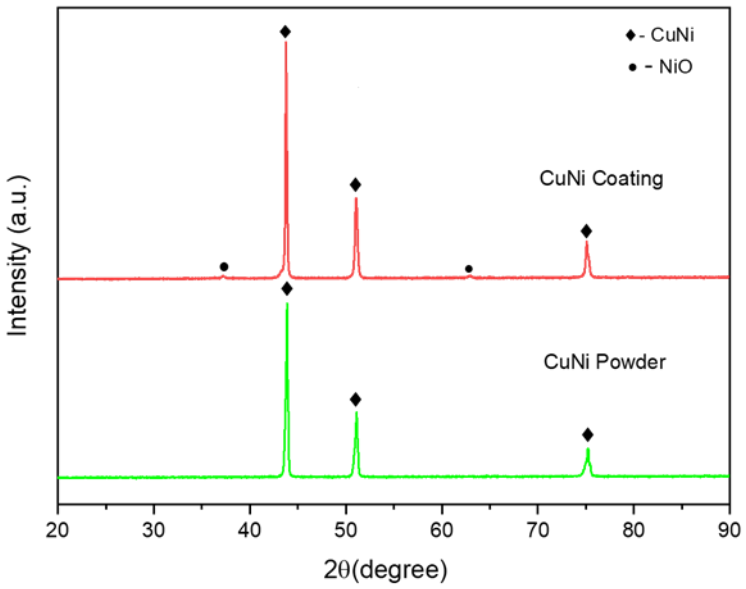

Figure 3.6 XRD patterns of Cu-Ni feedstock and Cu-Ni coating

Table 3.5 shows the microhardness of the coatings deposited on the different substrates was within the same range of no significant difference, due to similar spray conditions as well as the same batch of spray. The different substrate materials did not significantly influence the microhardness of the coatings, as thick coatings were obtained for each material. The average microhardness measurements obtained from the coating deposited on carbon steel, stainless steel, and aluminum alloy are reported to be 128±33 HV, 117±10 HV, and 136±23 HV respectively, which is comparable to previously reported studies on copper-based coatings [1,9,20]. The improvement of the hardness of APS Cu-Ni based coatings in solid solution as the arc current increases have been reported by Jin-Kun et al [1]. They also attributed hardness property enhancement in coatings to the oxide formed from the high temperature of the plasma jet [1,20].

3.4.3 Friction and Wear behavior of coatings

Figure (3.7a-c) illustrates the coefficient of friction (COF) as a function of the number of cycles for copper-nickel coatings deposited on different substrates at different temperatures (room temperature (RT), 300°C, and 450°C). The frictional measurement of all coatings tested at room temperature and 300°C followed a similar trend of two distinct phases, the running-in phase and the steady state regime. At room temperature sliding conditions, a sharp increase from 0.2 to 0.5 in the COF curves was observed during the initial cycles of around 500 for all the deposited coatings, indicating the running-in phase. Subsequently, a steady state regime was observed for all the coatings from 500 to 5000 cycles, with an average COF of 0.42. In contrast, under 300°C sliding conditions, the running-in phase period was slightly longer for

all coatings. Nevertheless, no significant difference in the COF curves was observed, with an average of 0.73, for all the Cu-Ni alloy coatings. There was an average COF increase from 0.42 to 0.73 with increasing temperature. The C.O.F at 450°C sliding condition for all coatings on each substrate, displayed a different behavior in comparison to RT and 300°C test conditions. There was an initial decrease in C.O.F at the beginning of sliding, followed by pronounced fluctuations of peaks up to the end of sliding, without attaining a steady state regime.

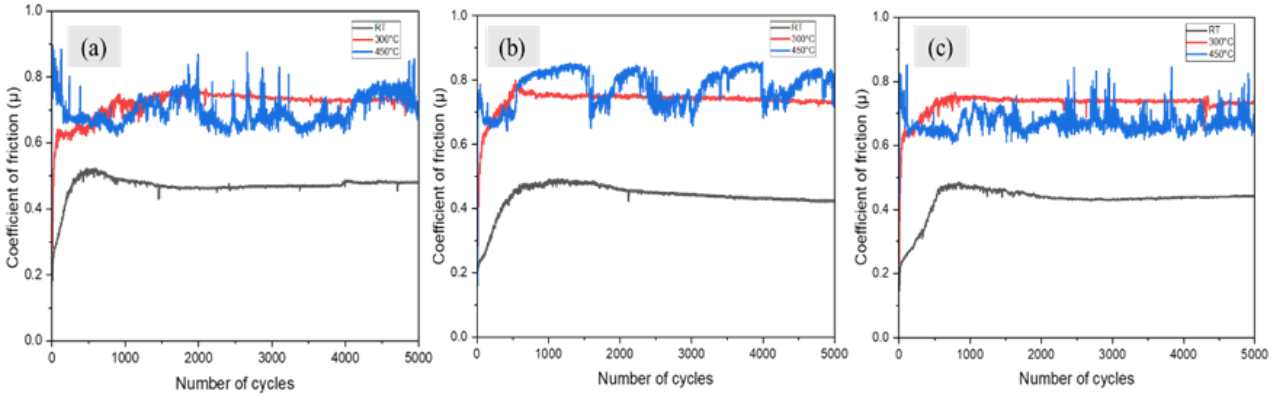

Figure 3.7 Coefficient of friction of copper-nickel coatings on (a) carbon steel (b) stainless steel (c) aluminum alloy at different temperature conditions.

Figure (3.8a-c) shows the wear depth profile of all coatings characterized at RT, 300°C, and 450°C respectively. It can be seen that the profiles obtained for the coatings deposited on different substrates showed no significant wear depths at room temperature, indicating low material removal during the sliding test process. In contrast to room temperature sliding, the wear depth increased for all the coatings tested at 300°C and 450°C. The wear depth of the worn coatings at 300°C condition was 15 µm, 14 µm, and 11 µm, for carbon steel, stainless steel, and aluminum alloy substrates respectively. Also, the wear depth of the worn coatings after the sliding test at 450°C was found to be 77 µm, 51 µm, and 89 µm, for carbon steel, stainless steel, and aluminum alloy substrates respectively. As with the C.O.F trend, the wear depth of all coatings increases as the temperature increases, which corresponds with the wear widths of each coatings.

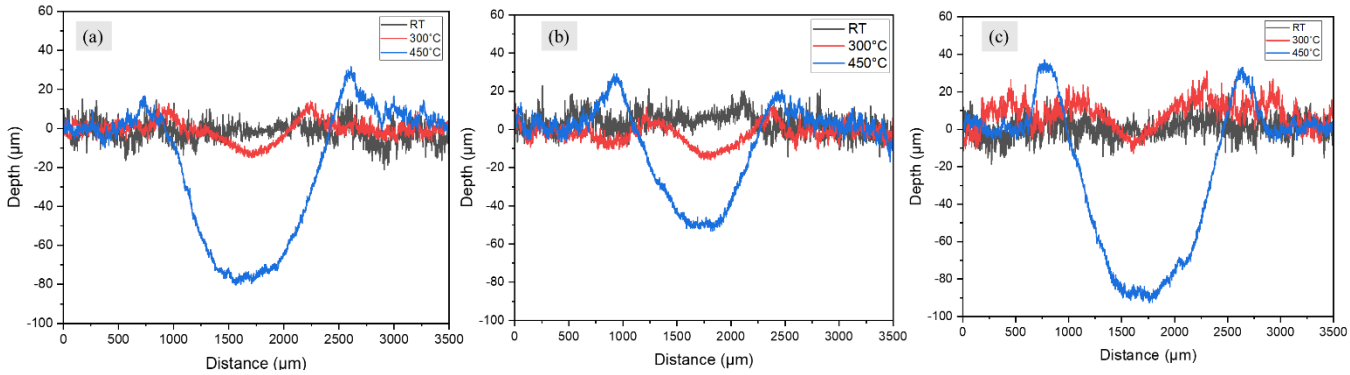

Figure 3.8 Wear depth profile of copper-nickel coatings on (a) carbon steel (b) stainless steel (c) aluminum alloy at different temperature conditions.

Figure 3.9 represents the specific wear rates of the coatings at 300°C and 450°C. The specific wear rate at room temperature was not computed for the reason stated above. However, at 300°C, the SWR was within the same range for coatings deposited on each substrate at $1.28 \times 10^{-4}\ mm^3$/N.m, $1.36 \times 10^{-4}\ mm^3$/N.m, and $1.45 \times 10^{-4}\ mm^3$/N.m for carbon steel, stainless steel and aluminum alloy respectively. At 450°C, the SWR for each coating increased, with a value of $14.6 \times 10^{-4}\ mm^3$/N.m, $11.5 \times 10^{-4}\ mm^3$/N.m, and $33.6 \times 10^{-4}\ mm^3$/N.m for carbon steel, stainless steel and aluminum alloy respectively. The result showed an increase in the SWR as the temperature increased from 300°C to 450°C.

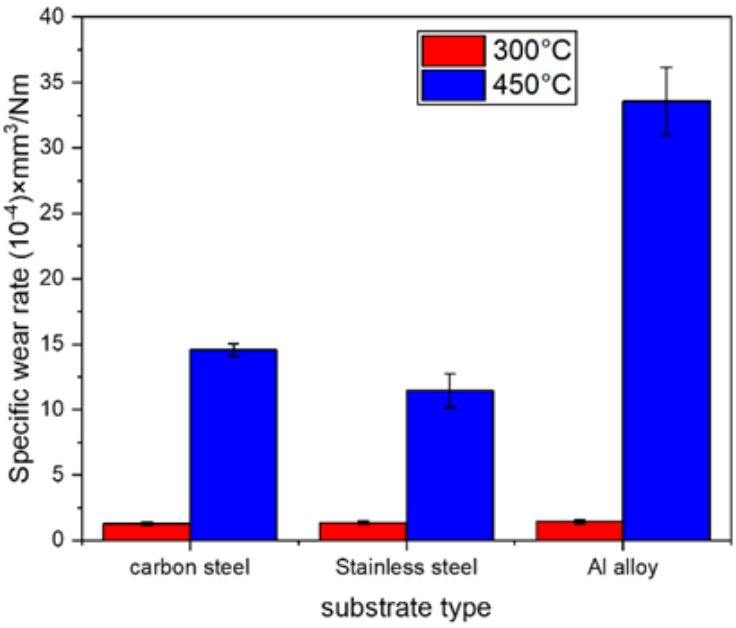

Figure 3.9 The specific wear rate of copper-nickel coatings on (a) carbon steel (b) stainless steel (c) aluminum alloy at 300°C and 450°C temperature conditions.

3.5 Ex-Situ Analysis

3.5.1 Worn Surface Morphologies

The worn surface morphologies of Cu-Ni alloy coatings deposited on each substrate at room temperature are shown in Figure 3.10. As shown in Figure 3.10, the damage severity is found to be lower at RT in comparison to elevated test conditions with no evidence of cracks. The wear track appears to be smoother with a uniform surface, which can be a result of the deformation of wear debris at the contact region of the coating and counter body [32]. Also, the occurrence of abrasive scars can be seen parallel to the sliding direction at room temperature sliding for all coatings. However, the worn surface morphologies of coatings tested at higher temperatures revealed the presence of cracks, loose particles and delamination. In addition to that, a significant degree of loose debris accumulation is also visible, which was not found at room temperature. The presence of these loose debris accumulation was significantly higher for 450°C test conditions compared to 300°C. It should be noted that the presence of abrasive scars are negligible for the Cu-Ni coatings tested at higher temperatures.

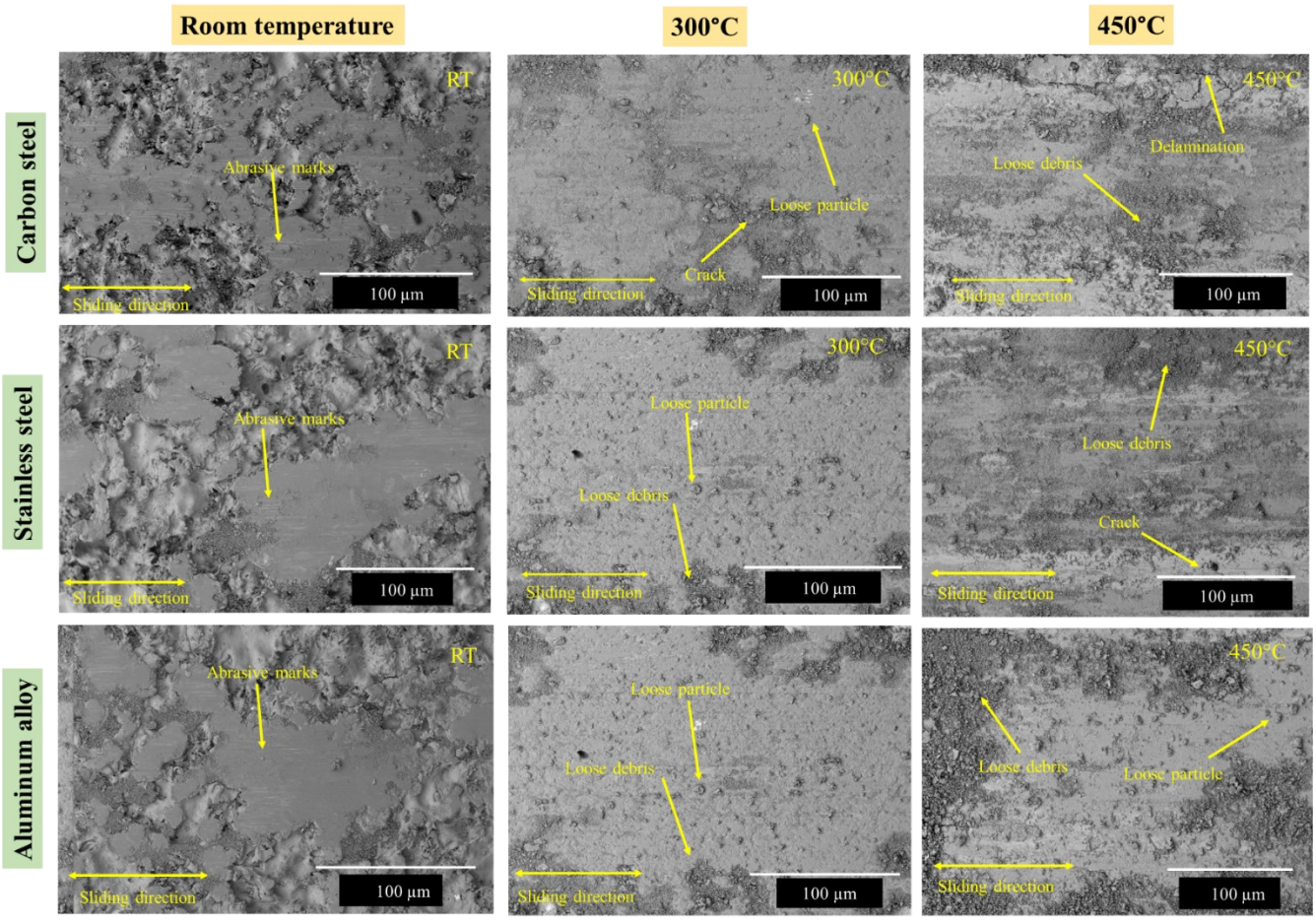

Figure 3.10 Worn surface morphologies of each coating tested at different temperature ranges at constant load.

Figures 3.11, 3.12, and 3.13 depict the elemental maps of the wear tracks for all coatings at different testing temperatures. The main components obtained from this analysis for all samples are Ni, Cu, O, and Al. The weight percentage of each element is displayed in Table 3.6 for carbon steel, stainless steel, and aluminum alloy substrates respectively. The EDS analysis revealed that the worn surface contained a significant amount of copper and nickel as well as a small fraction of aluminum for all coatings. The presence of traces of aluminum on the wear tracks is attributed to the alumina counterball used for the dry sliding test. The presence of oxygen on the wear tacks indicates the existence of oxides after the wear test and these oxide levels at each temperature condition were within the same level with no significant variations for all coatings. In summary, the results showed a homogeneous distribution of elements on the worn surface morphology for all coatings.

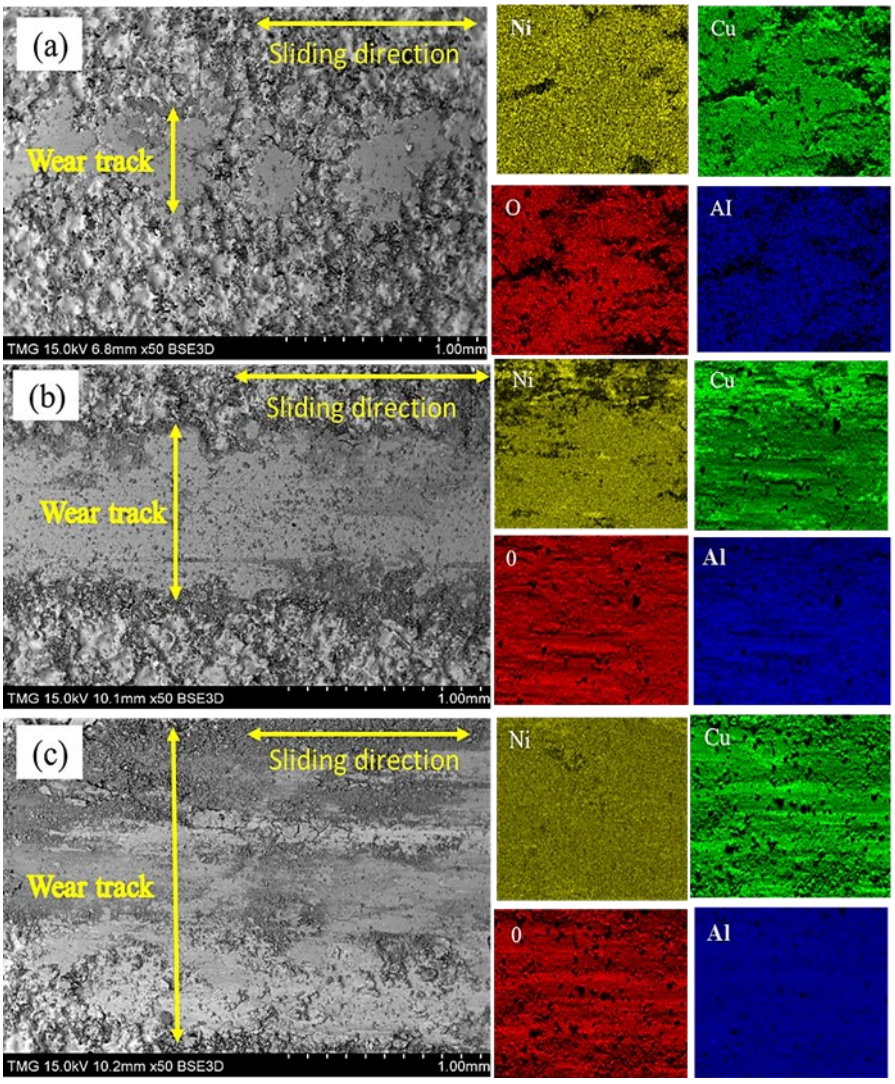

Figure 3.11 SEM analysis and EDS color mapping of the wear track on carbon steel substrate at (a) RT and (b) 300°C (c) 450°

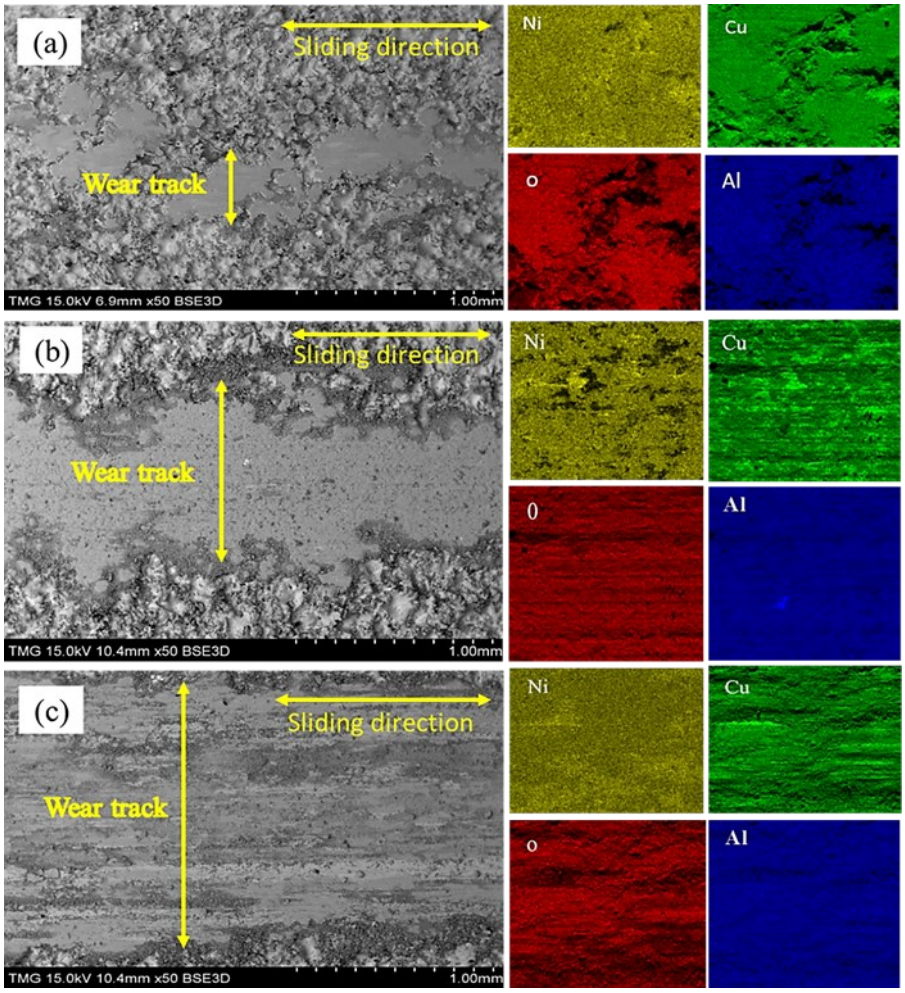

Figure 3.12 SEM analysis and EDS color mapping of the wear track on stainless steel substrate at (a) RT and (b) 300° (c) 450°C

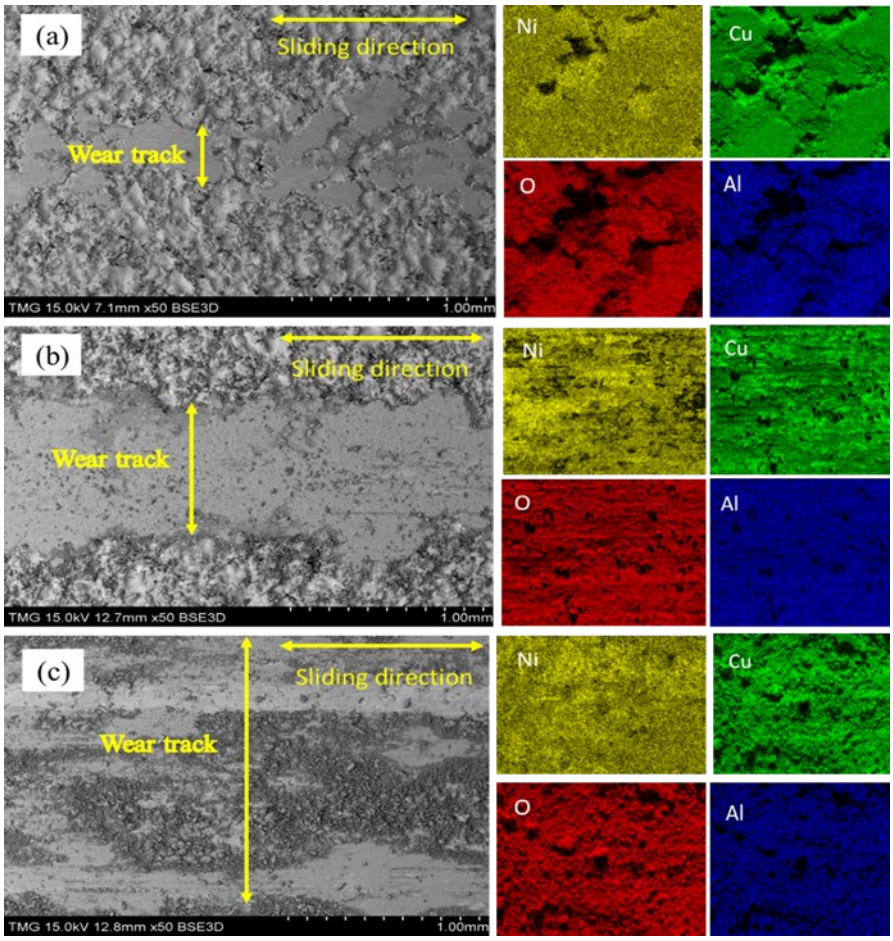

Figure 3.13 EDS color mapping of the wear track on aluminum alloy substrate at (a) RT and (b) 300°C (c) 450°C

Table 3.6 EDS evaluation of worn coatings on carbon steel, stainless steel, and aluminium alloy substrates (wt.%)

Substrate	Temperature	Cu	Ni	O	Al
Carbon steel	RT	44±2	41±4	14±3	1.1±0.6
	300°C	48±6	33±8	18±2	1.1±0.2
	450°C	53±6	31±7	17±5	0.1±0.1
Stainless steel	RT	51±3	31±3	17±2	1.3±0.2
	300°C	51±18	32±21	16±4	0.7±0.6
	450°C	51±5	31±7	18±4	0.2±0.1
Aluminum alloy	RT	52±3	31±4	16±4	1.2±0.4
	300°C	42±15	43±20	14±5	0.5±0.4
	450°C	39±15	49±20	12±6	0.1±0.1

3.5.2 Counterface analysis

Figure 3.14 represents the SEM micrographs of the alumina counterfaces after sliding test against copper-nickel coating for each substrate at different temperatures (RT, 300°C, and 450°C). In general, similar behavior occurred at each temperature condition on the counterballs sliding on the three different substrates. For each substrate, a slight amount of transfer layer from the coating to the surface of the alumina counter body was observed at room temperature Figure 3.14 (a, d and g). The counterface sliding at high temperatures experienced a higher amount of transfer film on the center and edges of its surface. This was more significant for the 450°C (see Fig. 3.14 c, f and i) conditions with a wider contact area in comparison to sliding at 300°C (see Fig. 3.14 b, e and h), indicating an increase in the amount of transfer film as well as the area of contact as the temperature increases.

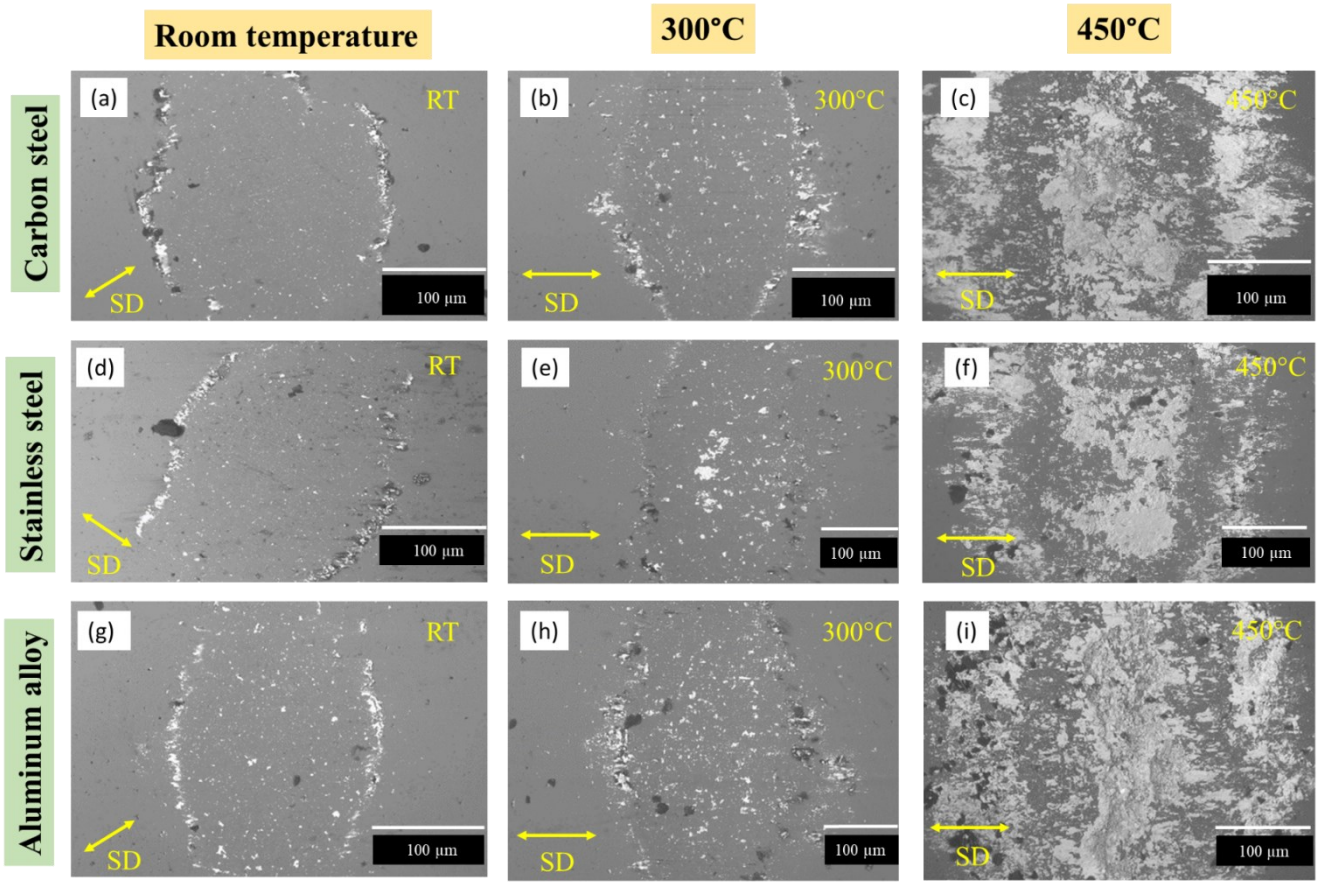

Figure 3.14 SEM analysis of alumina counter ball sliding on carbon steel substrate (a) RT (b) 300°C (c) 450°C stainless steel substrate (d) RT (e) 300°C (f) 450°C and aluminum alloy substrate (g) RT (h) 300°C (i) 450°C

3.6 Friction and wear mechanisms

Figure 3.15 provides a schematic representation of the friction and wear mechanism of the copper-nickel coatings on the substrate materials at room temperature and high temperature (300°C and 450°C) based on the ex-situ analysis that was performed on the worn surfaces. The coefficient of friction behavior at RT is consistent with copper-based alloys reported in previous studies [1,39,40]. As displayed in Figure (3.7a-c), the friction coefficient at room temperature was lower than coatings tested at high temperatures (300°C and 450°C). This can be related to the worn morphology of the wear tracks obtained at RT, which showed a smooth surface with abrasive marks parallel to the sliding direction, indicating abrasion as the dominant wear mechanism (figure 3.10).

As seen in (Fig. 3.8 a-c), a negligible wear rate was obtained for all sliding tests at room temperature. This behavior was similar for all coatings deposited on carbon steel, stainless steel, and aluminum alloy, and was also characterized by fewer transfer layers on the surface of the contacting alumina counter ball, as seen from the SEM images in Figure (3.14 a-g). In addition, the smeared smooth layer on the worn surface at RT condition can act as a protective layer during the sliding test, which in turn helps in the enhancement of wear resistance [41]. The formation of smooth surface film on the worn surface of HVOF Cr_2O_3 and Al_2O_3 coatings at room temperature has been reported to reduce the wear rates of the coatings [42].

At elevated temperatures (300°C and 450°C), the friction coefficient values were higher than the room temperature condition. The initial increase in the friction curve (i.e. during break-in) at 300°C can be attributed to contaminants removal from the sliding surface, resulting in exposure of the bare surface, which in turn enhances the coefficients of friction [43]. A high amount of adhesion between the alumina counterbody and CuNi coating results in the formation of cracks, loose particles and large debris on the wear tracks of coatings for 300°C and 450°C respectively (Figure 3.10). The presence of loose debris and particles at HT condition arises due to the ploughing of asperities. These wear debris entrapped in the mating surfaces can inhibit sliding, resulting in the enhancement of C.O.F [43]. This correlates well with the higher frictional values for coatings obtained at high temperatures (Figure 3.7). This wear debris was significantly higher for 450°C test conditions in comparison to 300°C. Also, it is important to note the fluctuations C.O.F curve for the 450°C test condition can be attributed to repeated localized fracturing of the CuNi coating layers resulting in the formation of loose debris on the wear tracks during the sliding test [33]. The debris accumulation on the wear surface during the sliding can create high COF with larger fluctuation behavior [44]. Similar

frictional fluctuation behavior at high temperature reciprocating sliding has been previously reported [45].

With regards to the wear, a high wear rate was observed for all coatings at high temperatures test conditions. The high contact temperature at this condition can lead to softening of the material and consequently enhance the wear rate of coatings. In addition, the higher amount of material transfer on the alumina counterball at high temperatures indicates a potentially higher amount of adhesion during the mating process, resulting in a higher wear rate of the coatings. The presence of these adhesive transfer films indicates the occurrence of continuous plastic shearing. This results in the fragmentation of materials as well as the formation of wear debris, before being transferred to the surface of the counterparts [45]. Furthermore, the splats from the coating surface are easily pulled out to adhere to the surface of the sliding counterparts at this test condition (450°C). In addition, the transfer film covered a greater area fraction at the contact surface of 450°C condition in comparison to 300°C, corresponding to the higher wear of 450°C sliding in comparison to 300°C. The enhancement in wear behavior due to an increase in the material transfer on the counterface during sliding has been reported by several authors [33, 46]. The worn coatings at high temperature sliding produced a rougher wear track with brittle fracture which promotes the formation of cracks, delamination as well as loose particles. The brittle fracture was more evident for the coatings tested under 450°C conditions. Indeed, the presence of cracks and delamination can create a detrimental effect because of the greater amount of material removal during reciprocating sliding, which results in high debris formation. As a result of high debris content, the three-body abrasion could take place, promoting enhanced wear and friction coefficient [41, 47]. Bilolli et al [42] reported an immense failure of the wear track of APS Cr_2O_3 coating sliding at high temperatures with characteristics feature of cracks propagating through the weak points of the interlamellar surfaces, resulting in a higher degree of material removal. At high temperature test conditions, heat generated through friction during the sliding process results in thermal softening and an increase in the real area of contact, leading to an enhanced adhesion between the surfaces of the alumina counterball and the CuNi coating. This enhanced adhesion experienced between the sliding surfaces promotes higher friction and wear behavior at high temperature test conditions [48]. Adachi et al [49] also reported a higher tendency to form adhesive film between contacting bodies when sliding at higher temperatures, resulting in higher friction forces due to tensile stresses near the surface. Thus, it can be implied that the wear mechanism at room temperature is mainly dominated by the features of abrasive wear, whilst the presence

of cracks, delamination and loose debris particles in conjunction with adhesive films being the dominant wear mechanism found for the coatings tested at higher temperatures.

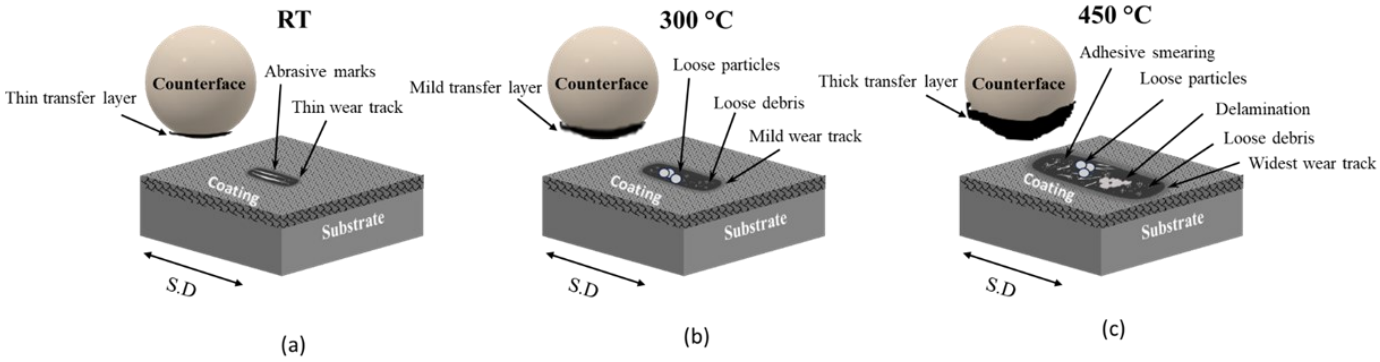

Figure 3.15 Schematic showing the wear mechanisms of copper-nickel coatings at (a) RT (b) 300°C and (c) 450°C.

3.7 Conclusion

In this present study, copper-nickel (Cu-38Ni) was deposited on carbon steel, stainless steel, and aluminum alloy using atmospheric plasma spray to critically evaluate the mechanical and tribological performance of the coatings. An attempt was made to investigate the influence of the substrate materials. Coatings deposited on each substrate exhibited a well-flattened splat, which is a characteristic phenomenon of plasma sprayed coatings. From the coating cross-section microstructure, CuNi deposited on aluminum alloy produced a better adhesion in comparison to other substrates. However, this did not significantly influence the performance, as the thickness, porosity, surface roughness, and microhardness of coatings for each substrate were fairly within the same range. The XRD analysis revealed and validated the formation of oxides in the coatings due to the high temperature plasma spray process. Also, the solid solution nature of the copper-nickel feedstock was confirmed by this analysis. The Cu-Ni coating deposited on the three substrates was subjected to sliding test at RT and HT (300°C and 450°). Similar frictional and wear behavior was observed for each substrate at the different temperatures. However, the friction and wear behavior of coatings exposed to HT was higher than the sliding test at RT. The high friction and wear behavior was ascribed to cracks, delamination, loose particles and larger wear debris particles on the wear track as well as a higher amount of material transfer on the alumina counter ball, exhibiting a dominant adhesive wear. However, at RT a smooth wear track region with abrasive marks was observed. The material transfer at this condition was lesser and significantly reduced the friction and wear rates.

References

1. J.K. Xiao, W. Zhang, L.M. Liu, X.P. Gan, K.C. Zhou, C. Zhang, Microstructure and tribological properties of plasma sprayed Cu-15Ni-8Sn coatings, Surface Coating Technology, 2018, 337, p 159–167. https://doi.org/10.1016/j.surfcoat.2018.01.016.

2. J.B. Singh, W. Cai and P. Bellon. Dry Sliding of Cu-15 wt%Ni-8 wt.% Sn bronze: Wear behaviour and microstructures, Wear, 2007, 263, p 830-841. https://doi:10.1016/j.wear.2007.01.061

3. Guangwei Peng, Xueping Gan, Yexin Jiang, Zhou Li and Kechao Zhou. Effect of dynamic strain ageing on the deformation behavior and microstructure of Cu-15Ni-8Sn alloy, Journal of Alloys and Compounds, 2017, 718, p 182-187. https://doi:10.1016/j.jallcom.2017.05.127

4. Dongdong Gu, Yifu Shen and Zhijian Lu. Microstructural characteristics and formation mechanism of direct laser-sintered Cu-based alloys reinforced with Ni particles. Materials and Design, 2009, 30, p 2099-2107. https://doi:10.1016/j.matdes.2008.08.036

5. J. Schell, P. Heilmann and D.A. Rigney. Friction and wear of Cu-Ni Alloys, Wear, 1982, 75, p 205-220. https://doi.org/10.1016/0043-1648(82)90149-1

6. Adrian Chua, Chanman Park, Troy Y. Ansell and Andy Nieto. Mechanical Behavior of Annealed Cold Sprayed Cu-Ni Coatings, Journal of Thermal Spray Technology, 2022, 31, p 574-584. https://doi.org/10.1007/s11666-021-01306-8

7. Bing Yin, Yansheng Yin, Yanhua Lei, Lihua Dong and Yijun Zhang. Experimental and density functional studies on the corrosion behavior of the copper-nickel-tin alloy, Chemical Physics Letters, 2011, 509, p 192-197. https://doi.10.1016/j.cplett.2011.04.100

8. Yan Wang, Lei Zhang, Jinkun Xiao, Wu Chen, Chunfang Feng, Xueping Gan and Kechao Zhou. The tribo-corrosion behavior of Cu-9 wt.% Ni-6 wt.% Sn alloy, Tribology International, 2016, 94, p 260-268. https://dx.doi.org/10.1016/j.triboint.2015.06.031

9. Yong-Sheng Xhu, Xiao-Tao Luo, Yin-Qiu Sun, Yuan Ren, and Chang-Jiu Li. Atmospheric plasma-spayed CuNiInB coatings of high fretting wear performance enabled by oxide-free metallic droplet deposition, Surface and Coatings Technology, 2023, 464, 129537. https://doi.org/10.1016/j.surfcoat.2023.129537.

10. Amin Ma, Daoxin Liu, Xiaohua Zhang, Guangyu He, Dan Liu, Chengsong Liu, and Xingchen Xu. The fretting fatigue performance of Ti-6Al-4V alloy influenced by

microstructure of CuNiIn coating prepared via thermal spraying, Tribology International, 2020, 145, 106156. https://doi.org/10.1016/j.triboint.2019.106156

11. C. Mary, S. Fouvry, J.M. Martin and B. Bonnet. Pressure and temperature effects on Fretting Wear damage of a Cu-Ni-In plasma coating versus TiI7 titanium alloy contact, Wear, 2011, 272, p18-37. https://doi.org/10.1016/j.wear.2011.06.008

12. C.H. Hager Jr, J.H. Sanders and S. Sharma. Unlubricated gross slip fretting wear of metallic plasma-sprayed coatings for Ti6AI4V surfaces, Wear, 2008, 265, p 439-451. https://doi.org/10.1016/j.wear.2007.11.026

13. B. Rajasekaran, S. Ganesh Sundara Raman, S.V. Joshi and G. Sundararajan. Performance of plasma sprayed and detonation gun sprayed Cu-Ni-In coatings on Ti-6AI-4V under plain fatigue and fretting fatigue loading. Materials Science and Engineering A, 2008, 479, p 83-92. https://doi.10.1016/j.msea.2007.06.019.

14. V. Fridrici, S. Fouvry and Ph. Kapsa. Fretting wear behavior of a Cu-Ni-In plasma coating, Surface and Coatings Technology, 2003, 163-164, p 429-434. https://doi.org/10.1016/s0257-8972(02)00639

15. B. Rajasekaran, S. Ganesh Sundara Raman, S.V. Joshi and G. Sundararajan. Effect of detonation gun sprayed Cu-Ni-In coating on plain fatigue and fretting fatigue behaviour of Al-Mg-Si alloy, Surface and Coatings Technology, 2006, 201, p 1548-1558. https://doi.org/10.1016/j.surfcoat.2006.02.023

16. C. Mary, S. Fouvry, J.M. Martin and B. Bonnet. High temperature fretting wear of a Ti alloy/CuNiIn contact, Surface Coating Technology, 2008, 203, p 691-698. https://doi.org/10.1016/j.surfcoat.2008.08.043

17. H. Murthy, G. Mseis and T.N. Farris. Life estimation of Ti-6Al-4V specimens subjected to fretting fatigue and effect of surface treatments, Tribology International, 2009, 42, p 1304-1315. https://doi.org/10.1016/j.tribont.2009.04.013

18. Yang Q, Zhou WL, Zhong YN, Zhang XH, Fu XS, Chen GQ and Li ZQ. Effect of shot peening on the fretting wear and crack initiation behavior of Ti-6Al-4V dovetail joint specimens, International Journal of Fatigue, 2018, 107, p 83-95. https://doi.org/10.1016/j.ijfatigue.2017.10.020.

19. Ruiz C, Boddington PHB and Chen KC. An investigation of fatigue and fretting in a dovetail joint. Experimental Mechanics, 1984, 24, p 208-217. https://doi.org/10.1007/BF02323167

20. Atul Ranjan, Aminul Islam, Manabendra Pathak, Mohd Kaleem Khan, and Anup Kumar Keshri. Plasma sprayed copper coatings for improved surface and mechanical properties, Vacuum, 2019, 168, 108834. https://doi.org/10.1016/j.vacuum.2019.108834

21. Maher I. Boulos., Pierre L. Fauchais., and Joachim V.R. Herberlein, Introduction to Thermal spray, Thermal Spray Fundamentals, From powder to part, second edition, Springer Press, 2021, p 3-14. https://doi.org/10.1007/978-3-030- 70672-2

22. Shujuan Dong, Yihui Wang, Jinyan Zeng, Xiong Yang, Panpan Liang, Dezheng Wang, Huiqi Liao, and Hanlin Liao. Performance of plasma sprayed CuNiIn coatings and Mo Coatings subjected to fretting fatigue. Nano Materials Science, 2020, 2, p 140 -150. https://doi.org/10.1016/j.nanoms.2019.07.003.

23. Heli Koivuluoto, Juha Lagerbom and Petri Vuoristo. Microstructural studies of Cold Sprayed Copper, Nickel, and Nickel-30% Copper Coatings, Journal of Thermal Spray Technology, 2007, 16, p 488-497. https://doi.10.1007/s11666-007-9060-5

24. Wen-Ya, Hanlin Liao, Jinglong Li and Christian Coddet. Microstructure and Microhardness of Cold-Sprayed CuNiIn Coating, Advanced Engineering Materials, 2008, 10, p 746-749. https://doi.1002/adem.200800044

25. Liuyan Zhang, Shuimei Yang, Xiao Lv and Xiaohua Jie. Wear and Corrosion Resistance of Cold-Sprayed Cu-Based Composite Coatings on Magnesium Substrate, Journal of Thermal Spray Technology, 2019, 28, p1212-1224. https://doi.org/10.1007/s11666-019-00887-9

26. Liuyan Zhang, Yanchao Zhang, Huishu Wu, Shuimei Yang and Xiaohua Jie. Structure and corrosion behavior of cold-sprayed Cu/Ni composite coating post-treated by Ultrasonic shot peening. SN Applied Sciences, 2020, 2. https://doi.org/10.1007/s42452-020-1997-8

27. ‘‘Standard Guide for Metallographic Preparation of Thermal Sprayed Coatings’’ ASTM-E1920-03, ASTM International, USA, 2009.

28. ‘‘Standard test methods for determining area percentage porosity in thermal sprayed coatings,’’ ASTM-E2109-01, ASTM International, 2014. https://www.iso.org/standard/60996.html. (Accessed 31 December 2021).

29. P. Patel, S.A. Alidokht, N. Sharifi, A. Roy, K. Harrington, P. Stoyanov, R. R. Chromik, C. Moreau, Microstructural and tribological behavior of thermal spray CrMnFeCoNi high entropy alloy coatings, Journal of Thermal Spray Technology, 2022, 31, p 1285–1301. https://doi.org/10.1007/s11666-022-01350-y

30. A. Roy, V.N.V. Munagala, P. Patel, N. Sharifi, S.A. Alidokht, M. Makowiec, R. R. Chromik, C. Moreau, P. Stoyanov, Friction and wear behavior of suspension plasma sprayed tantalum oxide coatings at elevated temperatures, Surface and Coatings Technology, 2023, 452, 129097. https://doi.org/10.1016/j.surfcoat.2022.129097

31. B.C.N.M. de Castilho, V.N.V. Munagala, S.A. Alidokht, N. Sharifi, S. Bessette, M. E. Makowiec, R. Gauvin, P. Stoyanov, C. Moreau, R.R. Chromik, Insights on silver migration mechanisms and their influence on the wear behavior of thermally sprayed self-lubricating coatings up to 350◦ C, Tribology Letters, 2022, 70, p 1-14. https://doi.org/10.1007/s11249-022-01662-8

32. Amit Roy, Navid Sharifi, Venkata Naga Vamsi Munagala, Sima A. Alidokht, Payank Patel, Mary Makowiec, Richard R. Chromik, Christian Moreau and Pantcho Stoyanov. Microstructural evolution and tribological behavior of suspension plasma sprayed CuO as high-temperature lubricious coatings, Wear, 2023, 524-525, 204874. https://doi.org/10.1016/j.wear.2023.204874

33. Raunak Supekar, Rakesh Bhaskaran Nair, Andre McDonald and Pantcho Stoyanov. Sliding wear behavior of high entropy alloy coatings deposited through cold spraying and flames spraying: A comparative assessment, Wear, 2023, 516-517, 204596. https://dor.org/10.1016/j.wear.2022.204596

34. J J Kauzlarich and J A Williams. Archard wear and component geometry. Proceedings of the Institution of Mechanical Engineers Part J: Journal of Engineering Tribology, 20001, 215, p 387-403. https://doi.org/10.1243/1350650011543628

35. Vandana Chaturvedi Misra, Y. Chakravarthy, Neelima Khare, K. Singh, S. Ghorui. Strongly adherent Al_2O_3 coating on SS 316L: Optimization of plasma spray parameters and investigation of unique wear resistance behavior under air and nitrogen environment, Ceramics International, 2020, 46, p 8658-8668. https://doi.org/10.1016/j.ceramint.2019.12.099

36. Andrew Siao Ming Ang and Christopher C. Berndt. A review of Testing Methods for Thermal Spray Coatings, International Materials Reviews, 2014, 59, p 179-223. https://doi.org/10.1179/1743280414Y.0000000029

37. Goudarzi Masoumeh, Saviz Shahrooz, Ghoranneviss Mahmood, and Salar Elahi Ahmad. Investigation of stand-off distance effect on structure, adhesion, and hardness of copper coatings obtained by the APS technique, Journal of Theoretical and Applied Physics, 2018, 12, p 85-91. https://doi.org/10.1007/s40094-018-0277-0.

38. Eric A. Brandes, Smithells Metals Reference Book, Sixth Edition, Butterworth and Heinemann Ltd, 1983.

39. X. Chen, Z. Han, X. Li, K. Lu, Lowering coefficient of friction in Cu alloys with stable gradient nanostructures, Science Advances, 2016, 2, e1601942. https://doi.org/10.1126/sciadv.1601942

40. K. Zhou, J. Xiao, L. Zhang, X. Xie, Z. Li, Tribological behavior of brass fiber brush against copper, brass, coin-silver and steel, Wear, 2015, 326–327, p 48–57. https://doi.org/10.1016/j.wear.2014.12.024

41. C. Bidmeshki, A.C. Liberati, A. Roy, F. Ben Ettouil, C. Moreau. Microstructural, mechanical, and tribological evaluation of CuAl-based coatings deposited by APS and HVOF, Journal of Thermal Spray Technology, 2023, 32, p 2321-2335. https://doi.org/10.1007/s11666-023-01665-4

42. G. Bolelli, L. Lusvarghi, T. Manfredini, F. Pighetti Mantini, E. Turunen, T. Varis and S-P. Hannula. Comparison between plasma- and HVOF-sprayed ceramic coatings. Part II: tribological behaviour, International Journal Surface Science and Engineering, 2007, 1, p 62-79. https://doi.org/10.1504/IJSURFSE.2007.013621

43. Payank Patel. Rakesh B. Nair, Raunak Supekar, Andre McDonald, Richard R. Chromik, Christian Moreau and Pantcho Stoyanov. Enhanced wear resistance of AlCoCrFeMo high entropy coatings (HECs) through various thermal spray techniques, Surface and Coatings Technology, 2024, 477, 130311. https://doi.org/10.1016/j.surfcoat.2023.130311

44. Li-Hui Tian, Wei Xiong, Chuan Liu, Sheng Lu and Ming Fu. Microstructure and Wear Behavior of Atmospheric Plasma-Sprayed AlCoCrFeNiTi High-Entropy Alloy Coating, Journal of Materials Engineering and Performance, 2016, 25, p 5513-5521. https://doi.org/10.1007/s11665-016-2396-6

45. Venkata Naga Vamsi Munagala, Sima A. Alidokht, Navid Sharifi, Mary E. Makowiec, Pantcho Stoyanov, Christian Moreau and Richard R. Chromik. Room and elevated temperature sliding wear of high velocity oxy-fuel sprayed Diamalloy3001 coatings, Tribology International, 2023, 178, 108069. https://doi.org/10.1016/j.triboint.2022.108069

46. Sima A. Alidokht, Venkata Naga Vamsi Munagala and Richard R. Chromik. Role of Third Bodies in Friction and Wear of Cold-Sprayed Ti and Ti-TiC Composite Coatings, Tribology Letters, 2017, 65, p 1-15. https://doi.org/10.1007/s11249-017-0899-4

47. Amit Roy, Vahid Jalilvand, Saeed Mohammadkhani, Payank Patel, Ali Dolatabadi, L.Roue, D. Guay, Richard R. Chromik, Christian Moreau and Pantcho Stoyanov. Enhanced Wear Resistance of Cobalt Oxide over Nickel Oxide, Tribology Letters, 2023, 71, p 1-14. https://doi.org/10.1007/s11249-023-01769-6

48. A. Gaard, N. Hallback, P. Krakhmalev and J. Bergstrom. Temperature effects on adhesive wear in dry sliding contacts, Wear, 2010, 268, p 968 – 975. https://doi.org/10.1016/j.wear.2009.12.007

49. K. Adachi, K. Kato and N. Chen, Wear map of Ceramics, Wear, 1997, 203-204, p 291-301. https://doi.org/10.1016/s0043-1648(96)07363-2

Chapter
4. Influence of solid-state deposition processes on the tribological behavior of copper coatings

In this chapter…

The tribological studies of copper powder deposited by high-velocity air fuel and cold spray technique are provided. The tribological testing at varying temperatures and various characterization techniques were performed to understand the friction and wear behavior of the coatings.

4.1 Abstract

Lower temperature deposition techniques, such as high-velocity air fuel (HVAF) and cold spray (CS) methods, have recently become potential candidates for manufacturing complex tribological coatings in extreme environments. Thus, this study aims to evaluate copper coatings deposited by HVAF and CS in terms of their microstructure, mechanical and tribological behaviour. Emphasis is placed on the correlation between the interfacial processes and tribological behavior. Reciprocating dry sliding wear tests were conducted against an alumina counterpart at 25°C and 300°C test conditions using a ball-on-flat tribometer. The results showed a similar friction behavior for both coatings with a higher friction coefficient at 300°C (0.48 and 0.47 for HVAF and CS respectively) in comparison to the sliding wear test at 25°C (0.41 and 0.39 for HVAF and CS respectively). The wear resistance at room temperature was similar for both coatings. At high temperature test conditions, the wear depth of cold spray coating was within the same level as room temperature. However, the wear depth of HVAF coating increased at elevated temperature sliding. Ex-situ characterizations performed on the worn coatings showed detached particles, cracks, mild abrasive wear and adhesion were the dominant wear mechanisms of HVAF coatings and contributed to higher wear of the coatings in comparison to cold spray coatings that were marked with cracks, mild abrasive wear and deep abrasive wear as the dominant wear mechanism.

Keywords: HVAF, Cold spray, Cu, Friction, wear

4.2 Introduction

The element copper is known to have good ductility, formability, malleability, and remarkable thermal and electrical properties. It is mostly used for thermal and electrical applications in industries [1-2] as well as a suitable material for conductive coatings [3]. They possess a face-centred cubic crystal structure with atomic weight, bulk density and melting point of 63.54 g/mol, 8.93 g/cm^3 and 1085°C respectively [4]. Pure copper coatings can be used to enhance or modify the surface properties of components to be used for different functions such as electronics, wear resistance, corrosion resistance and antibacterial coating applications [5-7].

The development of copper-based coatings is important in promoting excellent performance against fretting failure [8-11]. Fretting wear is a common cause of premature failure of critical components within gas turbine engines. It occurs at the contact interface between two surfaces undergoing slight relative motion or vibration under load, resulting in fatigue crack initiation and subsequently reduction in the endurance life of components [12-14]. An example of fretting failure is observed between the compressor blade dovetail and the fan, which impedes the safety and life span of aero-engines [15-17]. A feasible method to mitigate fretting wear involves improving the surface properties of components by employing thermal spraying techniques. Thermal spraying emerges as a viable surface modification technique to enhance the surface properties of copper-based alloys [15,18-19]. Thermal spraying techniques known for their versatility, cost-effectiveness, and widespread industrial adoption, are greatly applied in various sectors such as aerospace, turbines, and oil and gas due to their wide range of applications [20]. This process involves feeding feedstock material such as powder, wire, rod, or suspension into a spray torch, heating it to a molten or near-molten state, and then propelling it towards a base substrate material to create thick coatings [19-20]. These copper-based coatings which are applied to the tribological interfaces of gas turbine engines are generally deposited by traditional thermal spray methods such as atmospheric plasma spray (APS) and high-velocity oxygen fuel (HVOF). However, these high-temperature processes are faced with the presence of high oxide content and porosity in the coatings produced as well as undesirable phase transformations [15,21]. These undesirable properties of high deposition techniques can affect the wear performance of copper-based coatings.

Several researchers have explored the application of pure copper using thermal spraying methods such as detonation gun, arc spraying, high-velocity oxygen fuel (HVOF), and atmospheric plasma spraying (APS). For instance, Goudarzi et al [22] investigated the effect of stand-off distance (SOD) on the structure, adhesion and hardness of copper coatings using

the APS method. They reported an increase in voids in the coatings produced as SOD increases, which resulted in a decrease in the hardness of coatings as well as the adhesion strength between the coating and substrate. The oxygen content and the size of grains in the lamellae of the coatings also enhanced due to increasing SOD. Mohamed et al [7] evaluated the tribological properties of copper and copper alloy coatings using a twin arc deposition technique. Their studies revealed that Cu4%Sn (tin bronze) and Cu 17%AI 1%Fe (aluminum bronze) coatings enhanced the wear resistance of pure copper by 38% and 65% respectively. Also, the friction coefficient was lower than pure copper coatings. The enhancement of the copper alloy coatings in comparison to pure copper was attributed to high hardness and strongly bonded splats with high integrity of their microstructures. Stoltenhoff et al [23] worked on a comparative study of thermal sprayed pure copper coatings. Their results showed better performance of HVOF copper coatings in comparison to arc-sprayed deposition in terms of hardness, bond strength and electrical conductivity. HVOF copper coatings also produced lower oxygen contents than arc-sprayed coatings. Also, some studies have been reported regarding the application of copper-based alloy coatings for fretting fatigue failure using high temperature deposition techniques. For example, Ma et al. [24] reported on the fretting wear behavior of Cu-Ni-In alloy coatings on Ti-6Al-4V substrates deposited via APS and HVOF techniques. Their findings revealed that the CuNiIn coatings manufactured using APS exhibited a more pronounced lamellar microstructure and demonstrated superior fretting fatigue resistance. This outcome was attributed to the combined impact of the coatings high toughness and low microhardness, effectively impeding fatigue-crack initiation. Another study investigated by Shujuan et al. [25] reported the fretting wear mechanisms of CuNiIn coatings on Ti6Al4V and AI1050 substrates produced by APS method. Their study identified galling, third-body abrasive wear, and material transfer as the predominant fretting wear mechanisms in their investigation.

However, despite the promising potential of copper-based alloy coatings for tribological interfaces, assessing these interfaces under extreme environmental conditions using pure copper coatings remains unexplored. In addition, with the recent improvements in lower temperature deposition techniques, such as high-velocity air fuel (HVAF) as well as cold spray (CS) methods, these processes have recently become potential candidates for the manufacturing of complex tribological coatings in extreme environments. Cold spray is a solid-state deposition process that utilizes a supersonic particulate jet to produce coatings rather than a molten droplet jet of conventional thermal spray coatings. Plastic deformation of feedstock particles which occurs due to the high kinetic energy of the particles upon impact on the

substrate materials enables the formation of interlinking splats, resulting in the formation of coating [26-27]. HVAF is a relatively new thermal spray technique compared to the conventional high-velocity oxygen fuel (HVOF). Instead of pure oxygen as in the case of HVOF, this process utilizes the mixture of gaseous fuel and compressed air to accelerate powder particles on substrate material to form a protective coating [28]. Compared to more traditional thermal spraying techniques, these low temperature methodologies can deposit coatings with low porosity and oxide content, enhancing coating properties. However, there are limited studies on assessing these low-temperature deposition processes for copper-based coatings in tribological systems. Therefore, it is paramount that the tribological behavior of these coatings is well understood and characterized.

Therefore, this study aims to deposit pure copper coatings using high-velocity air fuel (HVAF) as well as cold spray (CS) technologies on mild steel substrates to understand the microstructure, mechanical and tribological performance of the coatings produced. The sliding wear test of the pure copper coatings was mated against alumina counter balls at room temperature and 300°C. Ex-situ analysis was performed on the worn coatings and counter balls using scanning electron microscopy (SEM) and X-ray spectroscopy (EDS) to investigate the wear mechanism of the coatings.

4.3 Experimental Details

4.3.1 Materials and Methodology

Commercially available pure copper (Sigma-Aldrich, Canada) of about 98% pure as indicated by the manufacturer was selected as the spray powder for the deposition process. The copper feedstock material was accelerated on mild steel of 1’’× 1’’× 0.19” (25.4mm × 25.4mm × 4.7mm) for both the HVAF and cold spray process. Before the spraying process, the substrates were grit blasted using #80 mesh alumina grit abrasive particles to improve the surface roughness and the adhesion of the coatings onto the substrates. The substrates were subsequently cleaned with compressed air to remove sand residue from the sample surface. For the HVAF process, the pure copper feedstock powders were deposited on the substrate material using an i7 ID-HVAF spray system (UniqueCoat Technologies LLC, VA, US). This spray system was also used to preheat the mild steel substrate with the application of propylene as the gaseous fuel. Table 1 lists the spraying parameters used for the spray process. The i7 gun is made with a length of 95 mm providing the possibility to spray internal diameters greater

than 140 at a 50 mm stand-off distance [29]. A short-dimension nozzle made with a converging-diverging fixture provided by UniqueCoat was used for the ID-HVAF deposition process. The nozzle dimension consists of a length of 26.17mm, an inside diameter of 9.2mm, and an outer diameter of 22mm. The cold spray deposition process was done using an LPCS system (EPX cold spray system, Centerline Ltd. Windsor, ON, Canada). An EVB nozzle was used for the cold spray process. The dimensions of the nozzle consist of a throat diameter of 2.5mm, an exit diameter of 5.6mm, and a diverging section length of 120mm. Table 2 lists the spraying parameters used for the spray process. Nitrogen carrier gas was used to accelerate the copper feedstock powder.

Table 4.1 High-velocity air-fuel spray parameters used for depositing copper coatings

Parameters	Values
Fuel flow rate (g/min)	150
Fuel pressure (psi, MPa)	120 (0.83)
Air flow rate (L/min)	2752
Air pressure (psi, MPa)	122 (0.84)
Powder feed rate (g/min)	25
Carrier gas flow rate (L/min)	40
Spray distance (inches)	2
Preheat passes	4
Number of spray passes	20
Substrate temperature	130±15°C
Gun linear speed (mm/s)	1000
DE (%)	48

Table 4.2 Cold spray parameters used for depositing copper coatings

Parameters	Values
Pressure (psi, MPa)	300
Temperature (°C)	475
Powder feed rate (g/min)	12
Spray distance (inch)	7
Preheat passes	1
Number of spray passes	1
Gun linear speed (mm/s)	50
DE(%)	70

4.3.2 Characterization

The morphology of the copper feedstock powders was characterized using scanning electron microscopy (SEM) (SU8230, Hitachi, Japan). The particle percentiles (d_{10}, d_{50}, and d_{90}) were analysed by using Spraytec (Malvern Panalytical Instruments, UK) made with a wet dispersion (water) accessory to measure the particle size distribution of the pure copper powder. The cross-section and top surface of the as-sprayed copper coatings were examined using the scanning electron microscope (SU8230, Hitachi, Japan). The cross-sectional surfaces were metallurgically cold-mounted using epoxy resin and dried at ambient temperature for 24 hours. Subsequently, the samples were grounded down to 1200 grit emery sheets followed by diamond polishing by applying a standard metallographic sample preparation method as per the ASTM Standard E1920-03 [30]. The energy-dispersive X-ray spectroscopy (EDS) was utilized to obtain the chemical composition of the coatings. The thickness of the coating was measured from the cross-sectional SEM images of the HVAF and cold spray coatings. Ten measurements were taken, and the average was reported as the coating thickness for each coating. Phase analysis was performed on the powder and coatings with the help of X-ray diffraction (D8 Advance DaVinci, Bruker, Germany) using Cu-kα radiation (step size = 0.02°, $\lambda = 1.54$ Å, $2\theta = 5°\text{-}100°$). This was operated using a voltage of 40 kV and a current of 40 mA. The surface roughness of the as-sprayed coatings was measured using a confocal laser microscope (Olympus LEXT 4000, Houston, USA). At least 10 measurements were obtained for each coating and the average value as well as the standard mean error was reported. The porosity of the coatings was measured using Image J analysis software. To ensure statistical repetition of results, fifteen high-magnified SEM images at 2.00K magnification of 20 µm scale bar on different locations of the as-sprayed coatings were taken according to ASTM E2109-01 standard [31]. The high magnification was chosen to allow resolution the of voids and best fills the screen with the entire coating thickness. This will ensure that inherent porosity (voids) can be clearly seen and are only measured. The measurement does not consider defects such as oxides, artifacts (pullouts, smearing), embedded grit, and other unwanted features. The average value as well as the standard mean error was reported. Microhardness measurements were performed on the polished cross-sectioned coating samples using a Vicker's microhardness tester (Anton Paar Micro combi tester-MCT^3, Switzerland). A Vickers diamond indenter was used for the hardness test with an applied load of 500g ($HV_{0.05}$) and a dwell time of 10 seconds. The average microhardness value was obtained for each coating from a 15-point indents measurement.

4.3.3 Wear Tests

Sliding wear tests under dry sliding conditions were conducted using a ball-on-flat configuration with a reciprocating tribometer (Anton Paar, TriTec SA, Corcelles, NE, Switzerland). The parameters used for the wear test were derived from previously published studies to provide a possibility of comparison of results [32-33], Also, based on the capability of the tribometer. A 6.3 mm diameter Al_2O_3 ball counterface material was used against the Cu HVAF and cold spray coatings. The choice of alumina as the counter body for the sliding wear test is due to its high hardness of 1500 HV (verified by McMaster-Carr, USA) and superior wear resistance [34-36]. The wear test was done at ambient temperature with a relative humidity maintained below 20% with the help of a desiccator. The wear testing was performed on the as-sprayed coatings at a constant load of 10 N and a velocity of 3.14 cm/s. The tests were conducted by varying the temperature conditions. i.e., room temperature (RT) and 300°C to determine the influence of heating on the friction and wear performances. For the high-temperature test condition, the coatings were heated to a temperature of 450°C with the help of a furnace connected to the tribometer. After which the surface of the sample was measured with a pyrometer, which recorded a value of 300°C. The stroke length and sliding distance were fixed for 10 mm and 100 m for the tests. All sliding wear tests performed for this study were conducted on as-sprayed coatings. The rationale behind testing the as-sprayed coatings is to replicate real-world conditions without additional surface finishing processes. The methodology not only ensures the applicability of the results to practical conditions but also helps reduce the lead time and overall component costs. Two repetitions were performed for each coating to ensure consistency of results, and the average value was reported as the friction coefficient of the coating. The depth of the wear tracks was measured using confocal laser microscopy (Olympus LEXT 4000, Houston, USA). Profiles were analyzed across the wear track and data obtained from this measurement was used to plot the wear depth profile of each coating using the OriginLab software. The ex-situ analysis was subsequently analysed on the wear tracks and counter balls using the field emission scanning electron microscope coupled with energy dispersive spectroscopy to interpret the wear mechanisms of each coating. Raman analysis was performed using an InVia Spectrometer (Renishaw, UK) on the unworn and worn coatings using an Ar^+ ion (λ= 532 nm) laser source to investigate the phases after the sliding test.

4.4 Results and Discussion

4.4.1 Feedstock material

Figure 4.1a. shows the SEM morphology of the pure copper feedstock used for the deposition process of both coatings. As seen in Figure 4.1a, the FE-SEM of the copper powder displays a mixture of spherical and irregular morphology containing both large and small particles. Figure 4.1b presents the surface morphology of a single copper particle showing the presence of equiaxed grains on the surface of the particle, as similarly reported by [37]. EDS analysis performed on the powder showed an oxygen content of less than 1%. The EDS color mapping shown in Figure 4.1c affirms the high purity copper feedstock with a small quantity of oxide. The particle size distribution of copper feedstock is shown in Figure 4.1d. The d_{10}, d_{50} and d_{90} values obtained from this measurement are 6.3µm, 12.09µm, and 23µm respectively.

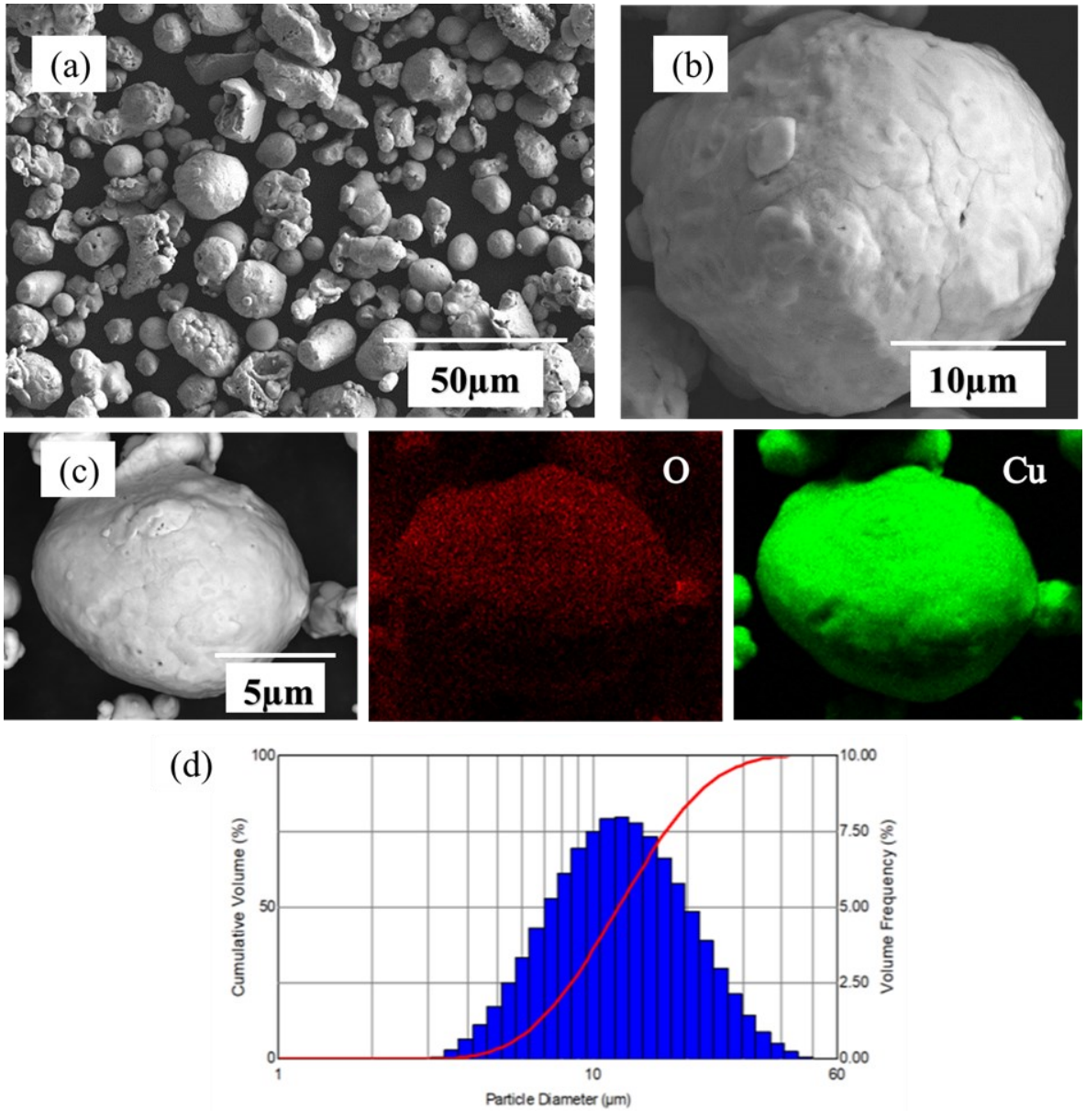

Figure 4.1. Scanning electron micrographs showing (a) low-magnified images of powder Cu powder particles, (b) high-magnification images of the Cu powder and (c) Energy dispersive spectroscopy mapping analysis of copper feedstock (d) particle size distribution of Cu feedstock.

4.4.2 Microstructure of coatings

Figure 4.2 shows the surface morphology of the HVAF and cold spray coatings. The surface of the HVAF coatings was characterized by the presence of splats, pores and a few unmelted particles. The HVAF spray process is a relatively higher temperature technique in comparison to cold spray, within a temperature range of 1000°C-1700°C[38]. This leads to heat transfer between the copper powder particles and the spray system, resulting in particles melting upon impact on the substrate, forming flattened splats. The surface of the cold spray coating showed numerous amounts of deformed particles. This is because the spray process consists of a gas and particle temperature well below the melting temperature of the copper feedstock. Thus, the particles are not melted but remain solid upon impact on the substrate material. The formation of coatings arises due to the high kinetic energy of the particles, resulting in deformation upon impact on the substrate [39]. Also, the cold spray coating surface offers a rougher surface morphology as confirmed by the surface roughness measurements of 9±1µm and 13±2µm for HVAF and cold spray coatings respectively.

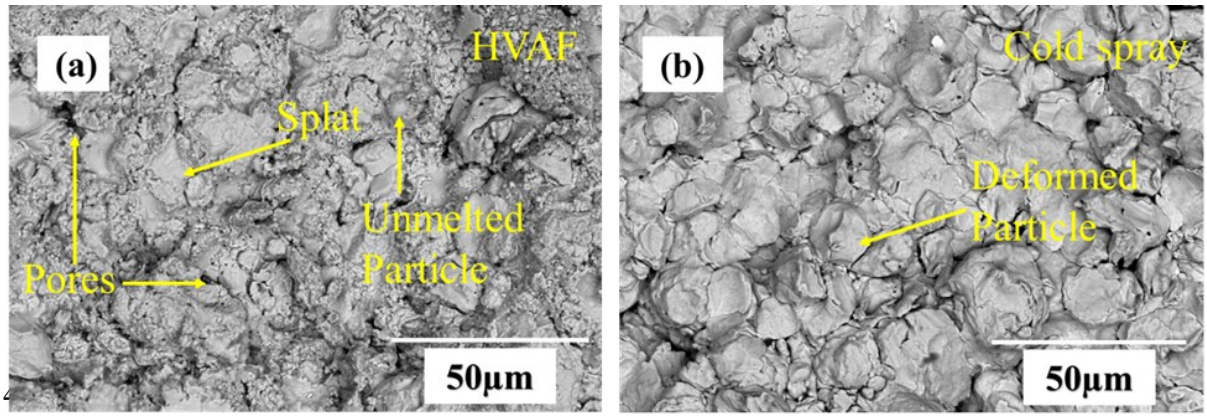

Figure 4.2 Scanning electron micrographs of the surface morphology of copper coatings (a) HVAF (b) cold spray.

The cross-sectional SEM images of the HVAF and cold sprayed Cu coatings are shown in Figure 4.3. It can be seen that both coatings produced a relatively dense and homogeneous microstructure with no visible distinct regions on the coatings. There was the absence of cracks and significant failure on the microstructure of both coatings. This can be attributed to

preheating of the substrate material before the deposition of both coatings. The preheating temperature has a significant effect on the distribution of residual stress in the coating [40]. Therefore, optimizing the preheating temperature of the substrate will promote evenness in the temperature distribution of the coating system. This will in turn reduce thermal stress in the coating and prevent cracks, peeling and failure that can arise due to excessive residual stress [41]. However, there was a presence of oxide contaminations on HVAF coatings which was less significant for cold spray coatings as verified by EDS mapping (see Figure 4.3). The weight percentage of oxide inclusions for the HVAF and cold spray coatings was found to be 6% and 1% respectively. The presence of oxides in the HVAF coatings is mainly due to the higher temperature working of the spray process as opposed to cold spray, as increasing heat input promotes oxidation. Furthermore, pores were also evidently found in both coatings, indicated by black regions. The average apparent porosity measured for all the coatings was less than 1.4% (see Table 4.3). However, the porosity defect was higher for the HVAF coatings. Generally, the increase of oxides in coatings enhances the increase of coating porosity, as the development of splat flashing which creates porosity, is promoted by oxidation [42]. In bibliography, other researchers have also reported low porosity below 0.5% of cold sprayed Cu [26,43,44] and Cu-based alloy [45], within the range of this study. The low porosity of the cold spray Cu coatings is due to the intense plastic deformation of the copper particles [26]. Regarding the thickness of the coatings, the copper coatings measured approximately 204µm and 187µm for the HVAF and cold spray coatings respectively.

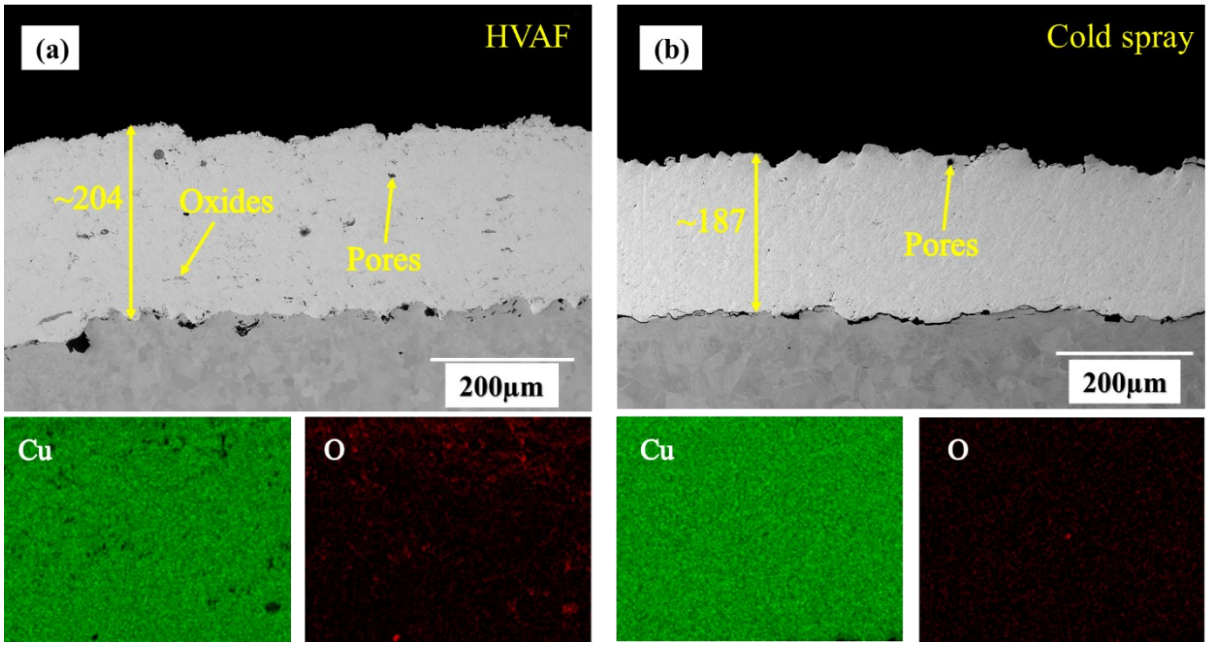

Figure 4.3 Scanning electron micrographs showing cross-section and elemental map analysis of Cu coatings produced by a) HVAF (b) cold spray

Table 4.3 Properties of the copper coating

Type of coating	Thickness (µm)	Porosity (%)	Roughness Sa (µm)	Microhardness ($HV_{0.05}$)
HVAF	204±7	1.37±0.1	9±1	111±1
Cold spray	187±4	0.36±0.1	13±2	136±1

The XRD pattern of the copper powder, HVAF and cold sprayed coatings is shown in Figure 4.4. The Cu diffraction peaks consist of 43.3°, 50.4°, 74.1°, 89.9°, and 95.1°, associated with (111), (200), (220), (311), and (222) planes respectively. This perfectly matches the standard data (PDF 00-004-0836). The Cu_2O diffraction peak appears at 36.4°, corresponding to the (111) plane. This resembles the standard data (PDF 01-071-3645). The XRD spectra for the powder and cold spray coating exhibit similar characteristics peaks. This indicates no phase transformation was observed from the powder before and after the cold spray, as no oxidation occurred during the cold spraying process. This result is consistent with other cu-based coatings deposited by cold spray [5,45]. However, in addition to the presence of Cu peaks, the HVAF diffraction peaks also showed a small peak corresponding to cuprous oxide or cuprite (Cu_2O). The XRD analysis depicts that a significant amount of Cu was retained for both HVAF and cold spray coatings, while a little amount of Cu_2O was formed in the HVAF coating. The small amount of Cu_2O formed on the HVAF coating was due to the oxidation process during the HVAF spray process. This validates the formation of oxides on the microstructure of the HVAF coatings produced (see Figure 4.3a).

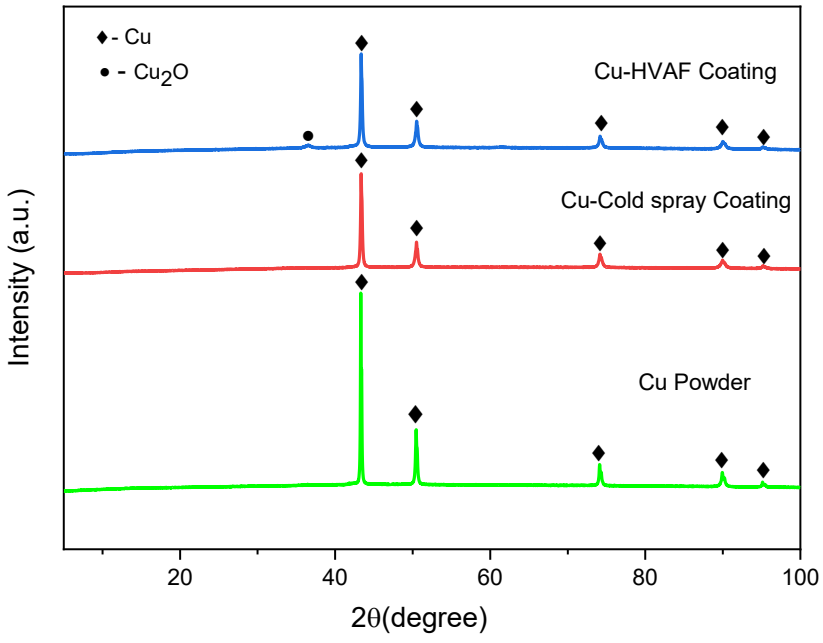

Figure 4.4. XRD patterns of Cu powder, Cold spray coating HVAF coating

Table 4.3 shows the microhardness of the HVAF and cold sprayed copper coatings. The average microhardness measurements obtained from both coatings were 111±1 $HV_{0.05}$ and 136±1 $HV_{0.05}$ for HVAF and cold spray coatings respectively. The hardness value obtained for cold spray coating was consistent with the study performed by Hutasoit et al. [46], they reported the hardness of cold spray copper coatings to be 136±8$HV_{0.1}$. The slightly improved hardness of the cold spray coatings can be attributed to the comparatively denser microstructure of the coatings. According to literature [2,23,26,47,45], the relatively high hardness of cold sprayed metallic coatings is due to the strain-hardening effect caused by a high level of plastic deformation during the high velocity impact of the particles. The shot peening effect that arises from particles rebounding during the deposition process can also enhance the coating hardness [26,48].

4.4.3 Friction and Wear behavior of coatings

Figure (4.5a-b) illustrates the variation of the coefficient of friction (COF) as a function of the number of cycles for both HVAF and cold spray copper coatings at different temperatures (RT and 300°C). The friction measurement of both coatings tested at room temperature followed a similar trend of two distinct phases, the running-in phase and the steady state regime. At room temperature sliding conditions, a sharp increase from 0.15 to 0.38 in the COF curves was observed during the initial cycles of around 1000 for all the deposited coatings, indicating the running-in phase. Subsequently, a steady state regime was observed for all the coatings from 1000 to 5000 cycles, with an average COF of 0.41 and 0.39 for HVAF and cold spray coatings respectively. In contrast, under 300°C sliding conditions, the friction behavior displayed a different behavior in comparison to RT. For HVAF coatings, there was an initial increase and decrease fluctuations behavior from 0.25 to 0.47 in the COF curves during initial cycles of around 1500 (run-in phase). After which a steady state value was obtained from 1500 to 5000 cycles with an average COF of 0.48. The cold spray coatings showed a sharp increase from 0.35 to 0.75 in the COF curves during the initial cycles of around 150, followed by a deceleration up to 400 cycles, before attaining a steady state regime at 0.47. Overall, the COF value at each test condition was within the same range for both coatings. However, there was an increase in COF with increasing temperature for both coatings.

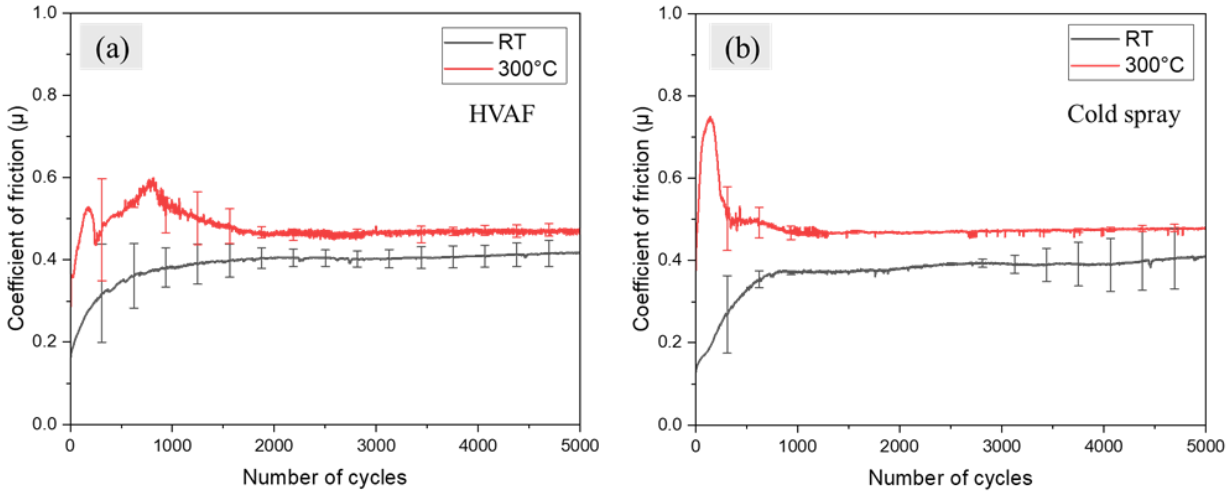

Figure 4.5 Coefficient of friction of copper coatings (a) HVAF (b) cold spray at different temperature conditions.

Figure (4.6a-b) shows the wear depth profile of HVAF and cold sprayed coatings characterized at RT and 300°C respectively. At room temperature, the wear depth of HVAF and cold spray coatings was relatively within the same range. At high temperatures, the wear depth of cold spray coatings was fairly within the same range as room temperature test conditions, However, the wear depth of HVAF coatings increased at elevated temperatures.

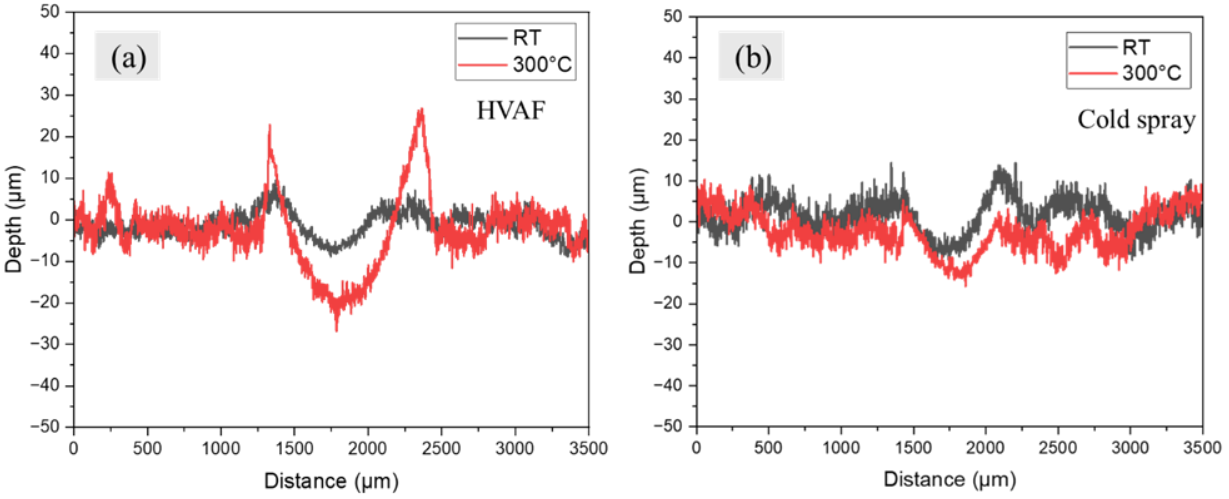

Figure 4.6 Wear depth profile of copper coatings (a) HVAF (b) cold spray at different temperature conditions.

4.5 Ex-Situ Analysis

4.5.1 Worn Surface Morphologies

The worn surface morphologies of HVAF Cu coatings (a,b) and cold spray Cu coatings (c,d) at room temperature are shown in Figure 4.7. As shown in Figure 4.7, the damage severity was

similar for both coatings, with a similar range of wear track width. For HVAF coating, cracks, detached particles, loose particles and accumulation of loose debris were found on the wear track worn surface. Furthermore, the occurrence of abrasive scars can be seen parallel to the sliding direction for the HVAF coatings. The worn surface of cold spray coatings was also characterized by similar features of cracks, loose debris accumulation, and abrasive scars parallel to the sliding direction. Elemental maps of the wear tracks for HVAF and cold spray coating at room temperature are shown in Figure 4.7. The main components obtained from this analysis for both coatings are Cu and O. The EDS analysis revealed that the tribo-layers are enriched by a significant amount of copper oxide for both coatings represented by the light gray region. The debris accumulation region for both coatings is rich in oxide as revealed by the analysis.

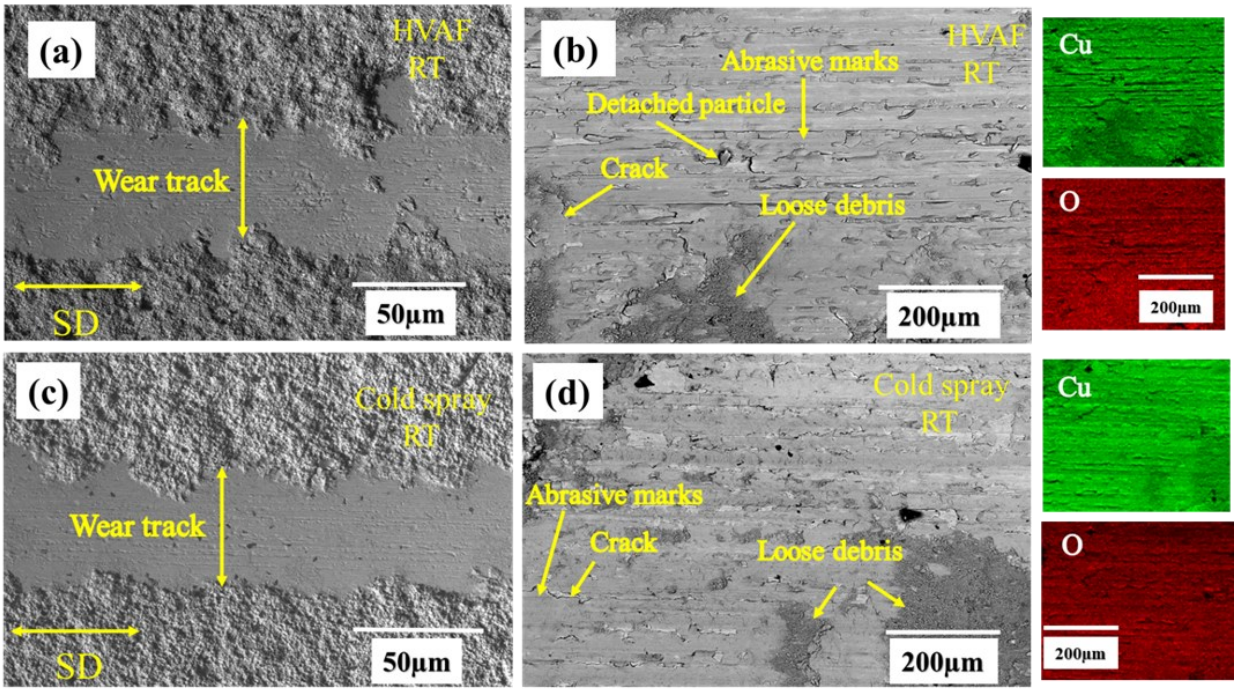

Figure 4.7 SEM worn morphologies and EDS mapping of (a,b) HVAF coating and (c,d) cold spray coating tested at room temperature.

The worn surface morphologies of HVAF Cu coatings (a,b) and cold spray Cu coatings (c,d) at 300°C are shown in Figure 4.8. The width of the wear track of HVAF coatings was significantly wider than the cold spray coatings. Also, the worn morphology of the HVAF coatings revealed the presence of two distinct regions represented by red and yellow boxes

respectively. The red region is presented with a smeared smoother surface while the yellow region shows the accumulation of rough patches with higher oxide content as verified by EDS analysis. The presence of loose particles was also found on the worn surface of the coating. For cold spray coatings, deep abrasive marks and grooves parallel to the sliding direction appeared throughout the worn surfaces. Elemental maps of the wear tracks for HVAF and cold spray coating at 300°C are shown in Figure 4.8. As with room temperature test conditions, the main components obtained from this analysis for both coatings were Cu and O.

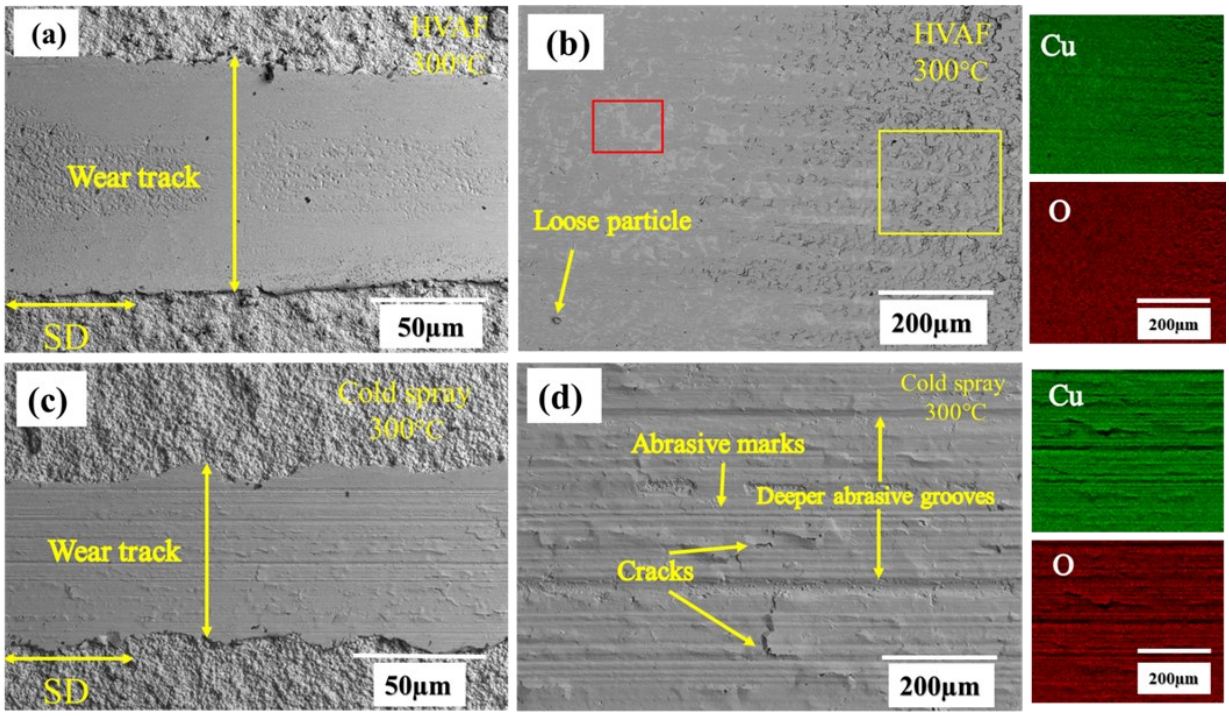

Figure 4.8 SEM worn morphologies and EDS mapping of (a,b) HVAF coating and (c,d) cold spray coating tested at 300°C.

EDS point analysis was performed at different locations of the unworn and worn region for both coatings tested at room temperature and 300°C. At room temperature, both coatings experienced an increased oxygen content ~10 wt.% for the worn coatings compared to the unworn coatings (~6 wt.% for HVAF and ~1 wt.% for cold spray). At 300°C, a similar occurrence of an increased oxygen content for the worn surface of both coatings (~20 wt.% for HVAF and ~21 wt.% for cold spray) compared to the unworn coatings (~15 wt.% for HVAF and ~16 wt.% for cold spray). The results indicate that after the wear tests, a higher oxide

content was obtained for both coatings at 300°C in comparison to room temperature sliding conditions as shown in Figure 4.9.

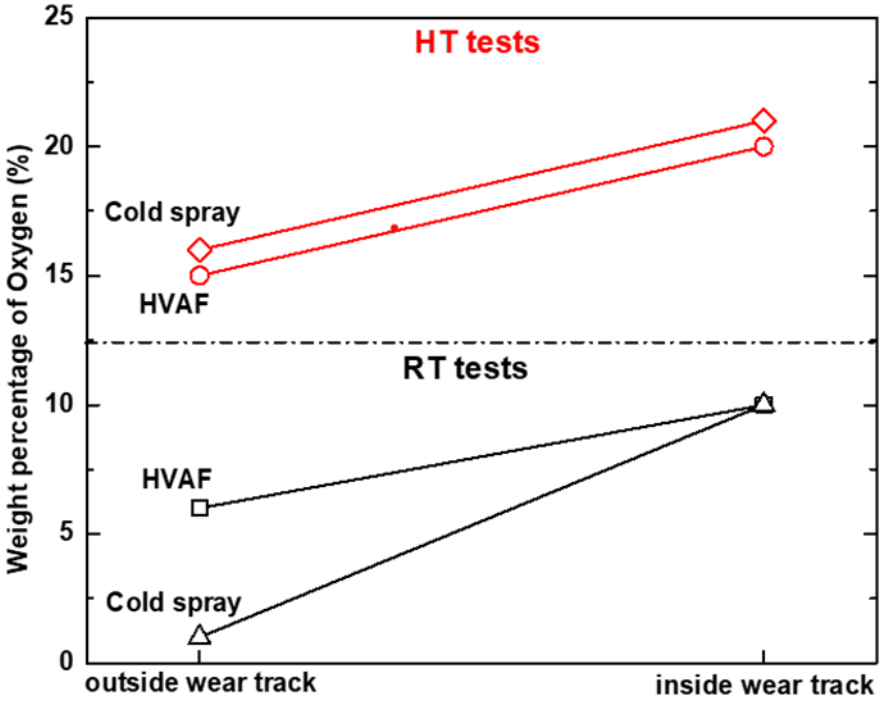

Figure 4.9. Weight percentage of oxygen (%) unworn and worn coatings of (a) HVAF and (b) cold spray coatings (wt.%)

Figure 4.10 a-b depicts the Raman analysis performed on the HVAF and cold spray unworn and worn coatings at room temperature and 300°C. For the HVAF unworn coatings at room temperature (see Figure 4.10a), the characteristic peaks at Raman shift 112 cm^{-1}, 151 cm^{-1} and 216 cm^{-1} correspond to the Cu_2O phase [49-51], while the peaks at Raman shift 302 cm^{-1} and 640 cm^{-1} are associated with the Cuo phase [52]. For the HVAF unworn coatings at 300°C (see Figure 4.10a), the characteristic peaks at Raman shift 112 cm^{-1}, 148 cm^{-1} and 216 cm^{-1} correspond to the Cu_2O phase [49-51]. In contrast, the peaks at Raman shift 302 cm^{-1} and 640 cm^{-1} are associated with the Cuo phase [52]. For the cold spray unworn coatings at room temperature (see Figure 4.10a), No Raman active phase was detected, indicating only metallic copper, which is not Raman active. For the cold spray unworn coatings at 300°C (see Figure 4.10a), the characteristic peaks at Raman shift 112 cm^{-1}, 151 cm^{-1} and 216 cm^{-1} correspond to the Cu_2O phase [49-51]. In contrast, the peaks at Raman shift 296 cm^{-1} and 632 cm^{-1} are associated with the Cuo phase [52-55]. For the HVAF worn surfaces at room temperature (see Figure 4.10b), the characteristic peaks at Raman shift 112 cm^{-1} and 216 cm^{-1} correspond to the

Cu_2O phase [49-51], while the peaks at Raman shift 283 cm^{-1} and 620 cm^{-1} matched with the Cuo phase [51,53]. For the HVAF worn surfaces at 300°C (see Figure 4.10b), the characteristic peaks at Raman shift 112 cm^{-1} and 216 cm^{-1} align to the Cu_2O phase [49-51], whereas the peaks at Raman shift 283 cm^{-1} and 620 cm^{-1} matched with the Cuo phase [51,53]. For the cold spray worn surfaces at room temperature (see Figure 4.10b), the characteristic peaks at Raman shift 112 cm^{-1} and 216 cm^{-1} correspond to the Cu_2O phase [49-51]. For the cold spray worn surfaces at 300°C (see Figure 4.10b), the characteristic peak at Raman shift 112 cm^{-1} is associated with the Cu_2O phase [50], whereas the peaks at Raman shift 296 cm^{-1}, 341 cm^{-1} and 623 cm^{-1} tallies with the Cuo phase [52-55]. In summary, Cu_2O and Cuo were found on both coating's unworn and worn surfaces.

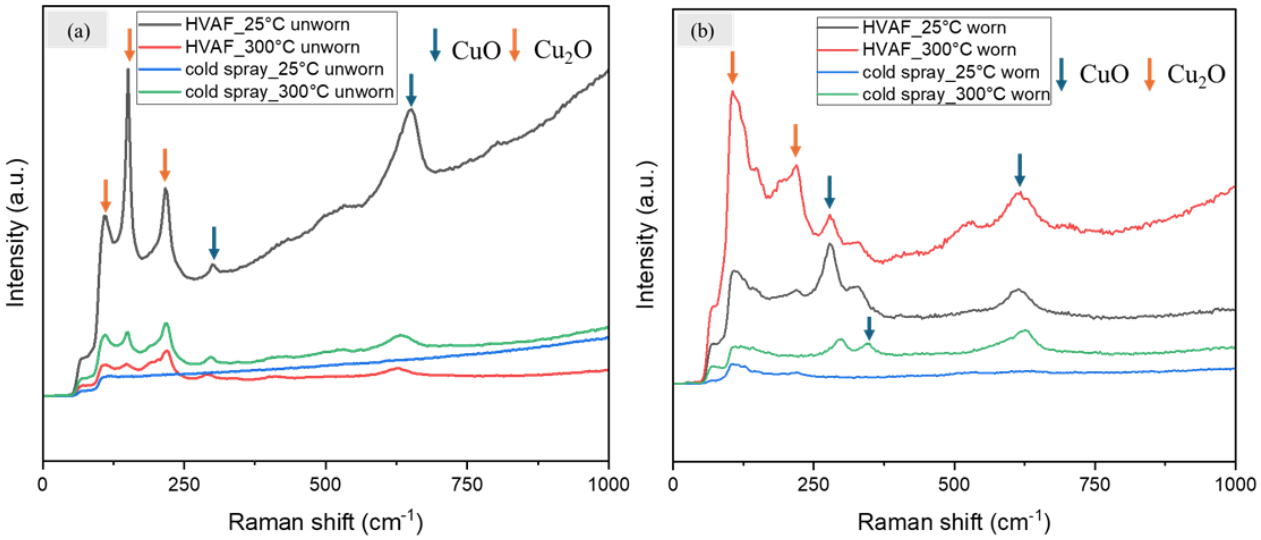

Figure 4.10. Raman spectrum of the (a) unworn HVAF and cold spray coatings at room temperature (25°C) and 300°C, (b) worn HVAF and cold spray coatings at room temperature (25°C) and 300°C.

Figure 4.11 shows the SEM imaging of the wear track cross-section of (a) HVAF and (b) cold spray coatings after sliding test at room temperature. Thin continuous tribo-films in the form of copper oxide film were formed on the surface of the HVAF coatings. Also, the subsurface of the wear track of the HVAF coatings revealed the presence of fragmentation, debonding (red circle) and cracks (yellow circle) as shown in Fig. 4.11a. On the other hand, the surface of the cold-sprayed coatings was characterized by thin tribo-film (copper oxide film) and fragmentation defects. However, there was no evidence of debonding and crakcs on its

subsurface (see Figure 4.11b). The EDS color maps of the worn HVAF and cold spray coatings cross sections at room temperature shown in Figure 4.11 indicate that both coatings had a small amount of oxygen content.

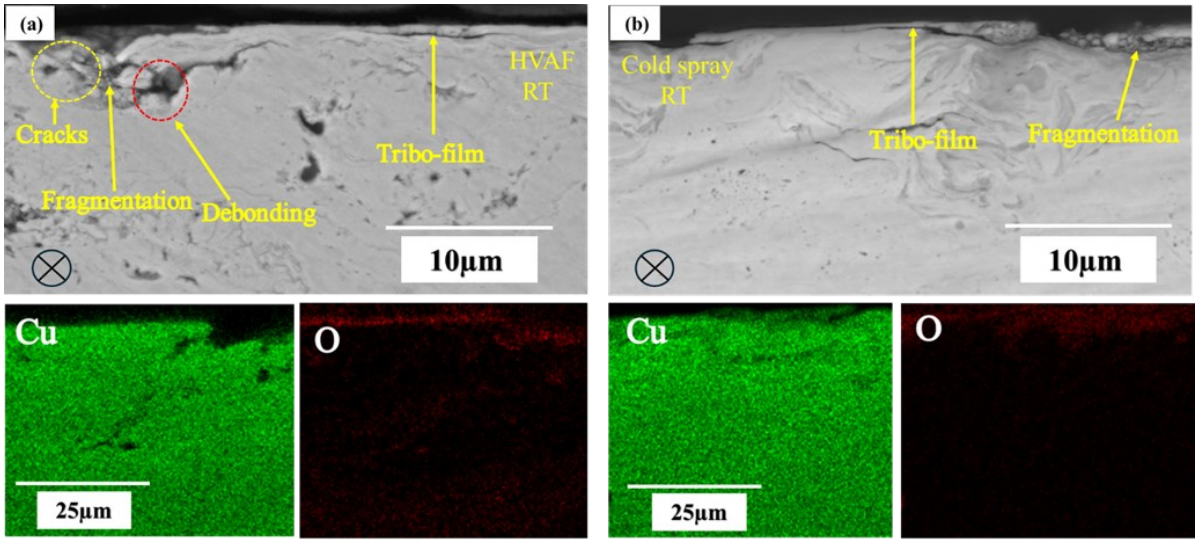

Figure 4.11. SEM and elemental map analysis of the wear track cross-sections of (a) HVAF and (b) cold spray copper coatings at room temperature.

Figure 4.12 shows the cross-sectional morphology of worn surfaces of (a) HVAF and (b) cold spray coatings after sliding test at 300°C. Tribo-layers (i.e., third body) with different distinct features were formed on the surface of both coatings. The third body exhibits distinct properties that are different from those of the original pair of mating materials. The tribo-layer for the HVAF coatings consists of oxide concentration and a higher level of crack formation. (see Figure 4.12a). Concerning the cold sprayed coating, the tribo-layer was also rich in oxide. However, the layer of oxides was mixed with a significant amount of copper and the crack formation was lesser in comparison to HVAF coatings (see Figure 4.12b). The EDS color maps of the worn HVAF and cold spray coatings cross sections at 300°C shown in Figure 4.12 confirm that the tribo-layer of both coatings was rich in oxygen content. However, the oxygen concentration was slightly higher for the tribo-layer of HVAF coatings than for cold spray coatings. The EDS point analysis performed on the coatings showed an oxygen concentration of ~16 wt.% and ~9 wt.% for HVAF and cold spray coatings respectively. The EDS line scan was performed along the arrow lines marked in the SEM images in Fig. 4.13, from the top of the tribo-layer to the coatings. The results corroborate the presence of Cuo and Cu_2O in the tribo-layer of both coatings, with a higher oxygen concentration at the surface of the tribo-layer

in comparison to the lower area. Also, the oxygen concentration at the surface of the tribo-layer was slightly higher for the HVAF coatings than the cold sprayed coatings.

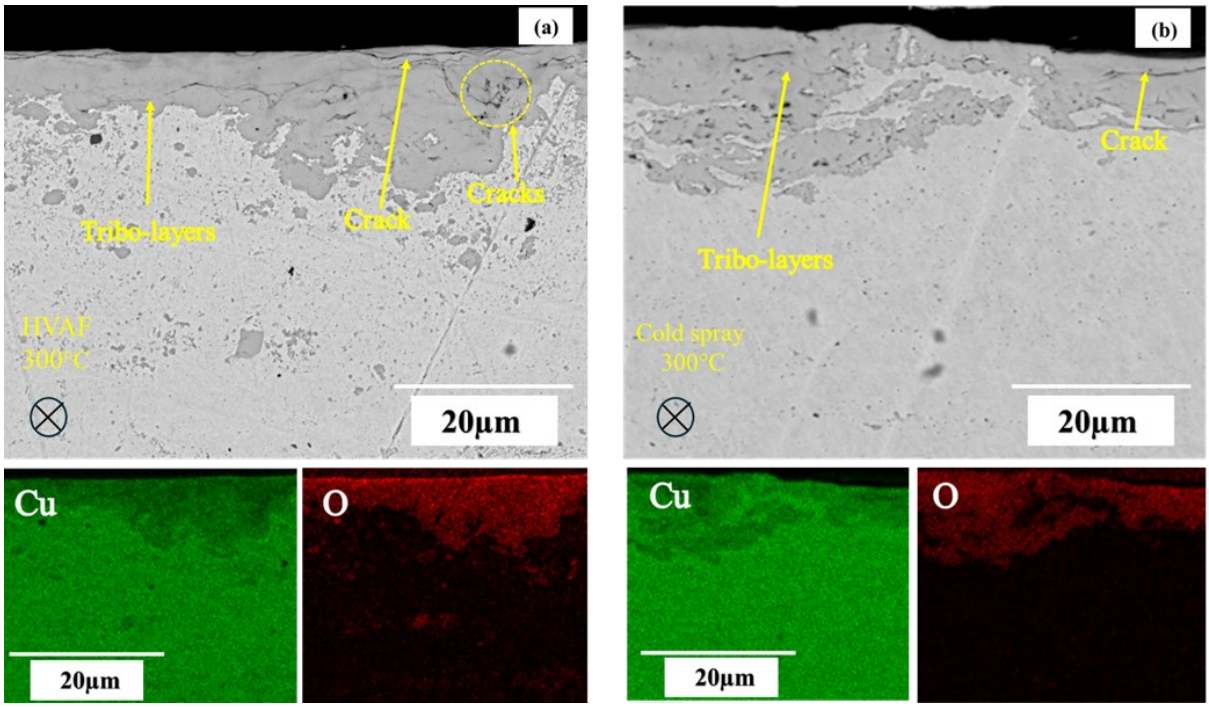

Figure 4.12. SEM and Elemental map analysis of the wear track cross-sections of (a) HVAF and (b) cold spray copper coatings at 300°C.

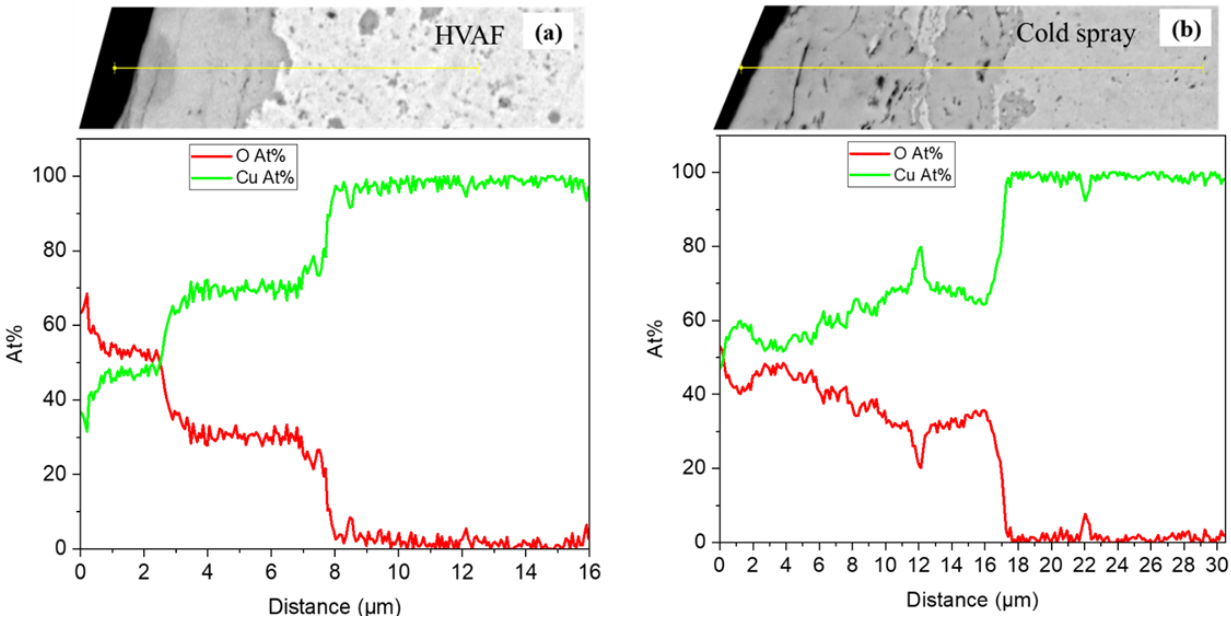

Figure 4.13 EDS line scan on the cross-section of wear track of (a) HVAF coatings and (b) cold spray coatings at 300°C.

4.5.2 Counterface analysis

Figure 4.14 a-b represents the SEM micrographs of the alumina counterfaces after sliding test against a) HVAF copper coating and b) cold spray copper coating at room temperature test conditions. At room temperature sliding, a thin layer of material from the coating to the surface of the alumina counter body, with a similar area of contact was observed for both coatings. The EDS mapping analysis performed on the transfer layer affirms the presence of copper and oxygen. Figure 4.14 c-d represents the SEM micrographs of the alumina counterfaces after sliding test against c) HVAF copper coating and d) cold spray copper coating at 300°C test conditions. The counterpart sliding at high temperatures experienced a higher amount of transfer film on the alumina counterparts, especially at the edge of the contact. The transfer layer for the counter ball sliding against the HVAF coating was higher than the cold spray coating with a wider contact area. Also, The EDS mapping analysis showed a higher copper content for the counter ball sliding against HVAF coatings. The counterface sliding against the cold spray coating showed abrasive marks along the sliding direction with transferred material covering some region of the marks at the center of the contact. In summary, the results depict an increase in the transfer film on the counter ball as the temperature increases.

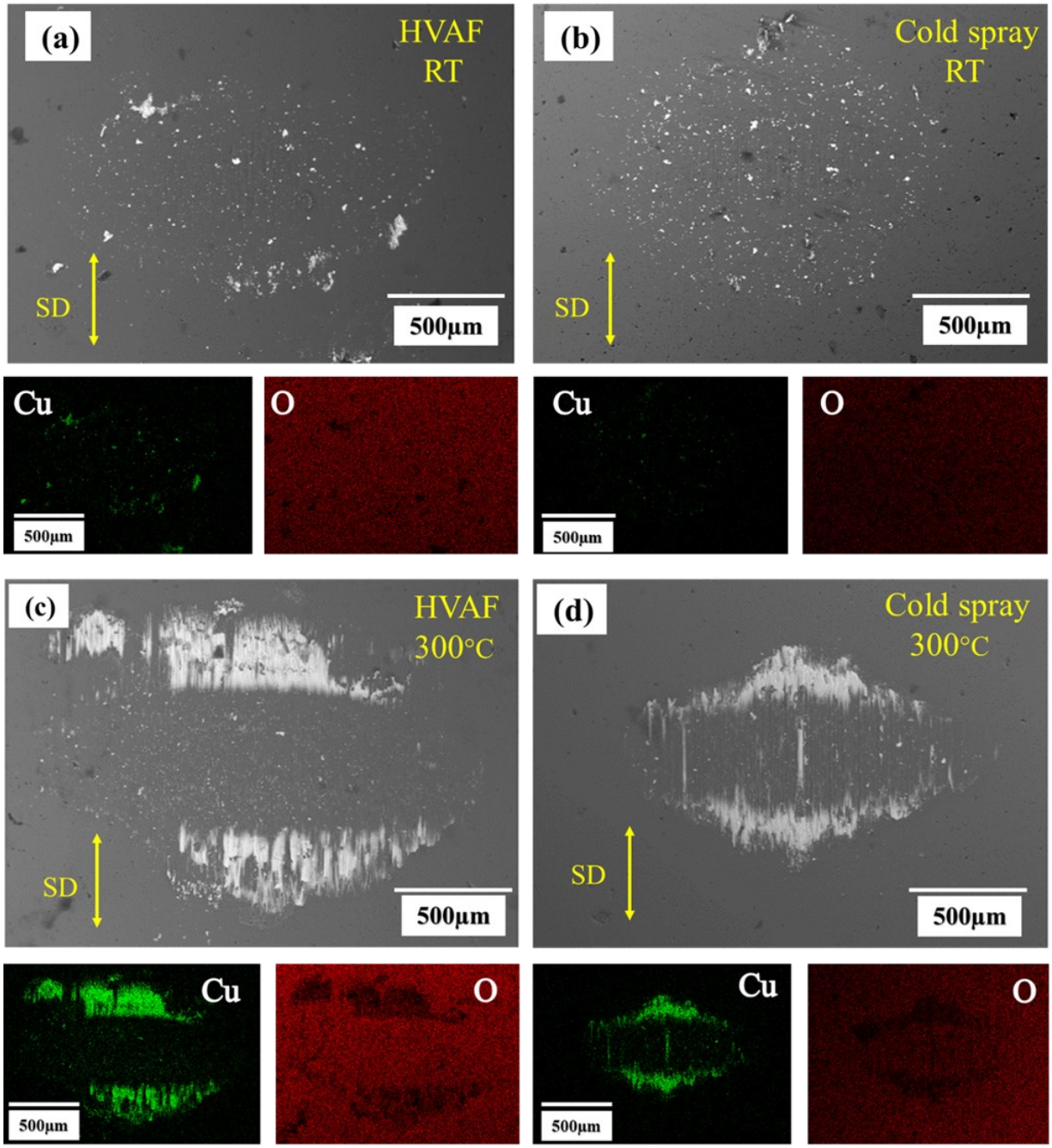

Figure 4.14 SEM analysis and EDS maps of alumina counter ball after sliding at room temperature (a) HVAF and (b) Cold spray and 300°C (c) HVAF and (d) Cold spray

4.6 Friction and wear mechanisms

Figure 4.15. provides a schematic representation of the friction and wear mechanism of the HVAF and cold spray coatings at room and elevated temperatures (300°C) based on the ex-situ analysis that was performed on the worn surfaces. The coefficient of friction behavior was similar for both coatings (HVAF and cold spray) at room temperature, as the different spray processes did not have variations in the wear mechanism. The coefficient of friction behavior at room temperature is consistent with copper coatings reported in the literature [26,44,56,57].

As shown in Fig. (4.5a-b) the friction coefficient at room temperature was lower than coatings tested at elevated temperatures (300°C). This can be attributed to the higher abrasion on the worn surface and reduced adhesion for the coatings sliding at room temperature. It could also be possible that some oxide debris present helps in promoting sliding friction reduction. The reduction of the coefficient of friction by oxide debris has been reported by previous studies [58,59]. Also, high temperature sliding condition stimulates higher stress levels in the coatings as well as an increase in the adhesion between mating bodies, promoting a higher coefficient of friction. Previous literature has observed an enhancement in the coefficient of friction of HVAF and HVOF WC-10Co4Cr coatings [60] and cold sprayed AISI 316L SS coatings [61] as the sliding test temperature increases.

As seen in Fig. 4.6a-b, similar wear behavior was obtained for both coatings sliding at room temperature as the sliding still occurs on the surface of the coatings at this test condition. Therefore, the porosity effect is minimal and not capable of liberating particles from the coatings during sliding. However, sliding wear tested at room temperature for both coatings was lower than the elevated test condition. Continuous tribo-film in the form of copper oxide film was formed on the surface of cross sections of both worn coatings at room temperature (see Fig. 4.11a-b). The formation of Cu_2O film on the sample surface of Cu sliding over Sapphire spheres at room temperature has been reported by Liu et [62]. This tribo-film can act as a protective layer between the counterface and the coating surface during sliding, assisting in decreasing the amount of adhesion as well as reducing wear [63,64]. At high temperature sliding conditions, heat generated through friction during the sliding process results in thermal softening and an increase in the real area of contact, leading to an enhanced adhesion between the surfaces of the alumina counterface and the Cu coating. This improved adhesion experienced between the mating bodies promotes higher friction and wear behavior at high temperature test conditions [65]. In addition, a higher amount of material transfer was observed on the alumina counterball mated with the Cu coating at elevated temperature sliding compared to room temperature, indicating a possible higher amount of adhesion between the mating bodies, resulting in higher wear of the Cu coatings (see Fig. 4.14). The appearance of adhesive transfer films on the counterface indicates the occurrence of continuous plastic shearing, causing the fragmentation of coating material during the sliding process before being transferred to the surface of the counterface [66]. Previous studies have reported the enhancement in wear due to increased material transfer on the counterball during the mating process [36,63, 67].

At high temperatures, the wear behavior of cold spray coatings was fairly low and within the same range as room temperature test conditions as there were no significant changes at both test conditions. This can be attributed to the uniform dense coating of the cold spray coating, which does not liberate particles or cracks easily during sliding. However, the wear of HVAF coatings increased at elevated temperatures. The higher wear behavior of HVAF coatings in comparison to cold spray at 300°C test condition can be attributed to the higher porosity of HVAF coating, which can create a significant effect during sliding, resulting in cracking and liberation of particles which can produce higher adhesive transfer and enhance wear rates. This indicates that debris particles formed from the liberation result in the smearing of the copper to adhere to the alumina counterface. Also, the worn surface of the cold spray coatings was characterized by cracks and deep abrasive scars parallel to the sliding direction (see Fig. 4.8 c and d). However, two distinct regions consisting of a smeared region (red circle) and a rough region (yellow circle) were obtained for the worn surface of HVAF coatings (see Fig. 4.8 a and b). This smooth region was verified by EDS to be rich in copper oxide, producing a higher metallic content. This promotes a higher level of adhesion between the mating surface, leading to higher wear rates. In addition, Raman analysis performed on the worn coatings at 300°C showed the presence of Cuo and Cu_2O (see Figure 4.10b). However, the intensity of the peaks of HVAF coatings was higher than that of cold spray coating. This correlates well with the higher oxidation concentration formed on the HVAF worn coatings, indicating that the higher oxide concentration of the HVAF coatings might have contributed to its enhanced wear behaviour. In summary, at room temperature, detached particles, cracks and mild abrasive wear appear to be the dominant wear mechanism for HVAF coating. Whereas cracks and mild abrasive were the dominant wear mechanisms for cold spray coating. At elevated temperature, cracks and adhesion were found to be the dominant wear mechanism for HVAF coatings. Whilst cold spray wear mechanism was dominated by deep abrasive wear.

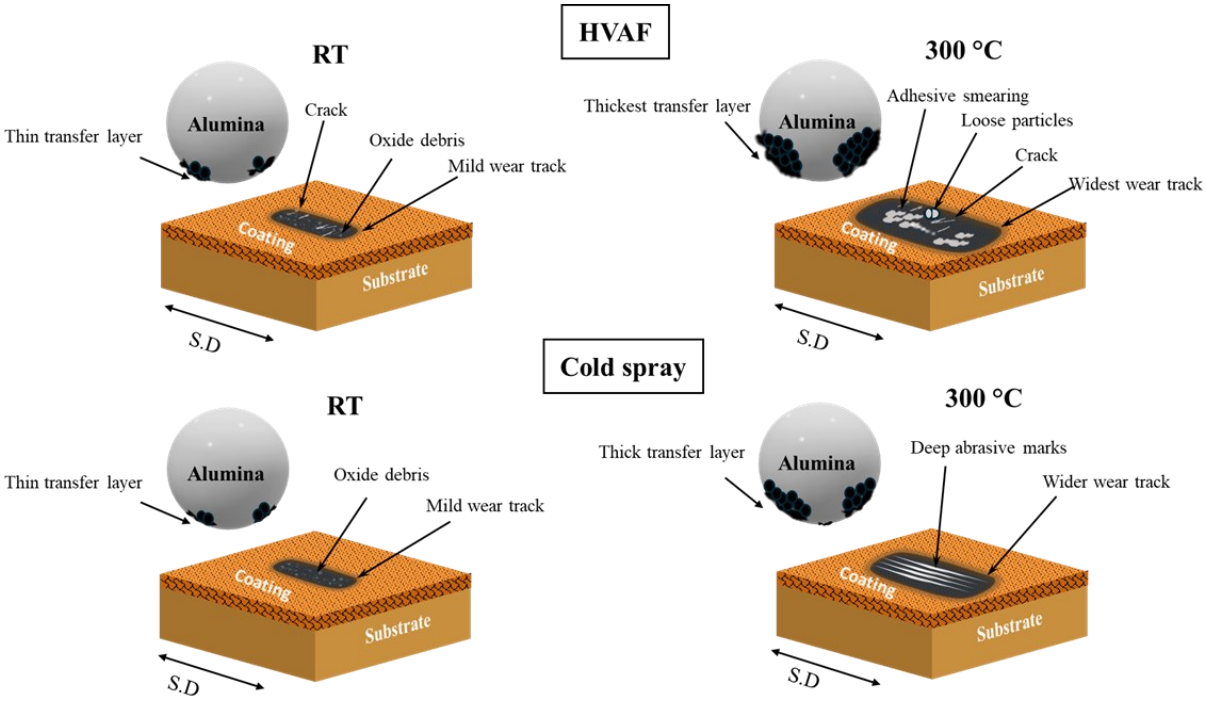

Figure 4.15 Schematic showing the wear mechanisms of HVAF and cold spray copper coatings at RT and 300°C

4.7 Conclusion

This study developed pure copper coatings using high-velocity air fuel (HVAF) and cold spray (CS) techniques to evaluate the microstructure, mechanical and tribological performance of the deposited coatings. The surface morphology of the cold spray coatings showed a larger amount of deformed particles than that of the HVAF coatings due to the deposition process. In regards to the cross-section of the coatings, cold spray coatings were denser with no or negligible oxide concentration. However, the HVAF coatings developed were marked with pores and oxides. The properties of the coatings measured showed that cold spray coatings produced a slightly higher roughness and hardness than HVAF coatings. However, HVAF coatings were thicker than cold spray coatings. The XRD analysis revealed and validated the formation of oxides in the HVAF coatings due to the higher temperature spray process compared to cold spray. The friction and wear behavior of copper coatings were investigated at room temperature and 300°C. At room temperature, the coefficient of friction and wear resistance were similar for both coatings. The dominant wear mechanism was ascribed to detached particles, cracks and mild abrasive wear for HVAF coatings. Also, cracks and mild abrasive wear were the main wear mechanisms for cold spray coatings. At elevated temperature test conditions, the friction behavior of both coatings was higher than the sliding test at room temperature. However, the coefficient of friction of both coatings was within the same range. While the wear behavior of cold spray coating at elevated temperature remains relatively on the same level with room temperature test conditions, that of HVAF coatings increased at high temperature sliding test. This was attributed to the ease of HVAF coatings to liberate particles to produce adhesive transfer during sliding due to their higher porosity. The dominant wear mechanism at this test condition was cracks and adhesion for HVAF coatings and deep abrasive wear for cold spray coating.

References

1. Vineeth Menon. Clodualdo Aranas Jr, Gobinda Saha. Cold spray additive manufacturing of copper-based materials: Review and Future Directions, Materials Science in Additive Manufacturing, 2022, 1(2), p 1-20. https://doi.org/10.18063/msam.v1i2.12

2. Swastika Banthia, Mohammad Amid, Srijan Sengupta, Siddhartha Das and Karabi Das. Reciprocating Sliding Wear of Cu, Cu-SIC Functionally Graded Coating on Electrical Contact, Journal of Materials Engineering and Performance, 2020, 29(6), p 3930-3940. https://doi.org/10.1007/s11665-020-04878-8

3. Heli Koivuluoto, Andrew Coleman, Keith Murray, Martin Kearns and Petri Vuoristo. High Pressure Cold Sprayed (HPCS) and Low Pressure Cold Sprayed (LPCS) Coatings Prepared from OFHC Cu Feedstock: Overview from Powder Characteristics to Coating Properties, Journal of Thermal Spray Technology, 2012, 21(5), p 1065-1075. https://doi.org/10.1007/s11666-012-9790-x

4. A.W. Blackwood and J.E. Casteras. Copper (Cu), Properties of Pure Metals, Properties and Selection: Nonferrous Alloys and Special-Purpose Materials, ASM Handbook, ASM International, 1990, 2, p 1099-1201

5. Jian Huang, Xingchen Yan, Cheng Chang, Yingchun Xie, Wenyou Ma, Renzhong Huang, Ruimin Zhao, Sgunhua Li, Min Liu and Hanlin Liao. Pure copper components fabricated by cold spray (CS) and selective laser melting (SLM) technology, Surface and Coatings Technology, 2020, 395. https://doi.org/10.1016/j.surcoat.2020.125936

6. Masoumeh Goudarzi and Hassan Ghaziasadi. The effect of gas flow rate on structural, mechanical and antibacterial properties of atmospheric plasma sprayed Cu coatings, Physica Scripta, 2021, 96. https://doi.org/10.1088/1402-4896/abf7fc

7. Mohamed Ibrahim, Mohammed Abdul Samad, Khaled Al-Athel, Abul Fazal Arif and Nasirudeen Olalekan. Evaluation of Tribological Properties of Thermally Sprayed Copper and Copper Alloy Coatings, Arabian Journal for Science and Engineering, 2018, 43, p 4899-4910. https://doi.org/10.1007/s13369-018-3222-2

8. C. Mary, S. Fouvry, J.M. Martin and B. Bonnet. Pressure and temperature effects on Fretting Wear damage of a Cu-Ni-In plasma coating versus TiI7 titanium alloy contact, Wear, 2011, 272 (1) p 18-37. https://doi.org/10.1016/j.wear.2011.06.008

9. C.H. Hager Jr, J.H. Sanders and S. Sharma. Unlubricated gross slip fretting wear of metallic plasma-sprayed coatings for Ti6AI4V surfaces, Wear, 2008, 265 (3-4), p 439-451. https://doi.org/10.1016/j.wear.2007.11.026.

10. B. Rajasekaran, S. Ganesh Sundara Raman, S.V. Joshi and G. Sundararajan. Performance of plasma sprayed and detonation gun sprayed Cu-Ni-In coatings on Ti-6AI-4V under plain fatigue and fretting fatigue loading, Materials Science and Engineering A, 2008, 479, p 83-92. https://doi.10.1016/j.msea.2007.06.019.

11. V. Fridrici, S. Fouvry and Ph. Kapsa. Fretting wear behavior of a Cu-Ni-In plasma coating, Surface and Coatings Technology, 2003, 163-164, p 429-434. https://doi.org/10.1016/s0257-8972(02)00639-4

12. B. Rajasekaran, S. Ganesh Sundara Raman, S.V. Joshi and G. Sundararajan. Effect of detonation gun sprayed Cu-Ni-In coating on plain fatigue and fretting fatigue behaviour of Al-Mg-Si alloy, Surface and Coating Technology, 2006, 201(3-4), p 1548-1558. https://doi.org/10.1016/j.surfcoat.2006.02.023

13. C. Mary, S. Fouvry, J.M. Martin and B. Bonnet. High temperature fretting wear of a Ti alloy/CuNiIn contact, Surface Coating Technology, 2008, 203(5-7), p 691-698. https://doi.org/10.1016/j.surfcoat.2008.08.043

14. H. Murthy, G. Mseis and T.N. Farris. Life estimation of Ti-6Al-4V specimens subjected to fretting fatigue and effect of surface treatments, Tribology International, 2009, 42(9), p 1304-1315. https://doi.org/10.1016/j.triboint.2009.04.013

15. Yong-Sheng Xhu, Xiao-Tao Luo, Yin-Qiu Sun, Yuan Ren, and Chang-Jiu Li. Atmospheric plasma-spayed CuNiInB coatings of high fretting wear performance enabled by oxide-free metallic droplet deposition, Surface and Coatings Technology, 2023, 464(129537). https://doi.org/10.1016/j.surfcoat.2023.129537.

16. Yang Q, Zhou WL, Zhong YN, Zhang XH, Fu XS, Chen GQ and Li ZQ. Effect of shot peening on the fretting wear and crack initiation behavior of Ti-6Al-4V dovetail joint specimens, International Journal of Fatigue, 2018, 107, p 83-95. https://doi.org/10.1016/j.ijfatigue.2017.10.020

17. Ruiz C, Boddington PHB and Chen KC. An investigation of fatigue and fretting in a dovetail joint, Experimental Mechanics, 1984, 24, p 208-17. https://doi.org/10.1007/BF02323167

18. J.K. Xiao, W. Zhang, L.M. Liu, X.P. Gan, K.C. Zhou, C. Zhang, Microstructure and tribological properties of plasma sprayed Cu-15Ni-8Sn coatings, Surface and Coating Technology, 2018, 337, p 159–167. https://doi.org/10.1016/j.surfcoat.2018.01.016.

19. Atul Ranjan, Aminul Islam, Manabendra Pathak, Mohd Kaleem Khan, and Anup Kumar Keshri. Plasma sprayed copper coatings for improved surface and mechanical properties, Vacuum, 2019, 168 (108834). https://doi.org/10.1016/j.vacuum.2019.108834

20. Maher I. Boulos., Pierre L. Fauchais., and Joachim V.R. Herberlein. Thermal Spray Fundamentals. From powder to part, second edition, 2021. https://doi.org/10.1007/978-3-030-70672-2

21. N. Espallargas, Future Development of Thermal Spray Coatings: Types, Designs, Manufacture and Applications, Woodhead Publishing is an imprint of Elsevier, 2015.

22. Goudarzi Masoumeh, Saviz Shahrooz, Ghoranneviss Mahmood and Salar Elahi Ahmad. Investigation of stand-off distance effect on structure, adhesion and hardness of copper coatings obtained by the APS technique. Journal of Theoretical and Applied Physics, 2018, 12, p 85-91. https://doi.org/10.1007/d40094-018-0277-0

23. T. Stoltenhoff, C. Borchers, F. Gartner and H. Kreye. Microstructures and key properties of cold-sprayed and thermally sprayed copper coatings. Surface and coatings Technology, 2006, 200, p 4947-4960. https://doi.org/10.1016/j.surfcoat.2005.05.011

24. Amin Ma, Daoxin Liu, Xiaohua Zhang, Guangyu He, Dan Liu, Chengsong Liu, and Xingchen Xu. The fretting fatigue performance of Ti-6Al-4V alloy influenced by microstructure of CuNiIn coating prepared via thermal spraying, 2020, Tribology International 145 (106156). https://doi.org/10.1016/j.triboint.2019.106156

25. Shujuan Dong, Yihui Wang, Jinyan Zeng, Xiong Yang, Panpan Liang, Dezheng Wang, Huiqi Liao, and Hanlin Liao. Performance of plasma sprayed CuNiIn coatings and Mo Coatings subjected to fretting fatigue. Nano Materials Science, 2020, 2, p140 -150. https://doi.org/10.1016/j.nanoms.2019.07.003.

26. Kostoula I. Triantou, Dimitris I. Pantelis, Vincent Guipont and Michel Jeandin. Microstructure and tribological behavior of copper and composite copper + alumina cold sprayed coatings for various alumina contents. Wear, 2015, 336-337, p 96-107. http://dx.doi.org/10.1016/j.wear.2015.05.003

27. R.J. Talib, S. Saad, M.R.M. Toff, and H. Hashim. Thermal spray coating technology – A review. Solid state science and technology, 2003, 11 (1), p 109-117.

28. Yasemin Yildiran Avcu, Mert Guney, and Egemen Avcu. High-Velocity Air Fuel Coatings for Steel for Erosion-Resistant Applications. Journal of Electrochemical Science and Engineering, 2023, 13(2), p 407-420. https://dx.doi.org/10.5599/jese.1369

29. Golnoush Asadiankouhidehkordi, Andre C. liberate, Fadhel Ben Ettouil and Christian Moreau. Inner Diameter High-Velocity Air Fuel (ID-HVAF) Spraying of Copper, compared to Cold Sprayed, 2023, Proceedings from the International Thermal Spray Conference. https://doi.org/10.31399/asm.cp.itsc2023p0531

30. ASTM Standard E1920-03, Standard Guide for Metallographic Preparation of Thermal Sprayed Coatings, ASTM International, USA, 2009.

31. ASTM international. Designation: E2109-01 (Reapproved 2014). Standard test methods for determining area percentage porosity in thermal sprayed coatings.

32. P. Patel, S.A. Alidokht, N. Sharifi, A. Roy, K. Harrington, P. Stoyanov, R. R. Chromik, C. Moreau. Microstructural and tribological behavior of thermal spray CrMnFeCoNi high entropy alloy coatings. Journal Thermal Spray Technology, 2022, 31, p 1285–1301. https://doi.org/10.1007/s11666-022-01350-y

33. A. Roy, V.N.V. Munagala, P. Patel, N. Sharifi, S.A. Alidokht, M. Makowiec, R. R. Chromik, C. Moreau, P. Stoyanov. Friction and wear behavior of suspension plasma sprayed tantalum oxide coatings at elevated temperatures. Surface and Coatings Technology, 2023 452 (129097). https://doi.org/10.1016/j.surfcoat.2022.129097

34. Bruno C.N.M. de Castilho, Venkata Naga Vamsi Munagala, Sima A. Alidokht, Navid Sharifi, Stephanie Bessette, Mary E. Makowiec, Raynald Gauvin, Pantcho Stoyanov, Christian Moreau and Richard R. Chromik. Insights on silver migration mechanisms and their influence on the wear behavior of thermally sprayed self-lubricating coatings up to 350◦ C. Tribology Letters, 2022, 70 (120). https://doi.org/10.1007/s11249-022-01662-8

35. Amit Roy, Navid Sharifi, Ventaka Naga Vamsi Munagala, Sima A. Alidokht, Payank Patel, Mary Makowiec, Richard R. Chromik, Christian Moreau and Pantcho Stoyanov. Microstructural evolution and tribological behavior of suspension plasma sprayed CuO as high-temperature lubricious coatings. Wear, 2023. https://doi.org/10.1016/j.wear.2023.204874

36. Raunak Supekar, Rakesh Bhaskaran Nair, Andre McDonal and Pantcho Stoyanov. Sliding wear behavior of high entropy alloy coatings deposited through cold spraying and flames spraying: A comparative assessment. Wear, 2023, 516-517(204596). https://doi.org/10.1016/j.wear.2022.204596

37. Jin-Kun Xiao, Hong Tan, Yu-Qing Wu, Juan Chen and Chao Zhang. Microstructure and wear behavior of FeCoNiCrMn high entropy alloy coating deposited by plasma spraying. Surface and Coatings Technology, 2020, 385 (125430). https://doi.org/10.1016/j.surfcoat.2020.125430

38. N. Markocsan. Comparison between High-Velocity-Air-Fuel-(HVAF) and Cold-Gas-Spray (CGS) by evaluating mechanical properties of Ti-6-4-and INCONEL 718 coatings. Report INCO718 2011-02-16.

39. Hamid Assadi, Frank Gartner, Thorsten Stoltenhoff and Heinrich Kreye. Bonding mechanism in cold gas spraying. Acta Materialia, 2003, 51(3), p 4379-4394. https://doi.org/10.1016/s1359-6454(03)00274-x

40. Dapei Tang. Effect of substrate preheating temperature and coating thickness on residual stress in plasma sprayed hydroxyapatite coating. Global Conference on Polymer and Composite Materials, IOP Conference Series: Materials Science and Engineering, 2015, 87 (012097). https://doi.org/10.1088/1757-899x/87/1/012097

41. Ming Pang, Xiao-Han Zhang, Quan-Xiu Liu, Yi-Xuan Fu, Guang Liu and Wen-Dan Tan. Effect of preheating temperature of the substrate on residual stress of Mo/8YSZ functionally gradient thermal barrier coatings prepared by plasma spraying. Surface and Coatings Technology, 2020, 385(125377). https://doi.org/10.1016/j.surfcoat.2020.125377

42. V.V. Sobolev and J.M. Guilemany. Effect of oxidation on droplet flattening and splat-substrate interaction in thermal spraying. Journal of Thermal Spray Technology, 1999, 8(4), p 523-530.

43. B. Yu, J. Tam, W. Li, H.J. Cho, J.G. Legoux, D. Poirier, J.D. Giallonardo and U. Erb. Microstructural and bulk properties evolution of cold-sprayed copper coatings after low temperature annealing. Materialia, 2019, 7(100356). https://doi.org/10.1016/j.mtla.2019.100356

44. Vladislav S. Shikalov, Tomila M. Vidyuk, Artem A. Filippov and Ivanna D. Kuchumova. Microstructure, mechanical and tribological properties of cold sprayed Cu-W coatings.

International Journal of Refractory Metals and Hard Materials, 2022, 106(105866). https://doi.org/10.1016/j.ijrmhm.2022.105866.

45. Wen-Ya Li, Hanlin Liao, Jinglong Li and Christian Coddet. Microstructure and Microhardness of Cold-Sprayed CuNiIn Coating. Advanced Engineering Materials, 2008, 10(8). https://doi.org/10.1002/adem.200800044

46. N. Hutasoit, R.A Rahman Rashid, S. Palanisamy and A. Duguid. Effect of build orientation and post-build heat treatment on the mechanical properties of cold spray additively manufactured copper parts. The International Journal of Advanced Manufacturing Technology, 2020, 110, p 2341-2357. https://doi.org/10.1007/s00170-020-06010-5

47. Y. Zou, A. Rezaeian, W. Qin, S. Yue, J. A. Szpunar and E. Irissou and J. Legoux. Effect of Gas Temperature on the Microstructure and Properties of Cold Sprayed Copper Coatings. Materials Science and Technology, 2009.

48. W.Y. Li, C. Zhang, X.P Guo, G Zhang, H.L. Liao, C.J. Li and C. Coddet. Effect of standoff distance on coating deposition characteristics in cold spraying. Materials and Design, 2008, 29. p 297-304. https://doi.org/10.1016/j.matdes.2007.02.005

49. R. David Prabu, S. Valanarasu, I. Kulandaisamy, V. Ganesh, Mohd Shkir and A. Kathalingam. Studies on copper oxide thin films prepared by simple nebulizer spray technique. Journal of Material Science: Mater Electron, 2017, 28, p 6754-6762. https://doi.org/10.1007/s10854-017-6371-2

50. M. Grandin and U Wiklund. Wear phenomena and tribofilm formation of copper/copper-graphite sliding electrical contact materials. Wear, 2017. https://doi.org/10.1016/j.wear.2017.12.012

51. Meral Balik, Veysel Bulut and Ibrahim Y. Erdogan. Optical, structural and phase transition properties of Cu_2O, CuO and Cu_2O/CuO: Their photoelectrochemical sensor applications. International Journal of Hydrogen Energy, 2018, p 1-12. https://doi.org/10.1016/j.ijhydene.2018.08.159

52. I. Debbichi, M.C. Marco de Lucas, J.F. Pierson and P. Kruger. Vibrational properties of CuO and Cu_4O_3 from First-Principles Calculations, and Raman and Infrared Spectroscopy. The Journal of Physical Chemistry, 2012, 116, p 10232-10237. https://doi.org/10.1021/jp303096m

53. J.F. Xu, W. Ji, Z. X. Shen, W. S. Li, S. H. Tang, X. R. Ye, D. Z. Jia and X. Q. Xin. Raman Spectra of CuO Nanocrystals. Journal of Raman Spectroscopy, 1999, 30, p 413 -415.

54. Yilin Deng, Albertus D. Handoko, Yonghua Du, Shibo Xi and Boon Siang Yeo. In situ Raman Spectroscopy of Copper and Copper Oxide Surfaces during Electrochemical Oxygen Evolution Reaction: Identification of Cu Oxides as Catalytically Active Species. ACS catalysis, 2016, 6, p 2473-2481. https://doi.org/10.1021/acscatal.6b00205

55. Y.S. Gong, Chiapyng Lee and C.K. Yang. Atomic force microscopy and Raman spectroscopy studies on the oxidation of Cu thin films. Journal of Applied Physics, 1995, 77(10). https://dx.doi.org/10.1063/1.359234

56. Zahra Shabani Chafjiri, Amir Abdollah-zadeh, Rajab-Ali Seraj and Amir Azarniya. Efeect of cold spray processing parameters on the microstructure, wear, and corrosion behavior of Cu and Cu-Al_2O_3 coatings deposited onhttps://doi.org/10.1 AZ231 alloy substrate. Results in Engineering, 2023, 20(101594). https://doi.org/10.1016/j.rineng.2023.101594

57. Shu Wen, Cuiying Dai, Weiguo Mao, Zhiqiang Ren, Xiaoming Wang, Yang Zhao and Guofeng Han. Microstructure and Wear Properties of HVAF Sprayed Cu-Zr-AI-Ag-Co Amorphous Coatings at Different Spray Temperatures. Coatings, 2022, 12(458). https://doi.org/10.3390/coatings12040458

58. H.L. Costa, M.M. Oliveira Junior and J.D.B de Mello. Effect of debris size on the reciprocating sliding wear of aluminium. Wear, 2017, 376-377, p 1399-1410. https://dx.doi.org/10.1016/j.wear.2016.10.025

59. M.M. De Oliveira Junior, H.L. Costa, W.M. Silva Junior and J.D.B. De Mello. Effect of iron oxide debris on the reciprocating sliding wear of tool steels. Wear, 2019, 426-427, p 1065-1075. https://doi.org/10.1016/j.wear.2018.12.047

60. G. Bolelli, L. M. Berger, T. Borner, H. Koivuluoto, L. Lusvarghi, C. Lyphout, N. Markocsan, V. Matikainen, P. Nylen, P. Sassatelli, R. Trache and P. Vuoristo. Tribology of HVOF- and HVAF-sprayed WC-10C04Cr hardmetal coatings: A comparative assessment. Surface and Coatings Technology, 2015, 265, p 125-144. https://dx.doi.org/10.1016/j.surfcoat.2015.01.048

61. A.V. Radhamani, Hon Chung Lau, Anirudh Venkatraman Krishnan, M. Kamaraj and S. Ramakrishna. AISI 316L Stainless Steel Tribological Behavior under Sliding and Erosive Conditions: A Comparison between Spark Plasma Sintering, Laser Metal Deposition, and Cold Spraying. Journal of Materials Engineering and Performance, 2023. https://doi.org/10.1007/s11665-023-08548-3

62. Zhilong Liu, Christian Patzig, Susanne Selle, Thomas Hoche, Peter Gumbsch and Christian Greiner. Stages in the tribologically-induced oxidation of high-purity copper. Scripta Materialia, 2018, 153, p 114-117. https://doi.org/10.1016/j.scriptamat.2018.05.008

63. Cyrus Bidmeshki, Andre C. Liberati, Amit Roy, Alejandra I. Encalada, Fadhel Ben Ettouil, Sima A. Alidokht, Richard R. Chromik, Christian Moreau and Pantcho Stoyanov. Microstructural, Mechanical, and Tribological Evaluation of CuAl-based Coatings Deposited by APS and HVOF. Journal of Thermal Spray Technology, 2023, 32, p 2321-2335 https://doi.org/10.1007/s11666-023-01665-4

64. N.N. Gosvami, J.A. Bares, F. Mangolini, A.R. Konicek, D.G. Yablon and R.W. Carpick. Mechanisms of antiwear tribofilm growth revealed in situ by single-asperity sliding contacts. 2015, 348(6230). https://doi.org/10.1126/science.1258788

65. A. Gaard, N. Hallback, P. Krakhmalev and J. Bergstrom. Temperature effects on adhesive wear in dry sliding contacts. Wear,2010, 268, p 968 – 975. https://doi.org/10.1016/j.wear.2009.12.007

66. Venkata Naga Vamsi Munagala, Sima A. Alidokht, Navid Sharifi, Mary E. Makowiec, Pantcho Stoyanov, Christian Moreau and Richard R. Chromik. Room and elevated temperature sliding wear of high velocity oxy-fuel sprayed Diamalloy3001 coatings. Tribology International, 2023, 178 (108069). https://doi.org/10.1016/j.triboint.2022.108069

67. Sima A. Alidokht, Venkata Naga Vamsi Munagala and Richard R. Chromik. Role of Third Bodies in Friction and Wear of Cold-Sprayed Ti and Ti-TiC Composite Coatings. Tribology Lettes, 2017, 65(114). https://doi.org/10.1007/s11249-017-0899-4

Chapter
5. CONCLUSIONS AND FUTURE WORK

In this chapter…

the main conclusions and potential future works of this thesis are presented.

5.1 Conclusions

Copper-based coatings are commonly used on tribological interfaces within gas turbine engines to enhance the wear resistance. This thesis illustrates the tribological behavior of Cu-based coatings (Copper-nickel and pure copper) at room and elevated temperatures. The specific conclusions for each study have been summarized in their respective chapters. The global conclusions of the thesis are summarized below.

1. The APS Cu-Ni coating deposited on each substrate showed well-flattened splats and the properties of coatings (thickness, porosity, surface roughness, and microhardness) were relatively comparable. The coefficient of friction and wear behavior of coatings sliding at high temperatures were higher than the room temperature test condition.
2. At room temperature sliding, the worn surface appeared to have a smeared smooth layer with abrasive scars as the dominant wear mechanism. A higher amount of adhesion between the mating bodies as well as the formation of cracks, delamination, loose particles and wear debris on the worn serves as the dominant wear mechanism at elevated temperature sliding conditions, resulting in a higher level of friction and wear.
3. Pure copper deposited by cold spray showed dense microstructure with no or negligible oxide concentration compared to HVAF coatings that were chacterized with pores and oxide concentration. Also, the measured properties of both coatings showed a slightly higher roughness and hardness of cold spray coatings compared to HVAF coatings. The friction and wear behavior of both coatings were higher at elevated test conditions in comparison to room temperature sliding. The formation of a continuous tribo-film layer at room temperature test might have acted as a protective layer during sliding reducing wear. However, the coefficient of friction for both coatings was within the same range at room and elevated test conditions. Cold spray coatings showed a similar wear resistance for both test conditions (room temperature and 300°C), However, there was an increase in wear from room temperature to elevated temperature sliding test for HVAF spray coatings.
4. At room temperature, the dominant wear mechanism was found to be delamination, brittle fracture and mild abrasive wear for HVAF coatings and mild abrasive wear for cold spray coatings. At elevated sliding test, the wear mechanism of the HVAF coating was dominated by brittle fracture and adhesion which contributed to the increase in wear of the coating compared to cold spray coating which was characterized by deep abrasive scar as the primary wear mechanism.

5. The wear behavior of cold spray coatings that did change with a function of temperature indicates the capability of the coating to adapt to different environmental conditions.

5.2 Future work

1. From the outcomes of the coatings developed via the spray methods investigated in this thesis, a further improvement can be targeted using a novel coating technique called the liquid cold spray (LCS). Such a process has the potential to deposit much larger particles and thus produce high quality coatings at a lower cost than the conventional cold spray process.
2. Pure copper feedstock powder with suitable particle size distribution should be deposited with the atmospheric plasma spray (APS) to understand the performance of the coating as well as to obtain a close comparison with the low temperature deposition Cu-coatings obtained in this study.
3. Advanced tribological characterization should be performed on the coatings using a component-based test rig that closely mimics the actual operating conditions of tribological interfaces of gas turbine engines.